INTEGRATION OF PALEOHYDRAULIC RECONSTRUCTION AND

PROVENANCE METHODS IN ANCIENT FLUVIAL AND AEOLIAN SYSTEMS

A Dissertation

by

CLYDE PITT FINDLAY III

Submitted to the Office of Graduate and Professional Studies of
Texas A&M University
in partial fulfillment of the requirements for the degree of

DOCTOR OF PHILOSOPHY

Chair of Committee,	Ryan C. Ewing
Co-Chair of Committee,	Nicholas D. Perez
Committee Members,	Julia S. Reece
	Franco Marcantonio
Head of Department,	Julie Newman

December 2020

Major Subject: Geology

ABSTRACT

Detrital zircon is a dense mineral used in provenance studies to translate the rock record into spatio-temporal reconstructions of climatic, tectonic, and autogenic processes that shaped ancient landscapes and continue to shape modern planetary surfaces. Such provenance techniques rely on accurately quantifying the abundance and variability of dense minerals, but dense mineral assemblages can be affected by hydraulic sorting during transport of a sediment load. I integrate paleohydraulic reconstruction and provenance techniques to disentangle allogenic and autogenic signals in detrital zircon age signatures in a case study of the Pennsylvanian–Permian Cutler Group in the Paradox Basin of UT and CO. I synthesize paleohydraulic reconstruction methods and demonstrate how to apply them to provenance problems, demonstrate how paleohydraulics and provenance can be used to investigate depositional environment and improve understanding of sediment dispersal patterns in the Paradox Basin, and expand the paleohydraulics and provenance approach to investigate fluvial and aeolian interactions. Measured sections, grain size, and cross-stratification set thickness measurements from outcrops in a source-to-sink transect, along with detrital zircon sampling of fluvial channel and aeolian deposits, were used to reconstruct and identify spatial variations in ancient flow conditions and provenance. Results show that sorting did not affect detrital zircon age signatures in the fluvial or aeolian systems, and instead implicate the mixing of different sediment sources from within the Uncompahgre Uplift, as well from extrabasinal sources. Integration of detailed sedimentologic, paleoflow,

sediment provenance, and paleohydrualic datasets indicate that both fan and axial dispersal patterns existed in the Cutler fluvial system, and these interacted with actively uplifting salt walls. Paleohydraulic results also reveal how sediment recycling between coeval fluvial and aeolian systems is likely linked to the combined influence of position within the active flexural foreland basin and salt wall topography and illustrate variable influence of these allogenic drivers on ancient fluvial and aeolian systems. Combining paleohydraulic reconstruction with provenance analysis provides the tools necessary to investigate the autogenic sorting effects on detrital zircon age data, and assess these in the context of allogenic controls on fluvial and aeolian systems.

DEDICATION

To Jenny, Isla, and Emery, your love and silliness motivated me through the whole thing.

ACKNOWLEDGMENTS

CONTRIBUTORS AND FUNDING SOURCES

TABLE OF CONTENTS

LIST OF FIGURES

LIST OF TABLES

1. INTRODUCTION

The sedimentary rock record and detrital zircon geochronology is utilized to interpret the provenance of sediment and determine paleogeographical setting. Different forcings on erosion and deposition can leave similar signatures in the record that are sometimes difficult disentangle. Allogenic drivers, such as tectonic and climatic events, can expose new sediment sources, divert transport systems, and remove a sediment source from the catchment, resulting in temporal changes in sediment provenance detected by detrital zircon age signatures in the basin. Inversely, those age signatures can be used to infer the driving tectonic or climatic events. However, autogenic processes, such as hydraulic sorting of zircon grains, may also change detrital age signatures by removing zircons from the sediment load, which can yield variations in age spectra downstream that could be interpreted as the result of allogenic events. Although sorting occurs in all transport systems, the effects of sediment transport on detrital zircon provenance signals is not well recognized in provenance studies. Established paleohydraulic reconstruction methods have not yet been applied to provenance studies to determine the role of sorting along a transport pathway, leaving open questions about the fidelity of paleogeographic reconstructions derived from detrital zircon age signatures.

An example of the current methods and potential pitfalls in basin scale provenance studies comes from the classic detrital zircon analysis of Paleozoic Colorado Plateau aeolian deposits, where single samples from aeolian systems are used to infer

continent scale paleogeography and sediment transport systems (Dickinson and Gehrels, 2003). In this specific study, Dickinson and Gehrels (2003) concluded that sediment was transported across the continent from Appalachia by a fluvial system, long-shore transport, and up onto the Colorado Plateau by wind. They predict that sediment was transported by different fluids and in different transport systems. Thus, it is reasonable to assume that sorting could have happened during transcontinental sediment transport, and during transitions between depositional environments, but it is unclear how this would be detected in the detrital zircon age signature.

Studies of modern depositional systems have found variable detrital zircon age signatures in sediment from different positions along the transport system and across depositional environment elements, even though the sediment was derived from the same source. For example, detrital zircon age signatures vary across the top of a single dune in the Amazon River (Lawrence et al., 2011). Grain size is finest on the stoss side of the dune, and coarsest on the lee side of the dune, so different sizes of zircon are deposited across the dune. They show that grain size sorting imparts variability on detrital zircon age results, where some detrital zircon ages may be more abundant, or are only present, in the coarse sediment on the lee side of the dune. Another study sampled sediment from the deepest part of a fluvial channel, halfway up a fluvial bar, and from the fluvial bar top in the Orinoco Delta (Ibanez-Mejia et al., 2018). They found that bulk sediment size, zircon grain size, and detrital zircon age spectra changed with position in the channel. Channel deposits from the deepest part of the channel are coarser than the bar top deposits and have detrital zircon age signatures that are statistically dissimilar

from the finest grain size samples. These studies demonstrate that sorting can affect age spectra at the bedform and channel scale. It remains unclear whether the sorting signal is transmitted to the basin scale, highlighting an emerging problem in provenance studies.

Complementary studies of ancient environments regarding the impacts of sorting on detrital zircon age signatures are less common because detailed sampling of sediment from different hydraulic environments across bedforms and channels is more difficult. Recognizing the effects of sorting from ancient sedimentary deposits requires reconstruction of ancient transport conditions, primarily the competency of the flow that transported the sediment load. Recent advances in paleohydraulic reconstruction are made possible by empirical studies of modern transport systems combined with physics-based transport modelling experiments that enable one to relate field measurements of grain size, bar thickness, and cross-stratification set thickness to the depth, slope, velocity, discharge, and competency of ancient channel flow. From these reconstructions, provenance data can be investigated for signals of sorting, and variability in provenance data can be more confidently attributed to allogenic events, but such methods have not been widely applied. Integrating paleohydraulic reconstruction and detrital zircon geochronologic methods requires an ancient sedimentary system with sediment derived from a known source that has a well-defined provenance signature and proximal to distal exposures of the transport system that allows reconstruction of a downstream profile.

The Pennsylvanian–Permian Cutler Group deposited in the foredeep and forebulge of the Paradox Basin of UT and CO presents an ideal natural laboratory for

testing the sensitivity and utility of paleohydraulic reconstruction of ancient fluvial and aeolian systems for provenance analysis. In the Cutler Group, fluvial deposits were derived from the basement-cored Uncompahgre Uplift, which acted as the structural load that drove flexural basin subsidence, and has a characteristic bimodal age signature dominated by 1441 Ma and 1723 Ma zircon U-Pb ages (Lawton et al., 2015; Leary et al., 2020). Aeolian deposits were derived from extrabasinal sediment sources scattered across Laurentia (Soreghan et al., 2002; Dickinson and Gehrels, 2003), resulting in multi-modal detrital zircon age signatures. The fluvial system transported sediment from the uplift to the forebulge, the aeolian system from the forebulge to the medial basin, and the two depositional environments interfinger in the medial foredeep. The Cutler Group is well exposed in the proximal basin, on the flanks of salt anticlines in the medial basin, and in deep canyon systems and Laramide uplifts in the distal basin. The Cutler Group fluvial system has been interpreted as a both a megafan and as an axial system that flowed between salt walls in the medial basin (Campbell, 1980; Cain and Mountney, 2009; Lawton et al., 2015; Venus et al., 2015). The aeolian system is interpreted to have been dominant in the distal basin, and the fluvial system dominant in the proximal basin (Langford and Chan, 1989; Mountney and Jagger, 2004). The known sediment sources, excellent exposure of the Cutler Group from the foredeep to the forebulge of the foreland basin, competing interpretations of fluvial style, and spatial variation in fluvial and aeolian interactions are key premises of this study. This study reviews and applies classic and state-of-the-art paleohydraulic reconstruction and detrital zircon provenance

methods to a ca. 100 km spatial transect of the basin to investigate the role of sorting on detrital zircon age results and grain size data.

In section two, I reconstructed flow depth, slope, discharge, and flow competency of ancient fluvial systems from field measurements of grain size and cross-stratification set thickness and compare the reconstructions to measured detrital zircon size from the Undifferentiated Cutler Group fluvial system in the proximal – medial foredeep of the Paradox Basin. Our results show reasonable trends in measured grain size and reconstructed flow depth, slope, and channel discharge, and illustrate the ability of gravel- and sand-bedded channels to transport detrital zircon grains without sorting them by size or age. The same reconstruction methods applied to a comprehensive dataset of modern rivers around the world indicate sorting is more likely to selectively deposit detrital zircon grains larger than 0.2 mm in silty environments. Variability in the Cutler Group fluvial provenance data is not related to sorting.

In section three, the same fluvial transect is investigated by integrating paleohydraulic reconstruction methods with detrital zircon age and size data and paleocurrent direction analysis. 3-way multi-dimensional scaling is used to statistically compare detrital zircon age and size data and reconstructed basal shear stress for each sample and confirms that sorting did not affect provenance data. Instead these results are consistent with changes in provenance of sediment resulting from the mixing of subtly distinct sources within the Uncompahgre Uplift, suggesting at least three alluvial fans draining distinct catchments into the proximal basin. Changes in provenance between salt-walled minibasins likely reflect the impact of active salt uplift on NW-flowing axial

fluvial systems that routed mixtures of sediment from the proximal fans to the medial basin.

In section four, provenance data and paleohydraulic reconstruction of both fluvial and aeolian systems of the Cutler Group are used to investigate interactions between the ancient transport systems across the foredeep to forebulge of the Paradox Basin. Fluvial data from the second and third chapters is combined with detrital zircon age and size data from aeolian deposits and paleohydraulic reconstructions of wind shear velocity and settling velocity of quartz and zircon grains. Results from the foredeep to forebulge fluvial and aeolian deposits of the Cutler Group show that sorting did not affect provenance results. Furthermore, these results demonstrate that the degree of sediment recycling and predominance of fluvial or aeolian depositional systems varies between the forebulge and foredeep and is likely driven by aggradation rate in both systems. In the fluvial system, sediment recycling increases from the foredeep, where high sediment supply and subsidence rate likely caused high aggradation and less sediment recycling, to the forebulge, where low sediment supply and subsidence rate likely caused low aggradation and promoted sediment recycling. In the aeolian system, sediment recycling increases from the forebulge, where extrabasinal sediment supply was high and recycling was minimal, to the medial basin, where salt-cored anticline likely acted as barricades to the wind-blown sediment supply.

This study shows that effects of sorting on detrital zircon provenance data can be detected by combining paleohydraulic reconstruction and provenance methods, and reveals that sorting likely only occurs in silty fluvial systems where basal shear stress is

too low to move all detrital zircon in suspension. These results demonstrate the utility of the methods for detailed reconstruction of ancient fluvial and aeolian systems and the allogenic forces that shaped them and reveals the impact of allogenic forces on fluvial and aeolian interactions. Such detailed reconstructions are invaluable for petroleum and water exploration because they inform the composition of sediment transported from sediment source rocks and can indicate expected locations and trends of high quality reservoir rocks in a basin. At the planetary scale, reconstructions of ancient fluvial and aeolian interactions are used to interpret ancient planetary surface processes and environmental conditions that may have affected early life forms in our solar system. Detailed provenance studies can be utilized in a variety of geoscience studies, and the results of this study further refine the methodology needed to confidently interpret sediment provenance.

2. IDENTIFYING HYDRAULIC FRACTIONATION OF DETRITAL ZIRCON AGE POPULATIONS IN ANCIENT FLUVIAL DEPOSITS, PART I: METHODS FOR PALEOHYDRAULIC RECONSTRUCTION OF ANCIENT FLUVIAL CHANNELS

2.1. Introduction

Detrital zircon geochronology is an established tool to study the provenance, routing, and composition of sediment (Rainbird et al., 1992; Ireland et al., 1998; Gehrels et al., 1996; Stewart et al., 2001; Dickinson and Gehrels, 2003). Many provenance techniques, however, rely on the abundance and variability of dense mineral phases (e.g. zircon), and are transported differently than common framework mineral species with lower density (e.g. quartz, feldspar) in the flows that disperse sediment. The possible impact on detrital zircon geochronologic age groups by hydraulic sorting is an emerging consideration in provenance studies, and its impact in gravel and sand bedded rivers remains debated (Garzanti et al., 2008; Hietpas et al., 2011; Lawrence et al., 2011; Malusà et al., 2016; Ibañez-Mejia et al., 2018).

Detrital zircon fractionation by spatial hydrodynamic changes occurs based on grain size, morphology, and density. Across a fluvial system, downstream decreases in flow competency occur (e.g. gravel-sand transitions) because shallowing slopes reduce flow velocity and basal shear stress, which in turn limits the size or density of grains able to be moved by that the flow (Fedele and Paola, 2007; Slingerland, 1977; Parker, 1991a, 1991b; Ferguson, 2003, 2007; Slingerland, 1984; Jerolmack and Brzinski, 2010; Knott et al., 2012; Miller et al., 2014; Trampush et al., 2014; Lamb and Venditti, 2016). Based on

modern river systems, changes in the abundance of age modes in the detrital zircon age

distribution due to grainsize fractionation introduces complexities to sediment

provenance interpretations and ancient sedimentary deposits (Gehrels et al., 1996;

Sircombe et al., 2001; Stewart et al., 2001; Kock et al., 2007; Hietpas et al., 2011;

Lawrence et al., 2011; Yang et al., 2012; Bonich et al., 2017; Ibañez-Mejia et al., 2018).

Despite recognition that dense mineral fractions of sediment are sorted along

modern fluvial systems and affect provenance signals, the effects of hydraulic sorting on

detrital zircon (e.g. zircon density = 4.65 g/cm^3) provenance signals from ancient strata

remain unquantified. Recent advances in paleohydraulic reconstructions allow

estimation of ancient fluvial transport conditions, such as the shear stresses, needed to

mobilize particles and paleoflow depths from ancient fluvial stratification (e.g., Hayden

et al., 2019). These new approaches, in turn, give rise to the opportunity to assess the

role of ancient fluvial hydraulics in detrital zircon geochronologic provenance analysis.

Here, I review the field methods used to collect paleohydraulic data, review

paleohydraulic analysis methodology, and evaluate how sorting of dense minerals in

both ancient and modern fluvial systems would affect provenance signals. As a case

study to demonstrate the paleohydraulic methodology applied to detrital zircon analysis,

I reconstruct the ancient paleohydraulic conditions of the fluvial environment in the

Permian Cutler Group in the Paradox basin of Utah and Colorado and determine detrital

zircon size distributions. To evaluate the effectiveness of the methodology in

determining the role of hydraulic fractionation on dense mineral distributions, I apply the

method to modern river systems to compare the reconstructed Permian conditions to modern fluvial environments.

2.2. Background

2.2.1. Linking Paleohydraulic Reconstruction and Provenance Data

Paleohydraulic analysis is emerging as a quantitative methodology to estimate the conditions of ancient fluvial and aeolian conditions, which has potential to advance provenance studies. Established paleohydraulic methods, based on theoretical and empirical relationships between modern rivers and both gravel and sand fluvial deposits, are used to reconstruct paleochannel flow depth, width, slope, velocity, and discharge based on observations from outcrops and thin sections (Ferguson, 2007; Engelund and Hansen, 1967; Paola and Mohrig, 1996; Leclair and Bridge, 2001; Mohrig et al., 2000; Bridge, 2009; Paola and Borgman, 1991; Wilkerson and Parker, 2011; Hajek et al., 2012; Lynds et al., 2014; Trampush et al., 2014; Bradley and Venditti, 2017; Hayden et al., 2019). These methods can relate slope and basal shear stress (discussed in detail below), which govern sediment transport in fluvial environments (Parker et al., 2007; Williams et al., 2009; Wilkerson and Parker, 2011; Trampush et al., 2014; Hayden et al., 2019). The principal utility of these methods has been to determine hydraulic conditions of ancient environments, but these same methods hold promise to examine spatial sorting of heavy minerals such as detrital zircons along a basin transect that could provide a more refined understanding of spatial variations in, for example, abundances of zircons in ancient environments.

Settling equivalency methods (Garzanti et al., 2009; Malusà et al., 2016), which

determines the zircon grain sizes transported with bulk sediment (quartz) grain size, is an

established method that determines which zircon size fractions would be transported at

positions along the transect, and the mode of sediment transport. However, settling

equivalency method cannot extract the level of detail about the fluvial system that the

paleohydraulic analysis. In conjunction, these two approaches provide a new quantitative

framework for understanding the distribution of zircons for detrital zircon

geochronology.

Detrital zircon geochronologic results from fluvial systems have resulted in both

similar detrital zircon age distributions in the upper and distal reaches (Sircombe et al.,

2001; Cawood et al., 2003; Link et al., 2005; Wissink et al., 2016; Wissink and Hoke,

2016), and spatially dissimilar detrital zircon grain size and age groups, which may be

symptomatic of hydraulic sorting of dense mineral assemblages (Gehrels et al., 1996;

Sircombe et al., 2001; Stewart et al., 2001; Wu and Zheng, 2004; Kock et al., 2007;

Lawrence et al., 2011; Hietpas et al., 2011; Yang et al., 2012; Malusà et al., 2016;

Bonich et al., 2017; Ibañez-Mejia et al., 2018). Combining the paleohydraulic results

with new and existing detrital zircon U-Pb geochronology, measured zircon grain size,

and statistical metrics that facilitate quantitative assessment of dissimilarity among

geochronology datasets (Vermeesch and Garzanti, 2015; Saylor and Sundell, 2016;

Vermeesch et al., 2016; Saylor et al., 2018; Sharman et al., 2018; Saylor et al., 2019),

provides a framework to assess whether spatial shifts in detrital zircon age spectra. The

goal of this review is to explicitly link state of the art methods from sedimentology,

fluvial hydraulics, and sediment provenance and connect these fields to demonstrate an opportunity to advance understanding of how autogenic and allogenic processes impact sediment dispersal, basin fill composition, and the preservation of geologic history. I describe the details of the paleohydraulic analysis and evaluate it utility in a case study across the Paradox Basin.

2.2.2. Grain Size Measurement For Paleohydraulic Reconstruction

Paleoflow conditions can be determined from the measurements of median grain size of the sediment load and measurements of cross-stratification height. Recent compilations of modern river and flume measurements of grain size, cross-stratification set thickness, flow depth, slope, and discharge constrain empirical relationships with physical parameters that control sediment transport (e.g. particle Reynolds number, Shields number, and shear stress) (Paola and Borgman, 1991; Leclair and Bridge, 2001; Wilkerson and Parker, 2011; Trampush et al., 2014; Bradley and Venditti, 2017; Hayden et al., 2019). These empirical relationships do not rely on a full grain size distribution. Rather, an accurate measurement of median grain size and cross-stratification thickness is sufficient.

Accurate grain size characterization is a critical first component to the paleohydraulic method. The median grain size (D_{50}) of a fluvial deposit accounts for movement of the total sediment load, which on Earth is typically composed of quartz and feldspar grains. Herein the total sediment load is referred to as the bulk sediment (Williams et al., 2009; Hayden et al., 2019). Despite recognizing the need for the D_{50} grain size, accurately representing the entire grain size distribution in deposits of

conglomerates with sand or finer matrix presents challenges. For example, surface sampling, or measuring gravel clasts in outcrop, underrepresents the fine fraction, whereas thin sections from a hand samples, or visual inspection using a grain size card at the outcrop, may not capture the coarsest grains (Wolman, 1954; Williams et al., 2009).

In the Paradox Basin example, at sites with mixed gravel and sand-sized grains, median grain size of each channel deposit was calculated using a weighted average of the median grain sizes of the coarse and fine fractions (Eq. 1). The weighted average is accurate if a lognormal grain size distribution is assumed (Lamb and Venditti, 2016). The approximate proportions of the gravel and fine fractions were determined by labeling 100 random points overlain on an image of a representative channel deposit as gravel or fines using ImageJ (FIJI) software (Fig. 1A) (Schindelin et al., 2012). The gravel and fine fraction grain sizes were weighted by their respective proportions in the image (Eq. 1), providing the median grain size that reflects the volume of gravel and fine sediment present at each location.

$$D_{50} = \frac{D_{50\,coarse}(\%\,gravel) + D_{50\,fine}(\%\,fines)}{100} \qquad (1)$$

The Wolman pebble count method, thin section grid counting method, and grain card estimates were used to for estimating the median grain size of the entire distribution present in fluvial sandstone. The Wolman pebble count method was used in outcrop to measure the intermediate axis of gravel clasts ($D_{50\,coarse}$) (Fig. 1) (Wolman, 1954; Williams et al., 2009). Grid counting method was used to measure median grain size in thin section or micrographs of freshly cut surfaces of hand samples ($D_{50\,fine}$) (Fig. 1) (Wohl et al., 1996). Equivalent spherical diameter (ESD), e.g. nominal diameter ($D_n =$

(D_{long} * $D_{intermediate}$ * D_{short})$^{1/3}$), was used to represent the size of the fine fraction because in thin section, the visible intermediate axis of a grain underestimates the actual intermediate axis (Komar and Reimers, 1978). ESD is particularly useful to compare the grain size of detrital zircon, which may have a range of morphologies from tetragonal prism to oblate spheroid to spherical, with the bulk sediment grain size (Komar and Reimers, 1978; Garzanti et al., 2008; Lawrence et al., 2011). The grain size card method ($D_{50 \text{ sand}}$) was used where hand samples were not collected and thin sections were not made (Wentworth, 1922). Once relevant D_{50} values were determined, I used Eq. 1 to determine the median grain size.
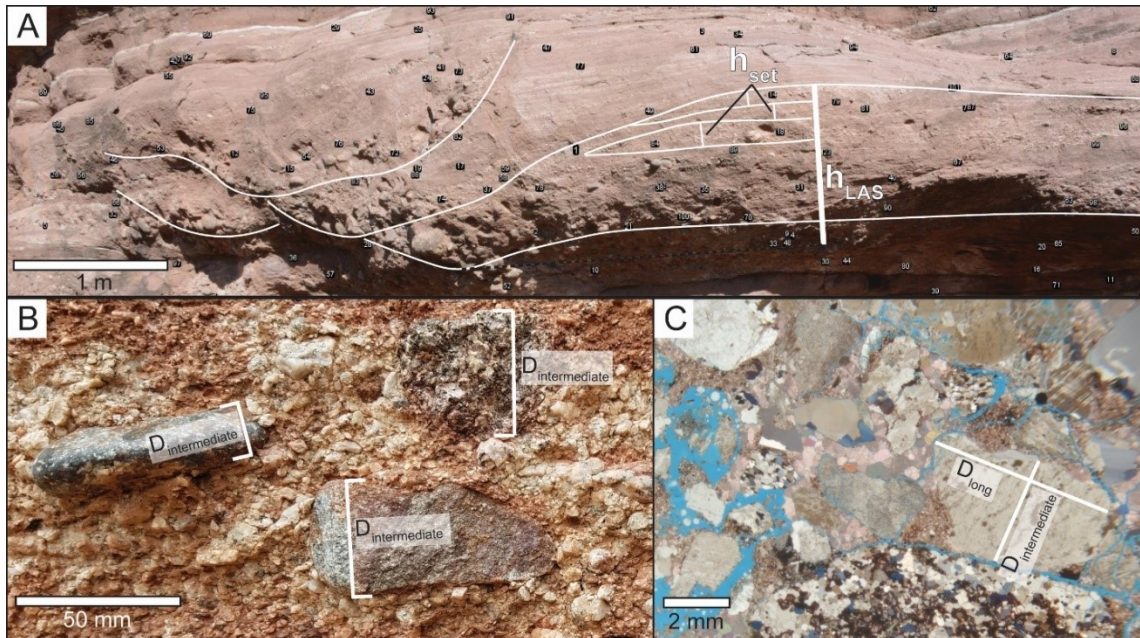
Figure 1: Images used to measure median grain size (D50) of a fluvial channel deposit at Gateway, CO. A) Fluvial channel deposits with coarser gravel in the base of the channel and dune scours. Random points are generated on the image using ImageJ software, and are used to point count the proportion of gravel to fines in the outcrop. The LAS (h_{LAS}) with superimposed dune cross-stratification (h_{set}) is a rare example that permits distinction between the two types of cross-strata. B) A close-up photo of gravel clasts in the outcrop is used to measure the intermediate axis of clasts larger than 2 mm using the Wolman pebble count method ($D_{50coarse}$). C) A thin section micrograph of the same deposit is used to measure the size of small grains (D_{50fine}) that are under-represented by pebble counts. In this example, the fines are still gravel size, but in many channel deposits are sand size. The proportionately weighted grain size (D_{50}) is calculated using Eq. 1.

15

Grainsize measurements from detrital zircons are needed to assess the hydraulics and settling equivalency of zircons. Detrital zircon grains were measured from zircon separates mounted in epoxy pucks after analysis in the LA-ICP-MS. The long and intermediate axis of each grain was measured, and the median equivalent spherical diameter (ESD) grain size of detrital zircon age groups was compared to the bulk sediment grain size (Komar and Reimers, 1978; Garzanti et al., 2008; Lawrence et al., 2011). Euhedral zircon grains have approximately equal intermediate and short axes, permitting the intermediate axis to be substituted for the short axis ($D_n = (D_{long}$ $D_{intermediate} D_{intermediate})^{1/3}$) (Poldervaart, 1955, 1956; Markwitz et al., 2017). Paleohydraulic transport conditions were calculated using these grainsize measurements from outcrops, thin sections, and zircon mineral separates.

2.2.3. Transport Calculations

2.2.3.1. Paleoflow Depth

Measurements of lateral accretion surfaces (LAS), and dune cross-stratification thickness provide the other key data needed to reconstruct and identify spatial changes in ancient transport conditions that could have sorted detrital zircon. LAS are formed by the migration of bar forms in fluvial channels (Miall, 1996; Mohrig et al., 2000). Distinctive sedimentologic features of LAS include sigmoidal low-angle bounding surfaces that contain low-angle cross-bed sets of conglomerate and sandstone (Miall, 1996; Mohrig et al., 2000) (Fig. 1A, 2B). The topsets of LAS rollover have a convex-up shape, and are typically fine-grained sandstone and contain ripple cross-stratification (Miall, 1996; Mohrig et al., 2000). Rarely observed, but required for confidently

differentiating LAS from dune cross-strata, are individual beds of the low-angle cross-bed sets contain laminae or more steeply dipping cross-bed sets interpreted as deposits from fluvial dune and ripple migration across the bar form (Miall, 1996) (Fig. 1A, 2B).

The particular utility of LAS for paleohydraulic reconstruction arises because bars grow in height up to the free surface of a river, and thus the height of untruncated LAS deposits (h_{LAS}) represents mean flow depth (d) (Eq. 2) (Mohrig et al., 2000).

$$d = h_{LAS} \qquad (2)$$

Truncated LAS represent 70% of the mean flow depth, on average (Paola and Borgman, 1991). Individual h_{LAS} were measured from the base of the bottom set to the top of the topset perpendicular to regional dip. Although LAS height is considered the most reliable estimation of flow depth (Mohrig et al., 2000; Hayden et al., 2019), finding and identifying complete LAS in the Permian Cutler Group in the field was difficult.
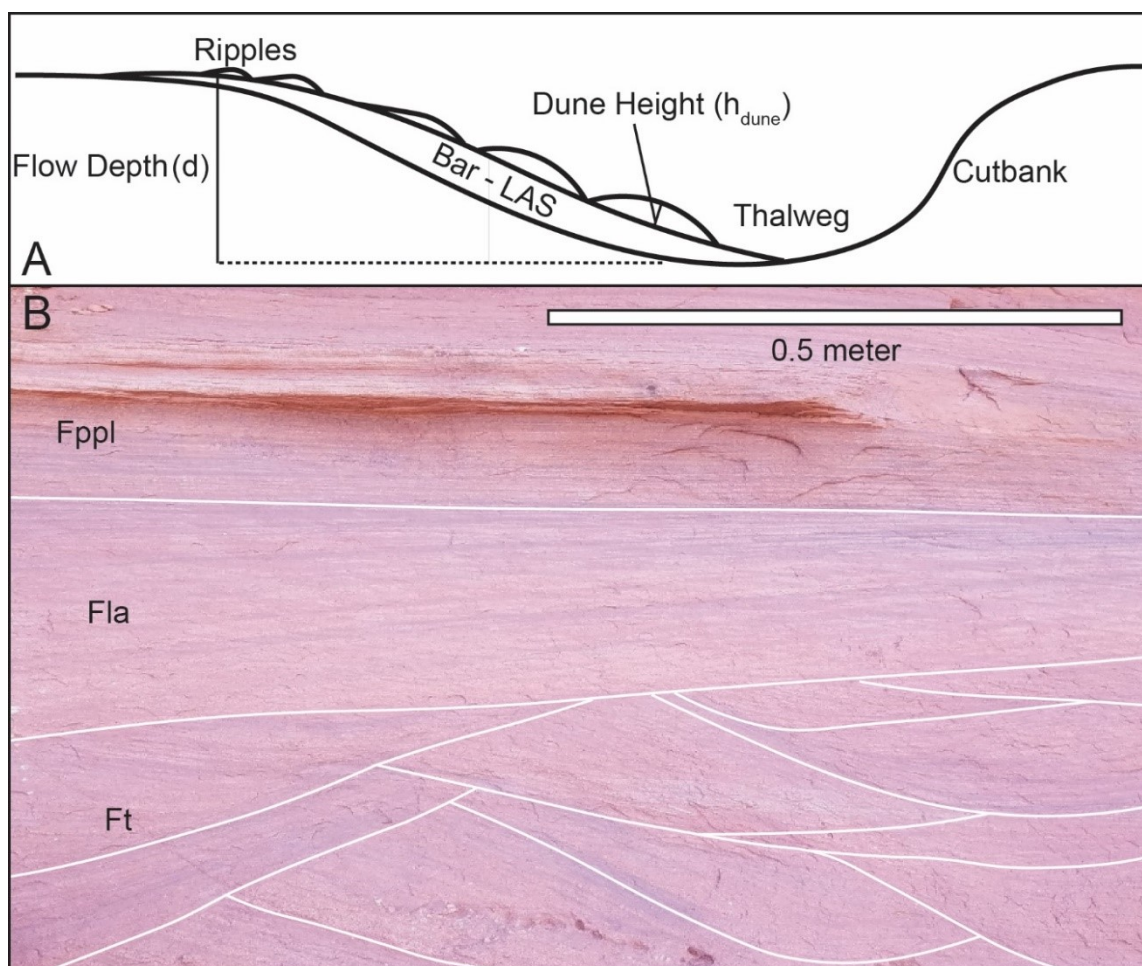
Figure 2: Schematic of fluvial bar facies and representative facies from the Permian Cutler Group. A) A schematic cross-section of a fluvial channel illustrates the thalweg, a laterally migrating bar with a lateral accretion surface (LAS), and dunes and ripples superimposed on the LAS. B) An example of planar parallel laminated (F_{ppl}) and low angle cross-stratified (F_{la}) sandstone from the top of a bar deposit overlying dune trough cross-stratified (F_t) sandstone from the base of a different bar. Although the full cross-section of the LAS is not observed, the bar is assumed to have accreted laterally with no vertical accretion and the minimum height of LAS in this example is measured from the base of the dune cross-strata to the top of the low angle cross-stratified sandstone.

Paleoflow depth (d) was also estimated from the thickness of dune-scale cross-stratification sets (t_{set}) (Eq. 3 and 4) (Fig. 3) (Paola and Borgman, 1991; Leclair and Bridge, 2001; Mohrig et al., 2000; Bridge, 2009; Hajek et al., 2012):

$$h_{dune} = \alpha t_{set} \qquad (3)$$

$$d = \gamma h_{dune} \qquad (4)$$

The thicknesses of dune cross-stratification sets were measured perpendicular to the basal and the top bounding surfaces of each set, with respect to regional dip (Fig. 2B, 3). A linear relationship exists between the original dune height (h_{dune}) and dune cross-stratification set thickness (t_{set}) scaled by a preservation potential constant (α) of the original dune height (Paola and Borgman, 1991; Leclair and Bridge, 2001). The lower, average, and upper values for α were used (the 5th percentile [2.2], the average [2.9], and 95th percentile [3.6]) (Eq. 3) (Paola and Borgman, 1991; Leclair and Bridge, 2001; Hayden et al., 2019). A linear relationship also exists between dune height (h_{dune}) and flow depth scaled by the empirical constant (γ). In rivers less than 2.5 meters deep, the lower, average, and upper values for γ were used (the 10th percentile [2.1], the average [3.5], and 90th percentile [9.9]) (Eq. 4) (Bradley and Venditti, 2017). In rivers more than 2.5 m deep, values of γ are larger and have a greater range (the 10th percentile [3.9], the average [7.7], and 90th percentile [26.3]) (Bradley and Venditti, 2017). The lower and upper values for α and γ represent the range of values reported in the studies mentioned above and yield minimum and maximum values of flow depth from t_{set}, respectively, which account for uncertainty in the reconstructions that propagates through the remainder of the calculations (Paola and Borgman, 1991; Leclair and Bridge, 2001;

Bradley and Venditti, 2017; Hayden et al., 2019). Not all sites yielded clearly

identifiable LAS or dune cross-stratification sets, and either of these measurements were

used where possible.

Figure 3: Trough cross-stratified sandstone and granule conglomerate viewed perpendicular to paleoflow direction (right to left) in the Undifferentiated Cutler Formation at Kane Springs (see Fig.4). Dune cross-stratification set thickness measurements were collected perpendicular to the bedding surface following a relatively straight line up the outcrop (blue lines).

2.2.3.2. Paleoflow Width

Paleoflow width was based on the Trampush et al. (2014) survey of modern

rivers that shows typical flow depths are 0.2–4.6 meters, and bankfull channel widths

(w_{bf}) are 3.9–35.2 meters. For ancient settings, w_{bf} was estimated from the mean ratio of

channel width and flow depth of modern rivers (Trampush et al., 2014; Hayden et al.,

2019), where:

$$w/d = 18 \qquad (5)$$

The Trampush et al. (2014) synthesis of modern rivers provides an ideal comparison against ancient rivers because grain size (D_{50}), flow depth (d), channel width (w), cross-sectional area (A), slope (S), and discharge (Q) data from gravel- and sand-bedded rivers were measured and compiled around the world. The maximum value from box and whisker plots (Q3 + 1.5*IQR) and the absolute minimum value for each parameter measured in modern rivers were used as typical values of modern rivers.

2.2.3.3. Paleoslope

Paleoslope was calculated using grain size and flow depth to find Shields stress. Shields stress (i.e. Shields number) is the ratio of forces of the flow that attempt to move the particle (lift and drag) to forces of the particle that resist movement (gravity and friction) (Middleton and Southard, 1984). Shields stress is a function of fluid and particle density, grain size, flow depth, and slope of a fluvial channel. Because no direct constraints on paleochannel slopes exist, an empirical relationship between particle bankfull Shields stress (τ^*) to particle Reynolds number (Re_p) was used to find Shields stress (Eq. 6, 7) (Wilkerson and Parker, 2011; Trampush et al., 2014; Hayden et al., 2019). Particle Reynold's number is a measure of laminar or turbulent flow around a particle in a fluid.

$$Re_p = (RgD_{50})^{1/2} \left(\frac{D_{50}}{\nu}\right) \qquad (6)$$

$$\tau^* = 17 \, Re_p^{-1/2} \qquad (7)$$

where R = $(\rho_s - \rho_f)/ \rho_f$, ρ_s is sediment density, ρ_f is fluid density, g is gravity, and ν (10^{-6} m^2/s) is kinematic viscosity of water. With a calculated τ^*, nondimensional slope (S)

(0.0001–0.015 in modern rivers) was quantified by relating τ^* to R, D_{50}, d, and S (Eq. 8) (Paola and Mohrig, 1996; Wilkerson and Parker, 2011; Trampush et al., 2014; Lynds et al., 2014):

$$\tau^* = \frac{dS}{RD_{50}} \qquad (8)$$

2.2.3.4. Paleoflow Velocity

Paleoflow velocity (U, m/s), was estimated by relating the forces that pull the flow downslope (i.e. gravity and fluid drag) to those that resist and decrease the flow velocity. Flow velocities in modern rivers range from 0.2–2.4 m/s (Trampush et al., 2014). Methods of calculating U are different for gravel-bedded streams and sand-bedded streams. Both apply skin friction, the drag created by viscous shear stress at low Reynolds numbers (e.g. sandy beds), and a grain roughness length scale, which corresponds to turbulent form drag created by the largest obstacles on the sediment bed at high Reynolds numbers (e.g. gravelly beds and bedforms), to account for the total drag force imparted by the sediment bed and bedforms that decreases flow velocity (Ferguson, 2007; Hayden et al., 2019). Flow velocities were calculated using approaches optimized for sand-bedded (Hayden et al., 2019) and for gravel-bedded channels (Ferguson, 2007), to assess which method yields values that are consistent with velocities in modern channels.

Flow velocity is related to the skin friction component of Shields stress (τ_s^*) and the drag of viscous forces caused by the flow of water over a sandy sediment bed (Eq. 9, 10) (Engelund and Hansen, 1967; Hayden et al., 2019):

$$U = \left(\frac{1}{\kappa}\right) \ln \left[11 \left(\frac{RD_{50}}{Sk_s}\right) \tau_s^*\right](RgD_{50}\tau_s^*)^{1/2} \qquad (9)$$

$$\tau_s^* = 0.06 + 0.4\tau^{*2} \qquad (10)$$

where $\kappa = 0.4$ is von Karman's constant and k_s is the grain roughness length scale. Logarithmic expressions describe flow velocity profiles for a wider range of channel depths and grain sizes, as long as roughness height (k_s), which accounts for form drag flow resistance, is inflated beyond the actual grain size of the bed, hence $k_s = 2.5(D_{50})$ (Ferguson, 2007).

The Variable Power Equation (VPE) method attributes flow resistance to skin friction in deep flows, and form drag and turbulent wakes around large objects in shallow flows (Ferguson, 2007). Flow velocity is related to the Darcy-Weisbach friction factor (f) (Eq. 11, 12):

$$\left(\frac{8}{f}\right)^{1/2} = \frac{U}{u_*} = \frac{a_1 a_2 \frac{d}{D}}{(a_1^2 a_2^2 \frac{d}{D}^{5/3})^{1/2}} \qquad (11)$$

$$u_* = (gdS)^{1/2} \qquad (12)$$

where a_1 and a_2 are empirical constants set to 6.5 and 2.5, respectively, and D is grain size. Although D_{50}, D_{84}, D_{90} have been used successfully, D_{50} was used to provide the upper limit on flow velocity because it represents the lower limit on flow resistance (Ferguson, 2007).

2.2.3.5. Paleo Discharge

Finally, discharge (Q_{bf}), typically 1–74 m^3/s (Trampush et al., 2014), was estimated by multiplying the cross-sectional area of the channel by flow velocity (Eq. 13):

$$Q = Udw \qquad (13)$$

The above methods and sequence of calculations describe the sediment transport conditions in ancient fluvial channels, and are used to identify locations along a source-to-sink transect where the competence of the flow to move grains might sufficiently decrease such that sorting could fractionate dense minerals from the bulk sediment. Despite this being a state-of-the-art approach, several limitations and uncertainties exist.

2.2.4. Limitations And Sources Of Uncertainties

Limitations and uncertainty arise from estimations of flow depth and calculations of flow resistance, which most significantly affect values of flow velocity and discharge. Determining flow depth from dune cross-stratification has high uncertainty because the relationship of dune height to flow depth is not the same in all rivers. Dune heights vary in rivers >2.5 m deep and <2.5 m deep such that dunes in shallow rivers are taller than 1/6 of flow depth, and deep rivers have dune shorter than 1/6 of flow depth (Bradley and Venditti, 2017). Further, flow depth and thus dune height scaling does not remain constant when flow conditions change (Leclair and Bridge, 2001; Nittrouer et al., 2011; Martin and Jerolmack, 2013). Constraining estimates of flow depth with measurements of LAS minimizes uncertainty in flow depth derived from measurements of dune set thickness.

Uncertainty in calculation of flow resistance stems from difficulty in estimating spatial variation of both form drag and skin friction from the range of objects that may apply resistance to a flow, such as bed forms, bars, woody debris, boulders, channel curvature, and changes in resistance with flow depth, slope, and median grain size (Trampush et al., 2014). If the magnitude of uncertainty is large enough, any significant changes in flow competence could be masked across the transect, and paleohydraulic reconstruction methods would be incapable of identifying positions where the effects of hydraulic sorting could impact dense mineral provenance indicators. Uncertainty increases because it is propagated through the exponential calculations for flow velocity. Flow depth, Shields stress, and slope (Eq. 2-8), which do not include flow velocity, have less error and are most sensitive to spatial changes in transport conditions. Thus, these are considered more reliable metrics to consider for provenance-related paleohydraulic problems.

2.2.5. Hydraulic-equivalence Calculation

The paleohydraulic reconstruction calculations above can be used to identify sites along a transect where flow competency decreases and sorting could have occurred. However, reconstructions of flow depth, slope, velocity, and discharge do not determine whether competency decreases sufficiently to selectively sort out dense minerals of a known size. To quantify flow competency, calculations of hydraulic parameters, such as settling velocity and basal shear stress that control the mobilization of sediment, are required (Cheng, 1997; Parker et al., 2007; Garzanti et al., 2008; Wilkerson and Parker, 2011). Settling or hydraulic equivalence approach calculates the size of zircon grains

transported with framework sediment, primarily composed of quartz and feldspar grains (Eq. 14-16) (Slingerland, 1984; Garzanti et al., 2008). The settling of sand in water is controlled by fluid viscosity and turbulence and is best predicted by a combination of Stokes' Law (viscous dominated settling) and Impact Law (inertia dominated settling) in the form of the empirically derived Cheng's formula (Cheng, 1997; Garzanti et al., 2008; Vermeesch et al., 2016). The size difference between sand-size sediment of different densities deposited by water was calculated as:

$$w = \left(\frac{\eta}{D_{50}}\right)\left[\sqrt{25 + 1.2\left(\frac{gRD_{50}^3}{\eta^3}\right)^{\frac{2}{3}}} - 5\right]^{\frac{3}{2}} \tag{14}$$

$$\Xi_{m,ref} = \left(\frac{w}{\eta}\right) + \sqrt{\left(\frac{w}{\eta}\right)^2 + 48\left(\frac{gR}{\eta^2}\right)^{\frac{2}{3}}} \tag{15}$$

$$SS_m = log_2\left(\frac{R_m}{R_{ref}}\right) - \left(\frac{3}{2}\right)log_2\left(\frac{\Xi_m}{\Xi_{ref}}\right) \tag{16}$$

where subscripts ref and m refer to the reference mineral and the mineral in question, respectively. SS_m is the size shift of the mineral in question, R is the submerged density of the mineral (quartz: 1.65 g/cm^3, zircon: 3.65 g/cm^3), D_{50} is the median grain size of the bulk sediment (cm), w is settling velocity (cm/s), η is fluid viscosity (0.01 g/cm s), and is g gravity (981 cm/s^2) (Garzanti et al., 2008; Vermeesch et al., 2016). D_{50} is input in centimeters and SS_m is output in phi units. w is only calculated once, using the D_{50} of the bulk sediment and density of quartz. Ξ is calculated for both the bulk sediment (Ξ_{ref}) and the dense mineral in question (Ξ_m), where w is the settling velocity of the bulk

sediment and only density is changed to the appropriate value for Ξ_m. The calculated

hydraulic-equivalent dense mineral grain size that would be transported with the bulk

sediment is equal to the median grain size of the bulk sediment sample in phi units plus

the calculated size shift in phi units of the mineral in question ($D_{50} + SS_m$) (Fig. 4). The

settling equivalency method predicts that any dense minerals larger than the hydraulic

equivalent grain size would not be transported further downstream.
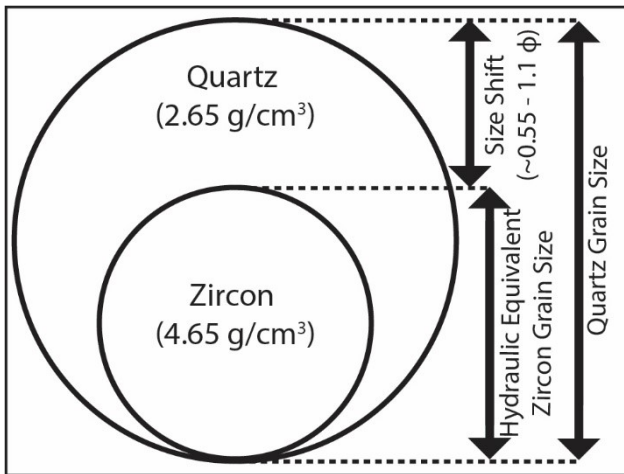
Figure 4: A schematic cross section of quartz and zircon grains that would be transported together under equal hydraulic conditions according to settling equivalency models of grains with different densities (Modified from Malusà et al., 2016b). The size of a dense mineral grain that would be transported with the bulk quartz and feldspar sediment in a sample is called the hydraulic-equivalent grain size, and the difference between the bulk sediment grain size and the dense mineral grain size is referred to as the size shift (Garzanti et al., 2008; Malusà et al., 2016).

2.2.6. Modified Shields Diagram To Assess Transport Mode

Settling equivalency models assume that particles with similar settling velocities

are transported together, but grains with different settling velocities are known to be

transported together in the same mode of transport (Ghosh et al., 1986; Hajek et al., 2010). The mode of sediment transport is determined using a modified Shields diagram (i.e. Trampush et al., 2014). For every grain size and density, the Shields curve defines the minimum Shields stress needed to move that grain. Likewise, the Rouse curves are the ratio of settling velocity of a particle to shear velocity of the flow (p) and are related to the Shields stress required to move a particle in bed load (points above the shields curve and below p=2.5), mixed load (points between p=2.5 and 0.8), or suspended load (points above p=0.8) (Trampush et al., 2014).

To examine the size of zircon grains that are transported in the same transport mode as the bulk sediment bulk sediment and detrital zircon grain sizes were plotted on a modified Shield's diagram. For bulk sediment, values of Shields stress and particle Reynolds number were calculated as above (Eq. 6, 7). The particle Reynolds number for detrital zircon was calculated using Eq. 6 and the density of zircon (4.65 g/cm^3). The basal shear stress of the flow (τ_b) was calculated by substituting the Shields stress (τ_*) of the bulk sediment (Eq. 17) (Wilkerson and Parker, 2011):

$$\tau_* = \frac{\tau_b}{\rho_f R g D_{50}} \qquad (17)$$

Shields stress for detrital zircon grains was calculated using τ_b calculated from the bulk sediment and the density and grain size of detrital zircon grains. With particle Reynolds number and Shields stress for both the bulk sediment and detrital zircon grains calculated, those values were plotted on the on the modified Shields diagram (Fig. 5).

To illustrate detrital zircon fractionation by different transport modes between bulk sediment and the zircons, three hypothetical D_{50} grain sizes ranging from gravel (10

28

mm) to sand (0.5 mm) to silt (0.062 mm) that represent bulk sediment, and include

detrital zircons of 0.05, 0.2, 0.31, and 0.5 mm, are plotted on the Shield's diagram with

Rouse curves using Re_p and τ_* calculated using equations 6, 7, and 17 (Fig. 5). Silt bulk

sediment plots in the suspended load with 0.05 mm detrital zircon, but zircon grainsizes

larger than 0.2 mm would be transported in the mixed load. In the silt-bedded scenario,

0.2 mm and larger detrital zircons would be preferentially deposited and fractionated

from smaller detrital zircon grains.
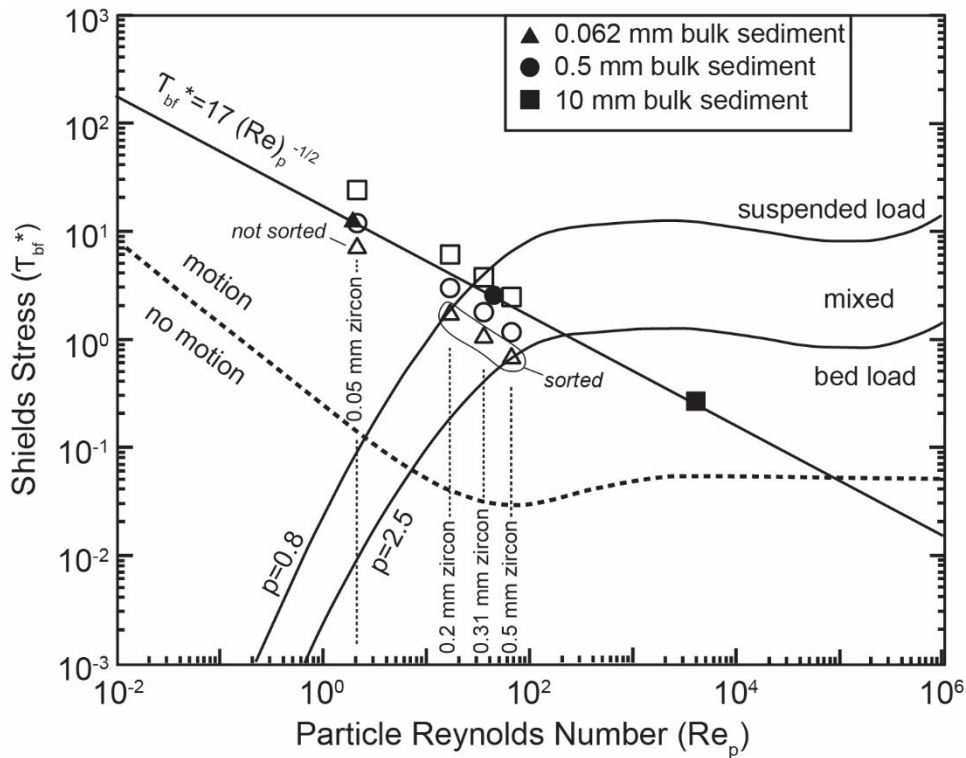
Figure 5: Hypothetical bulk sediment (solid shapes) and detrital zircon with grain sizes of 0.05, 0.2, 0.31, and 0.5 mm (hollow shapes) that would be transported with the bulk sediment. In the scenario of a 0.062 mm bulk sediment, 0.05 mm zircon would not be sorted because would be transported in suspension with the bulk sediment, but zircon larger than 0.2 mm would be sorted because it would be transported in the mixed load.

Despite advances made in hydraulic modeling, predicting the transport of grains outside of the median grain size of the bulk sediment is not well constrained. Hydraulic equivalence and Rouse curve transport models define distinct boundaries in grain sizes that are transported in the same mode, but field studies show the boundaries are more diffuse (Ghosh et al., 1986; Singer, 2008; Hajek et al., 2010; Wilkerson and Parker, 2011; Trampush et al., 2014; Pfeiffer et al., 2017). The settling equivalency and Rouse curve methods provide a means to assess detrital zircon sorting across a wide range of ancient fluvial systems, but the diffuse boundaries observed in field studies between grain sizes that are transported together are more realistic than the sharp cutoffs in flow competency.

The above sequence of methods is used to investigate possible sorting during deposition of the Permian Undifferentiated Cutler Formation fluvial system in the Paradox Basin of Utah and Colorado. The Undifferentiated Cutler Formation provides an ideal test for sorting in gravel- and sand-bedded channels because it is well exposed from proximal to distal reaches and the sediment was largely sourced from the Uncompahgre Uplift, which has distinct detrital zircon age groups.

2.3. Background – Paradox Basin

The Pennsylvanian–Permian Paradox Basin is a broken foreland basin that subsided adjacent to the Uncompahgre Uplift (UU) as a part of the Late Paleozoic Ancestral Rocky Mountains (Fig. 6) (Barbeau, 2003). The Permian Undifferentiated Cutler Formation fluvial system transported sediment from the UU into the Paradox Basin, yielding S-, SW- and NW-directed paleoflows (Campbell, 1980; Mack and

Rasmussen, 1984; Lawton et al., 2015; Venus et al., 2015) and detrital zircon U-Pb age results with three age modes centered at 520 Ma, 1440 Ma and 1721 Ma, consistent with derivation from the UU (Lawton et al., 2015; Leary et al., 2020). These ages reflect basement rocks in the UU from 503 – 583 Ma alkali intrusions, the ca. 1300–1500 Ma Granite–Rhyolite province, the ca. 1400–1490 Ma Picuris orogeny, and the ca. 1600–1860 Ma Yavapai–Mazatzal orogeny (Fig. 6) (Mose and Bickford, 1969; Bickford and Cudzilo, 1975; Olson et al., 1977; Livaccari et al., 2001; Jessup et al., 2006; Schoene and Bowring, 2006; Whitmeyer and Karlstrom, 2007; Jones et al., 2009; Daniel et al., 2013; Aronoff et al., 2016). The Undifferentiated Cutler Formation is exposed at the surface on the flank of the UU near Gateway, CO in Unaweep Canyon (Dubiel et al., 2009; Rasmussen, 2009; Soreghan et al., 2009). In proximal–medial regions of the basin, ~20–60 km from the uplift, the Undifferentiated Cutler Formation is exposed on the flanks of salt walls formed during the movement of Pennsylvanian Paradox Formation salt (Dubiel et al., 2009; Rasmussen, 2009; Trudgill, 2011). The fluvial strata of the Undifferentiated Cutler Formation become progressively more fine-grained to the southwest and interfinger with the time-correlative fluvial and aeolian systems of the Cedar Mesa and Organ Rock Formations (Condon, 1997; Dubiel et al., 2009; Lawton et al., 2015).
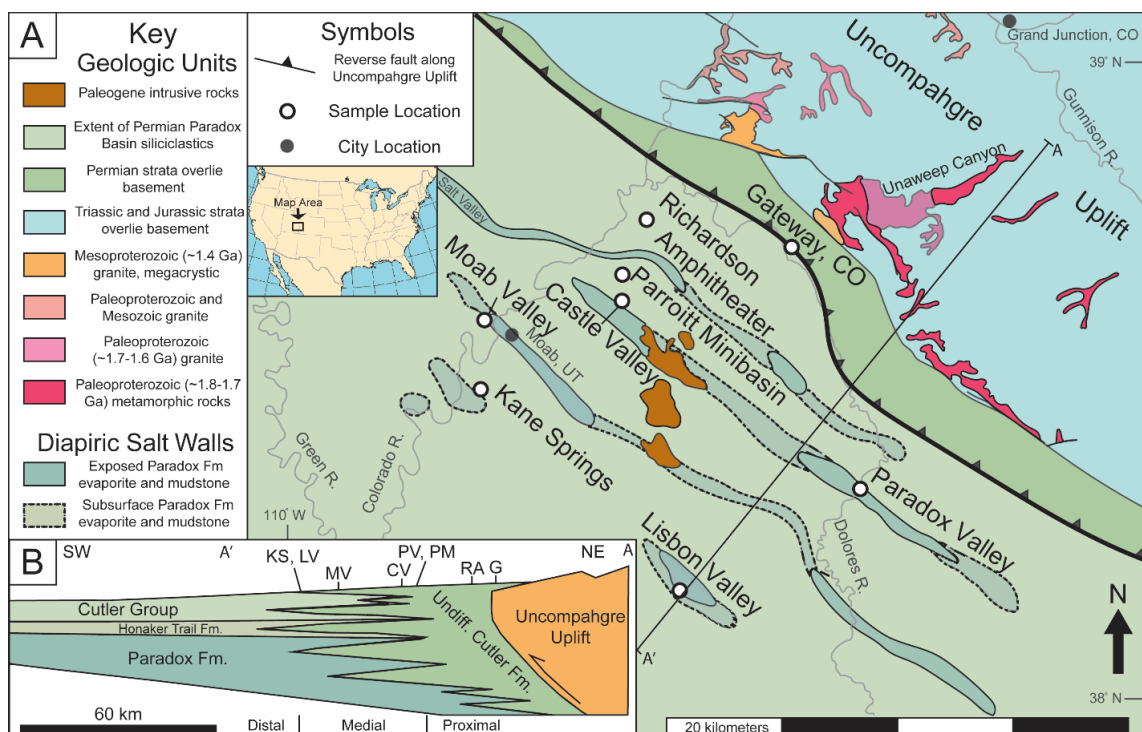
Figure 6: Sample locations are shown on a map and cross-section. A) Map of the Permian Paradox Basin with superimposed Paleogene intrusive rocks, modern rivers, salt walls formed from movement of Paradox Fm. evaporites (modified from Lawton et al., 2015). The Uncompahgre Uplift was uplifted along a crustal scale thrust fault, and the Paradox Basin subsided as a foreland basin. Sample locations are marked by white circles and cities by black circles. Latitude and longitude markers refer to the map in A, not the cross-section. B) Schematic cross section of the Paradox foreland basin follows line A – A' (modified from Barbeau, 2003). This study area focusses on the proximal – medial Undifferentiated Cutler Formation deposited in the foredeep region of the basin. Sample locations: G – Gateway, CO; PV – Paradox Valley; PM – Parroitt Minibasin; RA – Richardson Amphitheater; CV – Castle Valley; MV – Moab Valley; LV – Lisbon Valley; KS – Kane Springs.

2.4. Methods

2.4.1. Sampling

To assess the role of size-selective sorting of dense minerals on provenance results, field measurements, sample collection and analysis, and paleohydraulic

32

reconstructions were performed at sites situated along a NE–SW transect across the Paradox Basin from Gateway, CO to Lisbon Valley, UT (Fig. 6). This transect captured grain size variation in fluvial facies from pebble to fine sand. Eight stratigraphic sections (25 m to 300 m thick) were measured to assess facies variations. Nine samples were collected and analyzed for both thin-section grain size characterization and detrital zircon U-Pb geochronology within the Undifferentiated Cutler Formation (Fig. 6). Sample sites were located at Gateway, CO, Paradox Valley, UT, and Richardson Amphitheater in Undifferentiated Cutler Formation fluvial deposits proximal to the UU ($n_{outcrop}$=3, $n_{samples}$=4) and at Castle Valley, Moab Valley, Kane Springs, and Lisbon Valley in Undifferentiated Cutler Formation fluvial deposits in the medial salt deformed basin ($n_{outcrop}$=4, $n_{samples}$=5). These samples were strategically collected from outcrops proximal to the sediment source, along the flanks of salt-cored anticlines, and in the center of minibasins to test a range of possible topographic gradients and paleoflow conditions. All samples were collected from dune cross-stratified, low-angle cross-stratified, or planar parallel laminated pebbly sandstone or sandstone contained within channel forms observed in the outcrops.

2.5. Results

2.5.1. Transport Calculation Results

From field measurements, paleoflow velocity and discharge were calculated using methods for sand-bedded rivers (Hayden et al., 2019), and gravel-bedded rivers (Variable Power Equation [VPE]) (Ferguson, 2007). Reported here are: 1) ranges of measured modern grain size, flow depth, slope, flow velocity, and flow discharge from

Trampush et al., (2014); 2) values for reconstructed slope, Shields stress, skin friction

component of Shields stress, flow velocity, and flow discharge that were calculated

using paleohydraulic methods from modern measurements of grain size and flow depth

in modern rivers from Trampush et al., (2014) ; and 3) paleohydraulic reconstructions of

flow depth, slope, Shields stress, skin friction component of Shields stress, flow velocity,

and flow discharge calculated from grain size, dune cross-stratification set thickness

(t_{set}), and height of LAS (h_{LAS}) from the Undifferentiated Cutler Formation (Findlay,

2020a, 2020b). Valid ranges for reconstructed parameters are the absolute minimum and

the maximum of box and whisker plots from modern rivers (Trampush et al., 2014).

2.5.1.1. Grain Size

D_{50fine} and the proportionally weighted method (D_{50}), which best represents the

true D_{50} and results in the most reasonable paleohydraulic reconstructions, (Eq. 1) were

used for the lower and upper limits of bulk sediment grain size, respectively.

Measurements of D_{50} show that, as anticipated, grain size generally decreases away from

the uplift, with the minimum at Lisbon Valley (Table 1; Fig. 7). D_{50} values also reveal a

transition from gravel to sand median grain size at locations further away from the uplift

than Richardson Amphitheater and Paradox Valley. These sites are roughly 15 km from

the UU but situated at different positions along strike.

Table 1: Grain size measurements used for paleohydraulic reconstruction. D_{50fine} and $D_{50coarse}$ are measured from thin section and wolman pebble counts, respectively, and D_{50} is the proportionally weighted grain size calculated using those measurements and Eq. 1. Locations are listed in increasing distance from the UU (see Fig. 6).

Location	D_{50fine} (mm)	$D_{50coarse}$ (mm)	Fine (%)	Coarse (%)	D_{50} (mm)
G base	1.41	12.97	62	38	5.80
G top	3.73	14.80	62	38	7.94
RA	0.69	13.69	74	26	4.07
PV	0.73	12.46	48	52	6.83
PM	0.35	8.05	70	30	2.66
CV	0.22	10.15	89	11	1.31
MV lower	0.35	4.68	69	31	1.69
MV upper	0.21	4.68	69	31	1.59
LV	0.35	7.19	99	1	0.42
KS	0.66	3.34	36	64	2.37

2.5.1.2. Flow Depth

Key observations of LAS and dune cross-stratification sets in the field made it possible to differentiate the two structures and compare flow depths reconstructed from each. LAS were more common than dune sets in gravel deposits, whereas dune sets were more common in sand and finer-grained deposits. Dune cross-stratification sets in channel deposits were less than 50 cm thick and commonly less than 20 centimeters thick (Fig. 1–3). LAS were identified in low-angle cross-stratification sets with superimposed dune-scale trough cross-stratification in the foresets (Fig. 1, 2). LAS foresets dipped at a low-angle (<15°) and were typically 0.3–2 meters in height. The results from LAS show average depths from 0.34 meters at Moab Valley to 0.80 meters at Kane Springs. These depths are < 2.5 m, providing guidance on the appropriate choice

of values for α (5th percentile [2.2], average [2.9], and 95th percentile [3.6]) and γ (10th percentile [2.1], average [3.5], and 90th percentile [9.9]) (c.f. Paola and Borgman, 1991; Leclair and Bridge, 2001; Bradley and Venditti, 2017) for rivers in the Undifferentiated Cutler Formation (Eq. 3, 4).

Flow depths calculated from h_{LAS}, $t_{set\ min}$, and $t_{set\ avg}$ are consistent with modern gravel-bedded rivers, suggesting that the reconstructed flow depths of the Undifferentiated Cutler Formation are reasonable (Fig. 7B; Table 2) (Trampush et al., 2014). Calculated flow depths are shallowest when reconstructed from the height of LAS (h_{LAS}). The minimum limit of flow depth calculated from dune cross-stratification set thickness ($t_{set\ min}$) is typically closest to the values calculated from the height of LAS (h_{LAS}), while flow depths calculated from the average ($t_{set\ avg}$) and maximum limit ($t_{set\ max}$) are ca. 1–7 m greater. Calculated flow depths do not systematically increase or decrease from the proximal to distal sites (Table 2; Fig. 7B).

Table 2: Number of LAS and dune sets measured at each location and reconstructed flow depths.

	Measured		Calculated Flow Depths			
Location	h_{LAS} n=	t_{set} n=	h_{LAS} (m)	t_{setmin} (m)	t_{setavg} (m)	t_{setmax} (m)
G	6	40	0.53	0.55	1.2	4.21
RA	29	40	0.64	0.55	1.2	4.22
PV	2	24	0.55	0.38	0.84	2.94
PM	2	11	0.57	0.85	1.87	6.58
CV	36	61	0.59	0.63	1.38	4.84
MV	3	63	0.34	0.4	0.89	3.12
LV	1	20	0.39	0.7	1.53	5.37
KS	34	89	0.8	0.73	1.59	5.6
Total	113	348				

Figure 7: Grain size measurements and flow depth and slope reconstructions of the Undifferentiated Cutler Formation and modern rivers. A) Grain size values from thin section (D_{50fine}) and the proportionately weighted method (D_{50}) (Eq. 1). B) Flow depth results at each sample site from h_{LAS}, and the minimum, average, and maximum values of α and γ. C) Slope calculation results from both measures of grain size and the 4 flow depths. Red shaded background areas represent data ranges from modern gravel-bedded rivers, white background areas represent values of sand-bedded rivers, and yellow background areas are where values from gravel- and sand-bedded rivers overlap (data ranges from Trampush et al., 2014). Data at position "2014" on the X axis are paleohydraulic reconstructions of slope calculated from measurements of grain size and flow depth in modern rivers (data from Trampush et al., 2014). Sample locations: G – Gateway, CO; PV – Paradox Valley; PM – Parroitt Minibasin; RA – Richardson Amphitheater; CV – Castle Valley; MV – Moab Valley; LV – Lisbon Valley; KS – Kane Springs.
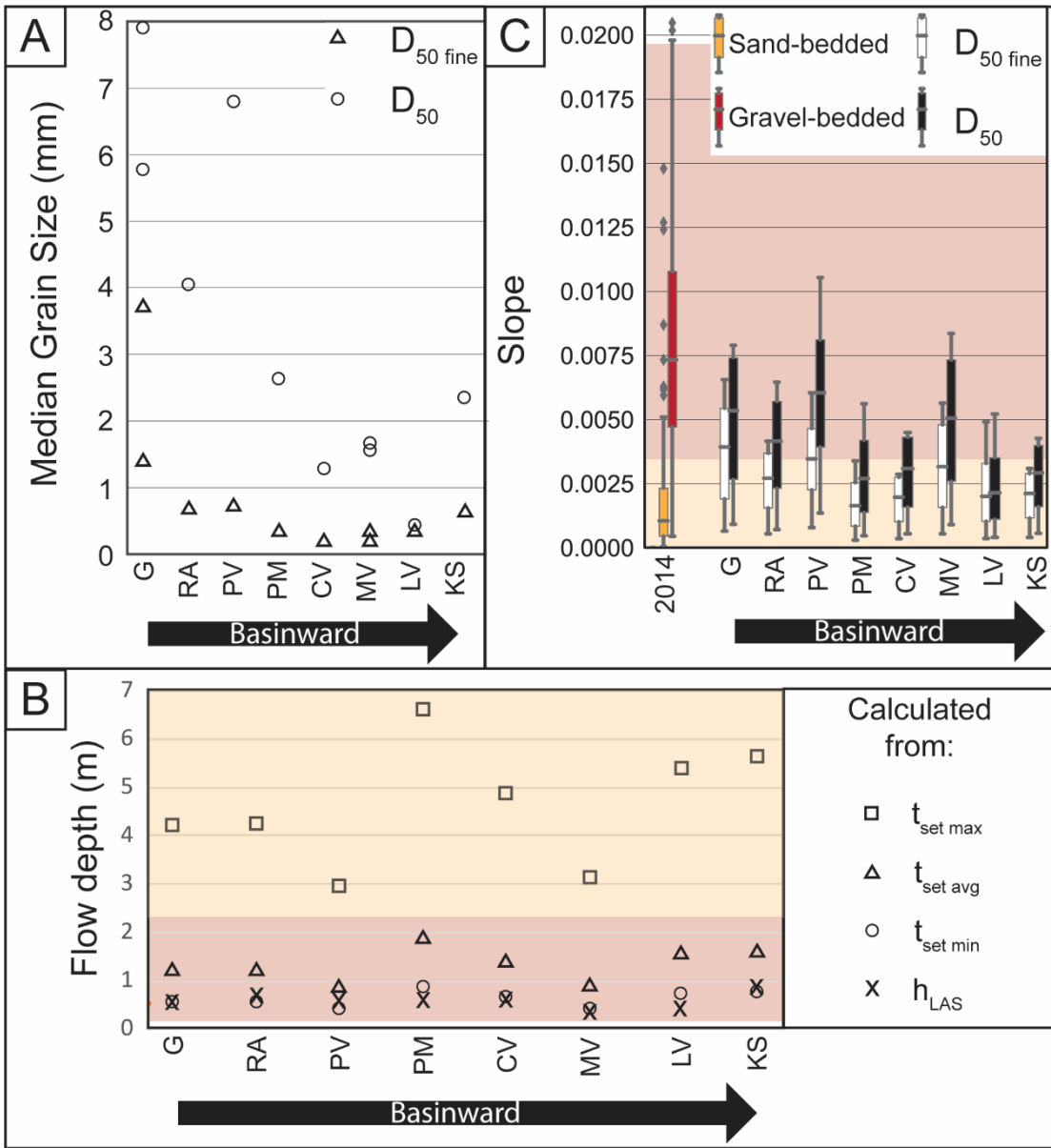
2.5.1.3. Slope

2.5.1.3.1. Modern Rivers

Calculated values of channel slope in gravel-bedded and sand-bedded rivers generally agree with measured slope values (Fig. 8). Calculated slope values in rivers with measured slope less than ca. 0.01 are generally double the measured slope, and in rivers with measured slope greater than 0.01 are generally half of measured slope. The trend line of measured to calculated slopes reflects overestimation of shallow slopes and underestimation of steep slopes and does not follow the 1:1 line, but the trend line has an r^2 value of 0.44 (Fig. 8).

2.5.1.3.2. Paradox Basin

Paleoslope was calculated by applying grain size measurements from both D_{50fine} and D_{50} to each of the four depth reconstructions (Eq. 8). Finer grain size and shallower flow depth result in a lower paleoslope. Paleoslope is greater at the proximal locations Gateway, Richardson Amphitheater, and Paradox Valley than at locations Parroitt Minibasin, Castle Valley, Lisbon Valley, and Kane Springs (Fig. 7; Table 3, 4). The maximum values of paleoslope, which result from using D_{50} and depth calculated from $t_{set\ min}$ or h_{LAS}, do not result in a trend of lower slopes further from the UU, but an irregular pattern with highs at Gateway and near salt walls at Paradox Valley, and Moab Valley.

All slope calculation results (using either D_{50} or D_{50fine}, and all flow depths) are within the range of measured values reported for modern gravel-bedded rivers (0.0001 – 0.0195) (Trampush et al., 2014) (Fig. 7). Slope calculation results from D_{50} and the

39

shallowest flow depths are greater than the measured values reported for modern sand-bedded rivers (0.000009 – 0.00395) (Trampush et al., 2014). The lower half of slope calculation results from D_{50fine} at Gateway, Richardson Amphitheater, Paradox Valley, and Moab Valley and all of the results from Parroitt Minibasin, Castle Valley, Lisbon Valley, and Kane Springs are within the range of measured slope values for modern sand-bedded rivers (Trampush et al., 2014).

Table 3: Reconstructed slope values from D$_{50}$ measurements.

Location	S (h_{LAS})	S (t_{setmin})	S (t_{setavg})	S (t_{setmax})
G base	0.0073	0.0071	0.0032	0.0009
G top	0.0079	0.0077	0.0035	0.0010
RA	0.0055	0.0065	0.0029	0.0008
PV	0.0073	0.0106	0.0048	0.0014
PM	0.0056	0.0037	0.0017	0.0005
CV	0.0045	0.0042	0.0019	0.0005
MV lower	0.0083	0.0070	0.0032	0.0009
MV upper	0.0082	0.0069	0.0031	0.0009
LV	0.0051	0.0029	0.0013	0.0004
KS	0.0039	0.0043	0.0019	0.0006

Table 4: Reconstructed slope values from D$_{50fine}$ measurements.

Location	S - h_{LAS}	S - t_{setmin}	S - t_{setavg}	S - t_{setmax}
G base	0.0051	0.0050	0.0023	0.0006
G top	0.0066	0.0063	0.0029	0.0008
RA	0.0035	0.0042	0.0019	0.0005
PV	0.0042	0.0060	0.0027	0.0008
PM	0.0034	0.0022	0.0010	0.0003
CV	0.0029	0.0027	0.0012	0.0004
MV lower	0.0056	0.0047	0.0022	0.0006
MV upper	0.0050	0.0042	0.0019	0.0005
LV	0.0049	0.0028	0.0013	0.0004
KS	0.0028	0.0031	0.0014	0.0004
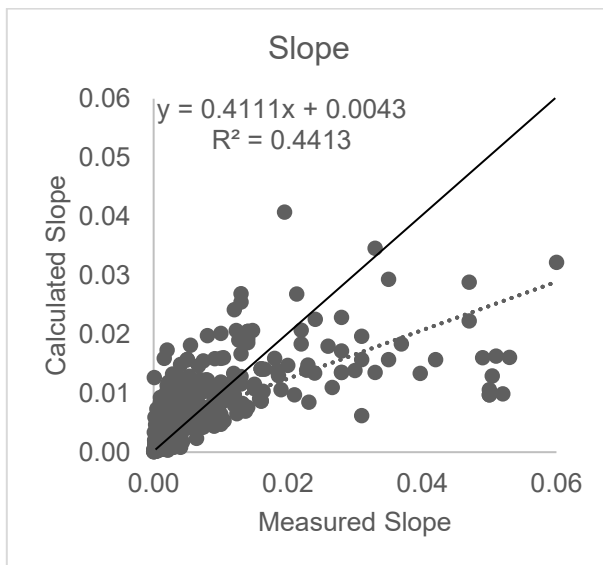
Figure 8: A plot of measured versus calculated slope of modern rivers shows slope reconstructions are accurate (Measured data from Trampush et al. (2014), slope was calculated from grain size and flow depth data from Trampush et al. (2014)). Each point represents the measured and calculated value for a single river.

2.5.1.4. Flow Velocity, Shields Stress, And Skin Friction

2.5.1.4.1. Modern Rivers

Reconstructed flow velocities are higher than measured flow velocities in modern rivers and do not fit to a trend line when calculated values are plotted against measured values (Fig. 9, 10) (Trampush et al., 2014). This is attributed to result from inaccurate calculation of τ_s^*. The Hayden et al. (2019) method uses the skin friction component of shear stress (τ_s^*) to account for a large part of the flow resistance caused by the sediment bed. Reconstructions of flow velocity likely overestimate the true value because of high τ_s^* results. τ^* must be greater than τ_s^* by definition, and, when τ^* is less

than τ_s^* , calculated flow velocity is unreasonably high. τ^* is less than τ_s^* in modern rivers where grain size is finer than ~0.5 mm or coarser than 74 mm. Even where τ^* is not less than τ_s^* , reconstructed flow velocity of modern rivers calculated using Hayden et al. (2019) methods is greater than measured values when grain size is finer than ~4 mm or coarser than ~50 mm (Trampush et al., 2014). The Trampush et al. (2014) dataset shows no correlation between slope and flow velocity ($R^2 = 0.08$), but our flow velocity results are greatest where grain size is smallest (Fig. 10B).

2.5.1.4.2. Paradox Basin

Shields stress, skin friction component of Shields stress (τ_s^*), and flow velocity increase at locations with finer grain size. Results for flow velocity are presented using two methods, from Hayden et al., 2019 and the VPE method from Ferguson (2007). Flow velocity was calculated with both D_{50} and D_{50fine}, and each grain size value with the four flow depth reconstructions from h_{LAS} and t_{set}. This results in eight calculated flow velocities for each method that capture uncertainty in the reconstructions (Eq. 9) (Table 6, 7; Fig. 10B).

Paleoflow velocity results from the Undifferentiated Cutler Formation where grain size is smallest, paleoflow depth is deepest, and paleoslope is shallowest are systematically higher than reasonable values of channel velocity constrained from modern examples in cases. Undifferentiated Cutler Formation reconstructions of paleoflow velocity for locations that use a grain size smaller than 1 mm and are calculated using Hayden et al. (2019) methods are not within the range of measured flow velocities of modern rivers (Trampush et al., 2014). Flow velocities increase past

43

Richardson Amphitheater and Paradox Valley at locations, which have D_{50} values finer than 0.5 millimeters and Shields stress (τ^*) values greater than 2.5. Undifferentiated Cutler Formation paleoflow velocities calculated using D_{50fine} yields a flow velocity minimum at the top of the Gateway section and a maximum at Castle Valley. Using D_{50}, the minimum occurs at Paradox Valley and maximum at Lisbon Valley.

Flow velocities calculated using Ferguson (2007) VPE methods also overestimate flow velocity at all locations measured in our Undifferentiated Cutler Formation transect because d / D_{50} is too large to apply significant flow resistance through form drag. The Ferguson (2007) VPE method was developed for gravel-bedded rivers where the ratio of d / D_{50} is 0.1–30 (Ferguson, 2007), and form drag over large bed elements applies most of the flow resistance and skin friction plays a minimal role. The shallowest flow depth results in our Undifferentiated Cutler Formation transect are 30–80 cm and D_{50} grain size measurements are 1–8 mm, resulting in d / D_{50} ratios ranging between 55–673 at Gateway and Lisbon Valley, respectively. The high d / D_{50} ratio shows that most of the preserved Undifferentiated Cutler Formation fluvial system is too deep and fine-grained for the form drag focused VPE method to be accurate.

Table 5: Measured grain size and reconstructed Shields stress (τ^*) and skin friction component of Shields stress (τ_s^*).

	D_{50}			D_{50fine}		
Location	D_{50} (mm)	τ^*	τ_s^*	D_{50fine} (mm)	τ^*	τ_s^*
G base	5.80	0.40	0.13	1.41	1.17	0.60
G top	7.94	0.32	0.10	3.73	0.56	0.19
RA	4.07	0.53	0.17	0.69	1.99	1.64
PV	6.83	0.36	0.11	0.73	1.90	1.51
PM	2.66	0.72	0.27	0.35	3.31	4.44
CV	1.31	1.23	0.67	0.22	4.74	9.05
MV lower	1.69	1.02	0.47	0.35	3.29	4.39
MV upper	1.59	1.06	0.51	0.21	4.86	9.51
LV	0.42	2.90	3.42	0.35	3.31	4.45
KS	2.37	0.79	0.31	0.66	2.06	1.76

Table 6: Reconstructed flow velocities (U) using D_{50} and Hayden et al. (2019) and Ferguson (2007) VPE methods.

	Hayden et al. (2019) (D_{50})				Ferguson (2007) VPE (D_{50})			
Location	h_{LAS}	t_{setmin}	t_{setavg}	t_{setmax}	h_{LAS}	t_{setmin}	t_{setavg}	t_{setmax}
G base	1.31	1.31	1.53	1.87	2.68	2.69	3.07	3.79
G top	1.29	1.30	1.52	1.88	2.64	2.65	3.03	3.74
RA	1.44	1.39	1.60	1.93	2.81	2.73	3.12	3.85
PV	1.30	1.20	1.42	1.76	2.68	2.51	2.87	3.55
PM	1.58	1.69	1.90	2.24	2.80	3.00	3.42	4.22
CV	2.07	2.09	2.33	2.70	2.91	2.94	3.35	4.13
MV lower	1.71	1.76	1.99	2.34	2.62	2.70	3.08	3.80
MV upper	1.76	1.81	2.03	2.39	2.63	2.71	3.09	3.81
LV	3.23	3.45	3.75	4.22	2.84	3.13	3.57	4.40
KS	1.73	1.71	1.92	2.26	2.98	2.93	3.35	4.13

Table 7: Reconstructed flow velocities (U) using D_{50fine} and Hayden et al. (2019) and Ferguson (2007) VPE methods.

Location	Hayden et al. (2019) (D_{50fine})				Ferguson (2007) VPE (D_{50fine})			
	h_{LAS}	t_{setmin}	t_{setavg}	t_{setmax}	h_{LAS}	t_{setmin}	t_{setavg}	t_{setmax}
G base	1.98	1.99	2.22	2.59	2.84	2.86	3.26	4.02
G top	1.41	1.42	1.63	1.96	2.73	2.74	3.13	3.86
RA	2.75	2.70	2.96	3.39	3.03	2.95	3.36	4.14
PV	2.63	2.51	2.77	3.19	2.94	2.77	3.16	3.89
PM	3.63	3.80	4.11	4.61	3.05	3.26	3.72	4.59
CV	4.47	4.50	4.85	5.41	3.14	3.16	3.61	4.45
MV lower	3.42	3.49	3.80	4.30	2.80	2.88	3.29	4.05
MV upper	4.29	4.36	4.72	5.28	2.86	2.95	3.36	4.14
LV	3.49	3.72	4.03	4.53	2.87	3.16	3.60	4.44
KS	2.88	2.85	3.12	3.55	3.14	3.10	3.53	4.35
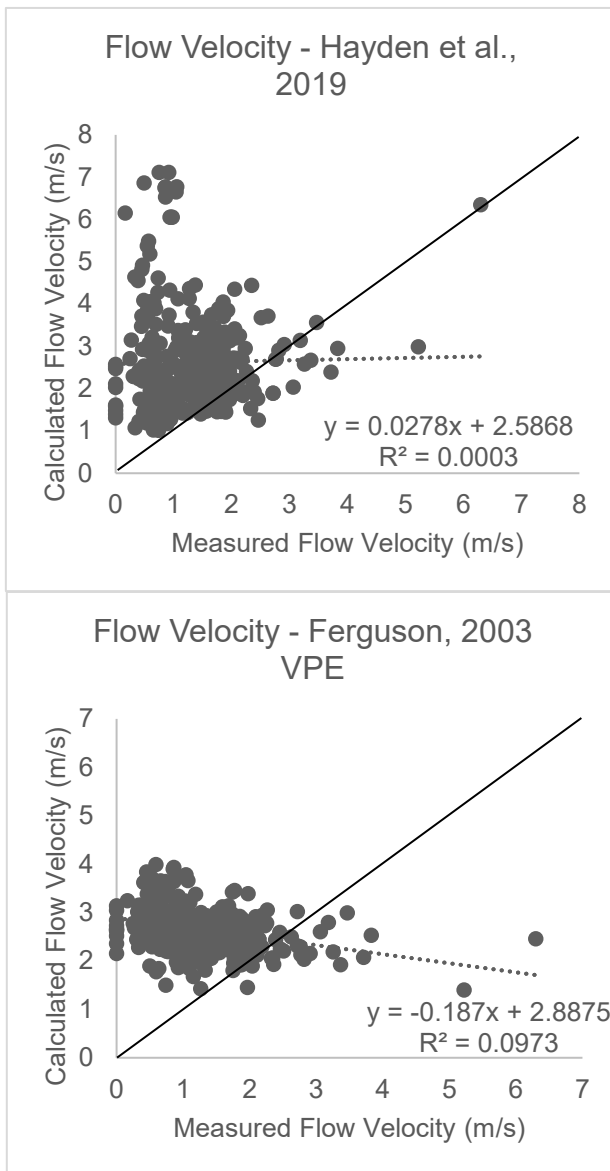
Figure 9: Measured versus calculated flow velocity of modern rivers shows calculated flow velocity is inaccurate (Measured data from Trampush et al., 2014). Each point represents the measured and calculated value for a single river, and dotted lines are linear trendlines of the data.

Figure 10: Shields stress, skin friction component of Shields stress, flow velocity, and discharge reconstructions of the Undifferentiated Cutler Formation and modern rivers. A) Shields stress and skin friction component of Shields stress results show that values are greatest where grain size is smaller than 0.5 mm. B) Flow velocity results from the Hayden et al. (2019) method show greatest flow velocity at locations furthest from the UU where grain size is less than 0.5 mm. C) Channel discharge calculation results reflect flow velocity results, keys in part B apply to part C as well. Red shaded background areas represent data ranges from modern gravel-bedded rivers, white background areas represent values of sand-bedded rivers, and yellow background areas are where values from gravel- and sand-bedded rivers overlap (data ranges from Trampush et al., 2014). Data at position "2014" on the X axis are paleohydraulic reconstructions calculated from measurements of grain size and flow depth in modern rivers (data from Trampush et al., 2014). Sample locations: G – Gateway, CO; PV – Paradox Valley; PM – Parroitt Minibasin; RA – Richardson Amphitheater; CV – Castle Valley; MV – Moab Valley; LV – Lisbon Valley; KS – Kane Springs.

49
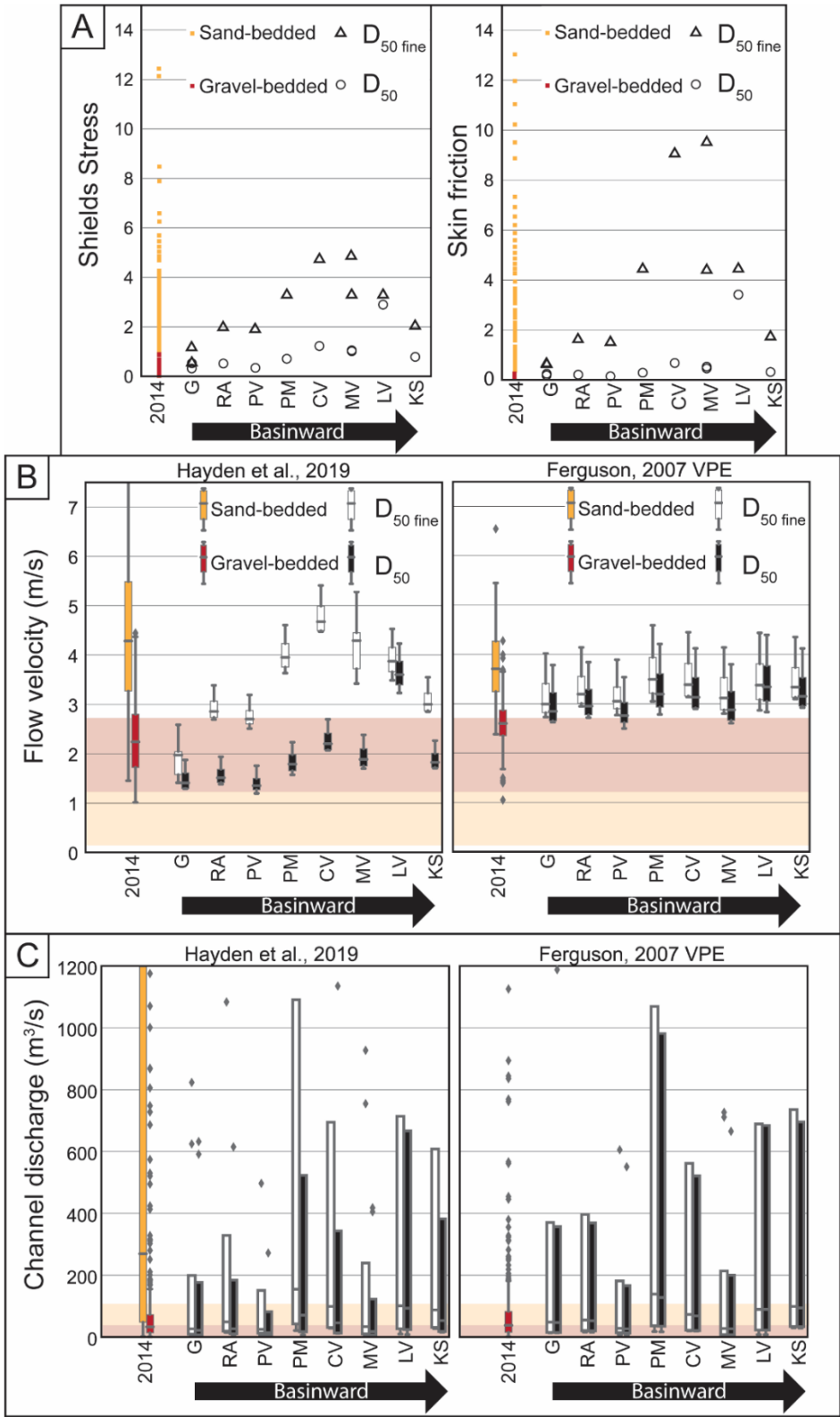
2.5.1.5. Discharge

2.5.1.5.1. Modern Rivers

The reconstructed values for channel discharge in modern gravel-bedded rivers generally agree with measured discharge and roughly fit to a trendline parallel to the 1:1 line, but reconstructed values for modern sand-bedded rivers have a larger spread of values and higher maxima than measured discharges values (Fig. 10C, 11). Modern sand-bedded rivers with a flow depth greater than 2 m have the highest calculated discharge values, but do not have measured discharge values to compare with, hence the range of discharge of deep sandy rivers is unknown. The modern dataset has little error in discharge reconstructions because it has well constrained flow depth.

2.5.1.5.2. Paradox Basin

Calculated discharge values for the Undifferentiated Cutler Formation are generally higher than measured discharges in modern rivers (Fig. 10C; Table 8, 9) (Trampush et al., 2014). Measured discharges from modern rivers have a narrow range (0.2 – 114 m^3/s), but deep sandy rivers (d > 2 m) are not included in the measured data because they are difficult to measure. Reconstructed discharge using D_{50} and Hayden et al. (2019) methods in the Undifferentiated Cutler Formation have a wide range (3.7 – 2188 m^3/s), as do results from D_{50fine} measurements and Ferguson (2003) methods (Trampush et al., 2014). Using D_{50} and flow depth from $t_{set\ min}$ or h_{LAS} at each location yield the lowest discharge, and using flow depth from $t_{set\ avg}$ discharge values in the measured range of gravel-bedded rivers except at Parroitt Minibasin and Lisbon Valley locations (Table 8). Parroitt Minibasin and Lisbon Valley have higher discharge and

50

deeper calculated flow depths than other locations. The wide range in calculated

discharge is a result of uncertainty in flow depth reconstruction, but realistic discharge

results for shallow flow depths lend confidence to calculated flow depths from h_{LAS},

$t_{set\ min}$, and $t_{set\ avg}$.
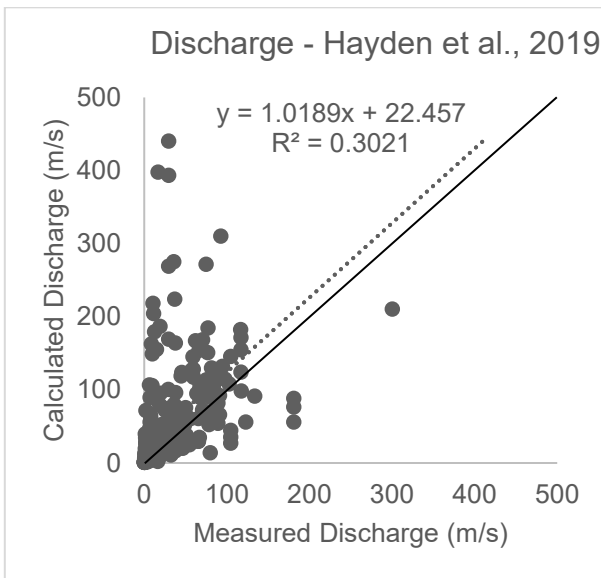
Figure 11: Measured versus calculated discharge of modern rivers shows discharge calculations are accurate when flow depth is well constrained (Measured data from Trampush et al., 2014). Each point represents the measured and calculated value for a single river, and the dotted line is a linear trendline of the data.. Rivers deeper than 2 m have the highest calculated discharge values, but the modern dataset does not contain measured discharge values for most rivers deeper than 2 m.

Table 8: Reconstructed channel discharges (Q) using D$_{50}$ and Hayden et al. (2019) and Ferguson (2007) VPE methods.

Location	Hayden et al. (2019) (D$_{50}$)				Ferguson (2007) VPE (D$_{50}$)			
	h$_{LAS}$	t$_{setmin}$	t$_{setavg}$	t$_{setmax}$	h$_{LAS}$	t$_{setmin}$	t$_{setavg}$	t$_{setmax}$
G base	6.5	7.0	39.4	594.5	13.4	14.4	79.3	1206.3
G top	6.4	6.9	39.2	597.2	13.2	14.2	78.3	1190.6
RA	10.7	7.5	41.6	618.9	21.0	14.7	81.0	1231.0
PV	7.1	3.1	17.9	274.7	14.6	6.6	36.3	551.7
PM	9.1	22.1	119.8	1740.8	16.1	39.2	215.9	3282.3
CV	13.1	14.8	79.5	1138.0	18.4	20.8	114.5	1740.8
MV lower	3.6	5.2	28.3	411.1	5.5	8.0	43.8	666.2
MV upper	3.7	5.3	28.9	419.8	5.5	8.0	43.9	667.9
LV	8.8	30.0	157.4	2188.4	7.8	27.3	150.1	2281.8
KS	19.7	16.2	87.9	1276.4	33.9	27.8	153.2	2328.9

Table 9: Reconstructed channel discharges (Q) using D$_{50fine}$ and Hayden et al. (2019) and Ferguson (2007) VPE methods.

Location	Hayden et al. (2019) (D$_{50fine}$)				Ferguson (2007) VPE (D$_{50fine}$)			
	h$_{LAS}$	t$_{setmin}$	t$_{setavg}$	t$_{setmax}$	h$_{LAS}$	t$_{setmin}$	t$_{setavg}$	t$_{setmax}$
G base	9.9	10.6	57.3	823.4	14.2	15.3	84.2	1279.6
G top	7.1	7.6	42.1	624.5	13.7	14.7	80.8	1228.7
RA	20.6	14.5	76.9	1083.7	22.6	15.8	87.2	1325.4
PV	14.3	6.6	35.0	496.9	16.0	7.2	39.8	605.6
PM	20.9	49.7	259.4	3585.6	17.5	42.7	235.0	3571.4
CV	28.4	31.9	165.9	2281.7	19.9	22.4	123.4	1876.2
MV lower	7.1	10.3	54.1	754.6	5.8	8.5	46.8	711.2
MV upper	8.9	12.9	67.2	927.2	6.0	8.7	47.8	726.8
LV	9.6	32.4	169.4	2346.9	7.8	27.5	151.2	2298.9
KS	32.8	27.0	142.9	2004.1	35.8	29.4	161.6	2456.7

2.5.1.6 Summary Of Paleohydraulic Reconstruction Results

        Our results emphasize that determining flow depth from h_{LAS}, and accurately characterizing D_{50}, reduces uncertainty and yields reasonable calculated values of particle Reynolds number, Shields stress, slope and discharge that are useful for provenance analysis. Results of modern river reconstructions show that slope and discharge calculations are the most reliable because they show best agreement with measured values from the same modern rivers within a factor of 2 (Fig. 7, 8, 10, 11). However, reconstructions of flow velocity are less reliable because reconstructions of modern rivers do not agree with measured values from the same modern rivers (Fig. 9, 10). Calculation of the skin friction component of Shields stress and flow velocity in rivers with a D_{50} finer than ~0.5 mm or coarser than 74 mm yields unreasonable values (Fig. 9, 10). The trend of greater skin friction component of Shields stress than Shields stress at fine grained locations, where flow velocity and discharge are most elevated, indicates that calculation of skin friction is a source of uncertainty (Trampush et al., 2014).

        Results from Undifferentiated Cutler Formation reconstructions show that D_{50} and channel flow depth determined from h_{LAS}, $t_{set\ min}$, and $t_{set\ avg}$ are reasonable calculations to use for provenance studies because reconstructions of slope and channel discharges fall within the range of measured values from modern rivers with similar grain size. Calculations incorporated the full range of possible values for variables (e.g. D_{50} and D_{50fine}; α and γ). Using the proportionally weighted method (D_{50}) is recommended for grain size determination over thin section measurement and hand

sample estimates (D_{50fine}) because D_{50} yields more realistic values of reconstructed slope and discharge (Eq. 1) (Fig. 7, 10). Grain sizes determined from thin section (D_{50fine}) and proportionately weighted grain size (D_{50}) methods result in significantly different values for slope, flow velocity, and discharge following Hayden et al. (2019) methods. Calculated using D_{50}, reconstructions of slope, flow velocity, and discharge results are generally within the measured ranges reported by Trampush et al. (2014). However, when D_{50fine} is used, slope is not in the range of measured values for gravel-bedded rivers at locations where gravel is observed, and τ_s^*, flow velocity, and discharge reconstructions are unrealistically high. These results reiterate that flow depth from h_{LAS} is preferable because it has lower uncertainty in comparison to flow depths from t_{set} (Fig. 7, 8). Flow depths calculated from $t_{set\ min}$ or h_{LAS} agree at all locations, and flow depths calculated from $t_{set\ min}$ yield values that are reasonable, but are twice as deep as flow depth from h_{LAS}. D_{50fine} and flow depth from $t_{set\ max}$ introduce significant error and destroy spatial trends in the reconstructions. Constraining flow depth with h_{LAS} and an accurate D_{50} reduces uncertainty and highlights spatial trends in particle Reynolds number, Shields stress, slope and discharge that are used for provenance analysis.

Despite some uncertainty regarding the precision of some reconstructed parameters, the spatial trends in the hydraulic reconstruction data remain useful because they highlight hydraulic boundaries where sorting most likely occurs. Modern rivers show a positive power law trend of larger grain size with steeper slope ($R^2 = 0.54$), and a power law trend of shallower flow depth with steeper slope ($R^2 = 0.78$) (Trampush et al., 2014). Our results agree with the positive power law trend of larger grain size with

steeper slope, and weakly agree with the power law trend of shallower flow depth with steeper slope (Fig. 7). The results show a SW trend of decreasing grain size and slope, except at Moab Valley, accompanied by increasing flow velocity and discharge towards the SW (Fig. 7, 8). There is a sharp decrease in grain size and Shields stress between Richardson Amphitheater and Parroitt minibasin that might represent a gravel-sand transition, which implies the location of an key ancient decrease in flow competency (Fig. 7) (Lamb and Venditti, 2016). The role of ancient salt walls on paleohydraulics remains equivocal. At Paradox Valley and Moab Valley, sites along the flanks of collapsed salt walls, results demonstrate that slope increases and discharge decreases. However, at Kane Springs and Lisbon Valley, I see no shift in slope or discharge (Fig. 6, 7). The hydraulic boundary identified in grain size and Shields stress data, and the increased slope and decreased discharge trend at Paradox Valley and Moab Valley, are used to find correlations between spatial changes in paleohydraulics and provenance data.

2.5.2. Detrital Zircon Data For Assessing The Effects Of Sorting

2.5.2.1. Detrital Zircon Age

Undifferentiated Cutler Formation fluvial samples have unimodal and bimodal age signatures with peaks centered on 1440 Ma and 1727 Ma, and a single sample from Lisbon Valley has a third peak at 526 Ma (Findlay, 2020c). These ages are consistent with expected derivation of sediment from the UU (Lawton et al., 2015; Leary et al., 2020). Paradox Valley and Moab Valley locations are outliers with unimodal 1727 Ma spectra, just as they are outliers in slope and discharge results. Details of detrital zircon

results are presented in a companion paper Findlay et al. (in review). For the purposes of this paper, I focus on the percentage abundance of the 1440 Ma and 1727 Ma age modes. Although these vary by sample, there is no systematic spatial trend in the distribution of either age mode (Table 10, Fig. 6).

Table 10: Proportions of 526 Ma, 1440 Ma, and 1726 Ma detrital zircon grains in each Undifferentiated Cutler Formation fluvial sample.

Location	% 1440 Ma	% 1727 Ma	% 526 Ma
G Base	93.8	3.1	
G Top	90.4	4.4	0.7
RA	28.0	65.2	
PV	1.2	97.6	
CV	67.8	18.3	0.6
MV lower	81.4	16.1	
MV upper	1.6	95.3	
LV	40.8	42.9	12.2
KS	75.0	24.2	

2.5.2.2. Detrital Zircon Grain Size

Relating detrital zircon grain size with grain age is a key relationship to investigating the possible impact of spatial sorting in the fluvial system. At Gateway, Richardson Amphitheater, Castle Valley, Lisbon Valley, and Kane Springs 1440 Ma and 1727 Ma zircons have similar median ESD grain sizes, which average 0.081 mm and 0.083 mm, respectively (Findlay, 2020d). Only at Paradox Valley and Moab Valley is there a difference in grain size between the age groups, where 1727 Ma zircons (D_{50} = 0.124–0.160 mm, average = 0.139 mm) are larger than 1440 Ma zircons (D_{50} = 0.094–0.115 mm, average = 0.101 mm) (Table 4; Fig. 11). The grain size of 1727 Ma zircon at

Paradox Valley and Moab Valley are larger than at other sites, complimenting the

unimodal 1727 Ma age spectra and outlying slope and discharge values at these

locations. There is no correlation between bulk grain size and detrital zircon median

grain size, indicating hydraulic equivalence with the bulk sediment did not control zircon

grain size (Fig. 12).

Table 11: Measured 1440 Ma, 1727 Ma, and 526 Ma age group detrital zircon grain sizes. Measured detrital zircon sizes are ESD median grain size. Standard deviation of the measured zircon size is given where more than one grain was measured, from which the D_{16} and D_{84} are calculated by subtracting and adding to the D_{50} value.

Location	1440 Ma Measured Zircon D_{50} (mm)	1727 Ma Measured Zircon D_{50} (mm)	526 Ma Measured Zircon D_{50} (mm)
G base	0.085±0.024	0.089±0.021	
G top	0.100±0.023	0.095±0.036	
RA	0.082±0.020	0.082±0.020	
PV	0.094	0.160±0.046	
CV	0.087±0.022	0.088±0.020	
MV lower	0.115±0.027	0.133±0.040	
MV upper	0.094±0.018	0.124±0.042	
LV	0.067±0.021	0.068±0.019	0.087±0.035
KS	0.062±0.022	0.077±0.038	
Average	0.08	0.09	0.09
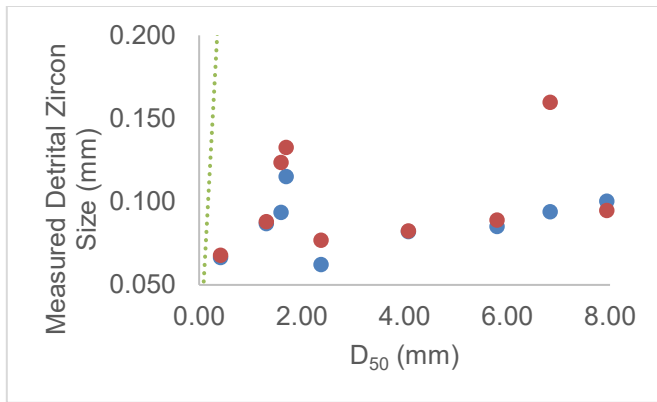
Figure 12: A plot of measured bulk sediment grain size (D_{50}) versus measured detrital zircon grain size shows that there is no correlation between the two. Orange points are 1727 Ma grains, and blue points are 1440 Ma grains. Grey dashed line is the zircon size predicted by hydraulic equivalency (Garzanti et al., 2008).

2.5.3. Hydraulic Equivalent Zircon Grain Size

Detrital zircon grain size results demonstrate spatial and temporal (vertical stratigraphic) variations, however, measured zircon grain size values do not correlate with hydraulic equivalent zircon size calculations (Table 10). Paradox Valley and Moab Valley have 0.160 mm 1727 Ma zircon that are the largest in the transect, but bulk sediment grain size and hydraulic equivalent grain size are largest at Gateway, suggesting that hydraulic equivalence method provides limited prediction regarding where the largest zircon are located. Measured zircon is the smallest at Lisbon Valley, and yields the smallest hydraulically equivalent zircon grain size (0.26 mm). However, this hydraulic equivalent grain size is larger than all measured zircon sizes in this study from the Undifferentiated Cutler Formation, suggesting that the fluvial system had sufficient competency to transport all detrital zircon grain sizes.

58

Table 12: Bulk sediment D_{50} (Eq. 1), D_{50fine}, and calculated hydraulic equivalent detrital zircon (Eq. 9–11).

Location	Bulk D_{50} (mm)	Hydraulic Equivalent zircon to D_{50} (mm)
G Base	5.803	2.775
G Top	7.937	3.745
RA	4.072	1.986
PV	6.831	3.243
PM	2.657	1.336
CV	1.309	0.704
MV Lower	1.693	0.887
MV Upper	1.595	0.840
LV	0.418	0.255
KS	2.373	1.205

2.5.4. The Modified Shields Diagram

The modified Shields diagram with Rouse curves provides another method for predicting which grain size fractions of bulk sediment and detrital zircon would be transported together. The Reynolds Number and Shields Stress of the Undifferentiated Cutler Formation samples (calculated from the both the D_{50} and D_{50fine} bulk grain size) are plotted on the modified Shields diagram. These results show that all detrital zircon grain sizes observed here were transported in suspension, regardless of the mode of transport during of the bulk sediment grain size during mean and bankfull flow (Fig. 12). Rouse curves indicate that most locations would have moved the D_{50} bulk sediment in the bed load, and the D_{50fine} bulk sediment in the mixed or suspended loads (Fig. 9). Calculated hydraulic equivalent zircon sizes from all sites would have been transported in the same mode of transport as the bulk sediment, but those hydraulic equivalent zircon

sizes (0.225–3.75 mm) were not observed in the Undifferentiated Cutler Formation (Table 11, 12).

The sizes of detrital zircon grain in the Undifferentiated Cutler Formation are smaller than the grain sizes predicted from the settling equivalency method, which suggests all detrital zircon grains could have been transported. The Rouse curves provide an additional level of detail, predicting that all zircon were transported together in suspension, and that even the largest 0.160 mm detrital zircon grains (observed at Paradox Valley) would have been transported in suspension at all locations (Fig. 12). Furthermore, Rouse curves emphasize that the Undifferentiated Cutler Group detrital zircons transported in suspended mode could have experienced winnowing from the D_{50} bulk sediment at all locations because the bulk sediment would have been transported as mixed or bed load. When considering similar results based on the D_{50fine}, zircons would have been winnowed only from Gateway, Richardson Amphitheater, Paradox Valley, and Kane Springs sites, which have gravel-size D_{50}.
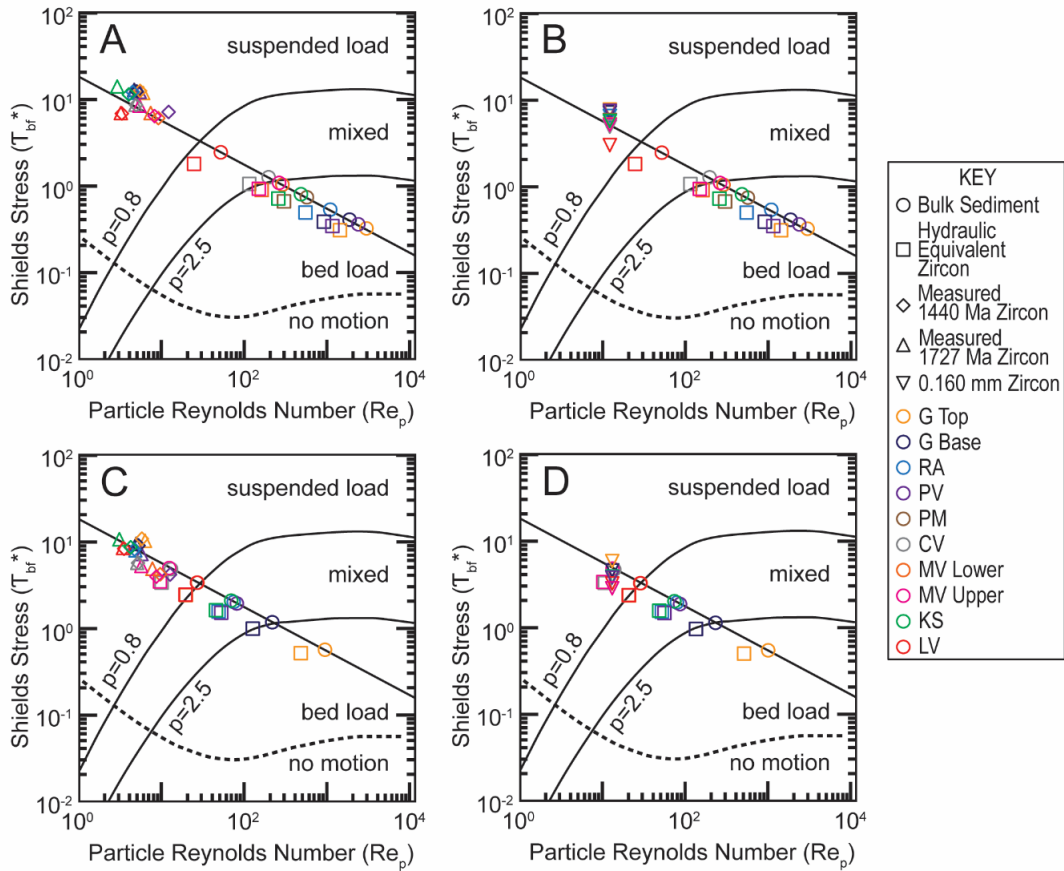
Figure 13: Modified Shields diagram with Shields curve and Rouse curves that indicate transport mode of bulk sediment and detrital zircon (Modified from Trampush et al. (2014)). Measured detrital zircon grain size plots in the suspended mode of transport at all locations. A) D_{50} bulk sediment grain size and measured detrital zircon grain size plotted for all locations. B) D_{50} bulk sediment grain size and 0.160 mm detrital zircon plotted for all locations. Inferring a 0.160 mm zircon grain size at all locations results in the same transport modes as measured detrital zircon sizes. C) D_{50fine} bulk sediment grain size and measured detrital zircon grain size plotted for all locations. Measured detrital zircon from every location plot in the suspended mode of transport. D) D_{50fine} bulk sediment grain size and 0.160 mm detrital zircon plotted for all locations. Inferring a 0.160 mm zircon grain size at all locations results in the same transport modes as measured detrital zircon sizes.

61

2.6. Discussion

2.6.1. Strengths And Limitations Of Paleohydraulic Reconstructions Of The Cutler

Group For Identification Of Sorting Of Dense Minerals

Hydraulic reconstruction methods are founded in robust physics-based theory,

supported by empirical data, and are widely used for assessing modern environments,

but have not been widely tested on ancient environments and strata, leaving untested the

utility of this method in combination with detrital zircon geochronology. Paleohydraulic

reconstruction approaches help constrain boundary conditions of ancient environments,

which improves environmental and climate reconstructions and basin analysis. The

review of methods and case study of the Paradox basin described herein show that

Shields stress, slope, and discharge reconstructed by paleohydraulic methods yield both

reasonable and unreasonable results in comparison to modern fluvial systems, and guide

the integration between detrital zircon provenance methods and paleohydraulics. Below I

further explore why some results are reasonable, while others are not, and show that

variation in provenance data of the Undifferentiated Cutler Group likely reflects changes

in provenance and is not an effect of hydraulic sorting on age spectra.

Hayden et al. (2019) methods yield τ_s^* and flow velocity results that show a trend

of higher flow velocity where grain size is finer. Although sand bedded rivers can have

higher flow velocity than gravel bedded rivers, this is unreasonable as a general trend

because modern rivers have a weak trend ($R^2 = 0.31$) of larger grain size with higher

flow velocity (Trampush et al., 2014). The cause of unreasonably high flow velocity

results in sand bedded channels is greater calculated τ_s^* than τ^* when grain size is finer

than coarse sand (ca. 0.5 mm) (Fig. 10). Likewise, paleoflow velocity calculated using the Ferguson (2007) VPE method overestimates flow velocity and shows no trend in the Undifferentiated Cutler Formation because it is only accurate in shallow gravel-bedded rivers, where d/D_{50} is less than 30. The Ferguson (2007) VPE method for flow velocity calculation is likely sufficiently sensitive to identify changes in hydraulic conditions that might preferentially sort dense minerals in shallow streams with cobble and boulder size objects on the bed, but, along with the Hayden et al., (2019) method, provides very limited utility in fluvial systems with similar or finer grain size than the Undifferentiated Cutler Formation system described here. This limits the utility of these parameters towards identifying locations in an ancient fluvial system where dense minerals could be sorted.

Despite limitations in reconstructing paleoflow velocity, our results show that values for slope and discharge in the Undifferentiated Cutler Formation are consistent with modern values when calculated using D_{50} and flow depth constrained by h_{LAS}. Our results for slope and discharge have wider spread than the modern dataset because D_{50} and flow depth in the Cutler Group are not as well constrained (Fig. 10C, 11). In the modern dataset, slope and discharge reconstructions agree with measured discharge because D_{50} and flow depth is known. Constraining D_{50} with Eq. 1 and flow depth with h_{LAS} decreases uncertainty in flow depth, and leads to reasonable basinward trends of slope and discharge results. Hayden et al. (2019) also found discharge results generally more accurate when flow depth was better constrained. This is a useful tool to identify

spatial changes in ancient fluvial systems and help determine where dense minerals might be preferentially sorted along a transport pathway.

Overall, trends in the Undifferentiated Cutler Formation data indicate no correlation of paleohydraulics with detrital zircon grain size. This indicates that age spectra are also unaffected. The hydraulic boundary between Richardson Amphitheater and Parroitt Minibasin does not correlate with a change in detrital zircon grain size, indicating no effects of sorting. Most spatial variations in age spectra are not associated with shifts in bulk grain size or paleohydraulic trends, except at Paradox Valley and Moab Valley. These two locations have higher slope, lower discharge, larger detrital zircon grain size, a difference in grain size between the 1440 Ma and 1727 Ma age groups, and more abundant 1727 Ma grains than all other locations, indicating unique provenance or sorting of detrital zircon by winnowing the finer 1440 Ma age group downstream. Both samples from Moab Valley have the same range of zircon grain sizes present in the sample (0.067–0.214 mm). The lower sample at Moab Valley has coarser bulk sediment (D_{50} = 1.69 mm) than the upper sample, yet the lower sample has a higher proportion of the finer 1440 Ma age group (0.094 mm), indicating winnowing did not decrease the abundance of 1440 Ma zircon grains at Moab Valley.

Measured zircon size does not correlate with distance from the uplift, bulk sediment size, or hydraulic equivalent grain size, and does not decrease at the hydraulic boundary (between Richardson Amphitheater and Parroitt Minibasin) identified by bulk sediment grain size and reconstructed slope (Fig. 7; Table 11). At proximal sites, such as Paradox Valley and Gateway, 1727 Ma grains (0.160 mm) are larger than the 1440 Ma

(0.85 – 0.1 mm), respectively, and our settling equivalency models show that the conditions were sufficient to transport all zircons of those sizes. Significantly, our results predict that the system could have transported hypothetical zircons up to 3.74 mm, larger than any zircon except for pegmatitic crystals (Poldervaart, 1956). Because the fluvial system was capable of transport zircon grains much larger than were supplied by sediment sources, it is unlikely zircon would have been preferentially deposited and sorted based on grain size, and thus there would be minimal impact on detrital zircon U-Pb geochronologic results (Table 11). This means that in the proximal reaches of the fluvial system detrital zircons would not have been preferentially deposited because all zircons were capable of being transported, but unimodal age spectra are present because the proximal samples have unique provenance.

Integrating results from detrital zircon grain size, geochronologic data, and paleohydraulic conditions is key to investigating possible impacts of sorting in ancient strata, and a strength of this approach. For example, Lisbon Valley and Kane Springs locations are situated at similar distances from the UU and have similar slope and discharge values but have different bulk grain sizes and age signatures. Hydraulic equivalence results predict that Kane Springs should have larger detrital zircons but measured median zircon grain sizes are roughly the same at both locations (0.062–0.077 mm) and Rouse curves show all zircon was transported in the suspended load at both locations, indicating sorting did not fractionate age groups and cause differences in zircon grain size and age spectra. Our paleohydraulic results suggest that sorting is

65

unlikely to have affected age signatures between these two sites. In turn, this indicates these differences are more likely linked to different sediment provenance.

The Shields diagrams with Rouse curves provide a more nuanced view of flow competency that shows zircon might have been winnowed from the bed load, but zircon is present in the samples with bed load sediment, suggesting that the winnowing predicted from Shields diagrams does not always occur (Fig. 5 and 12). Based on results from the modified Shield's diagram, all locations could have winnowed detrital zircons because zircon grains were transported together in the suspended load and thus at a different rate compared to transport rate of bulk sediment, which would have been transported as mixed and bed loads when coarser than ca. 1.5 mm. However, field and flume results from modern fluvial systems are more equivocal than the Rouse curve model, showing that the grain size distribution of suspended, mixed, and bed load material significantly overlaps (Ghosh et al., 1986; Singer, 2008; Pfeiffer et al., 2017; Hajek et al., 2010; Wysocki, 2015). A key example from gravel-bedded fluvial channels are slackwater deposits. Although sand and finer sediment, including detrital zircon grains, comprise the majority of the total sediment load, it is carried in the suspended/wash load and winnowed downstream (Lamb and Venditti, 2016). Slackwater deposits formed by settling of suspended grains to the bed in the sheltered region of flow separation behind dunes and bars contain the silt and clay grain size fraction not present in the bed load and do not contain the gravel fraction that is present in the bed load (Hajek et al., 2010). Flow fluctuations, slackwater behind bars and large objects on the bed, and less exposure to the flow behind shielding objects on the bed causes suspended

material to be deposited on the bed in gravel-bedded channels, contributing to the formation of dense placer deposits in many gravel-bedded rivers (Kartashov, 1971; Slingerland, 1977, 1984; Best and Brayshaw, 1985; Hattingh and Rust, 1993; Hajek et al., 2010; Lynds et al., 2014; Viparelli et al., 2015; Wysocki, 2015). This means that grains predicted to be transported in different modes by Rouse curves may be deposited together in fluvial channels on the lee sides of bars and dunes and between gravel sized grains. The detrital zircons and fine fractions of the bulk sediment in Undifferentiated Cutler Formation samples were deposited and preserved with gravel- and sand-sized material in the cross-strata of bars and dunes, arguing against predictions of winnowing based on Rouse curves, and instead consistent with previous results emphasizing the overlap in grain size distributions between suspended loads and bed loads.

2.6.2. Sorting In Fine Grained Fluvial Systems

To give paleohydraulic calculations perspective, results are compared to the range of zircon sizes reported in literature. Typical zircon ESD grain size ranges reported in literature are between 0.03 mm and 0.31 mm (Poldervaart, 1956). The median grain length of nearly all zircon in igneous rocks is between 0.05 mm and 0.5 mm in length with a length to width ratio (elongation) of 2–3 for the medium to large size zircons, and elongation of 1–2 for the smallest zircon grains (Poldervaart, 1956; Markwitz et al., 2017). Pegmatitic zircon grows up to 19 cm long, but most are 0.1 – 0.5 mm long with elongation ratios of 2-4 (Poldervaart, 1956). Median grain length detrital zircon separated from sedimentary rocks are typically 0.05 – 0.5 mm, the same as in igneous rocks, but elongation varies because the length decreases downstream faster

than the width (Poldervaart, 1955; Lawrence et al., 2011; Markwitz et al., 2017). Studies that identified effects of sorting on provenance data in the Amazon River found zircon grains with ESD sizes of 0.035 – 0.25 mm deposited with very fine to coarse sand size bulk sediment, and in the Orinoco delta found zircon grains with mean ESD sizes of 0.075 – 0.22 mm (Lawrence et al., 2011; Ibañez-Mejia et al., 2018). Following these observations, the ESD of most zircon from igneous rocks and detrital zircon expected to be found in fluvial deposits is 0.03 – 0.31 mm, which provides a basis to evaluate the hydraulics of how zircons move major river systems.

The hydraulic equivalence method places a lower limit on the movable size of detrital zircon and predicts more sorting than the Rouse curves in sand- and silt-bedded rivers. Two sites where sorting has been proposed to impact detrital zircon U-Pb geochronology data is in the fine grained Amazon and Orinoco rivers (Lawrence et al., 2011; Ibañez-Mejia et al., 2018). Predictions from hydraulic equivalence methods in large, fine-grained fluvial systems with $D_{50} < 0.5$ mm, including the Amazon, Mississippi, Niger, Mekong, Parana, Brahmaputra, and Indus rivers (Trampush et al., 2014), suggest that those rivers would not transport 0.3 mm ESD zircon grains. However, Rouse curves predict that 0.3 mm zircon would still be transported in the mixed load with the bulk sediment because sand bedded rivers operate at a higher shear stress than the threshold shear stress for moving the median grain size (Fig. 5) (Singer, 2008; Wilkerson and Parker, 2011; Trampush et al., 2014; Pfeiffer et al., 2017). Ten rivers in the modern dataset have a $D_{50} < 0.062$ mm and hydraulic equivalence models predict they would not transport any zircon with an ESD larger than 0.035 mm, and

Rouse curves predict that they would not transport zircon larger than 0.2 mm in the same mode of transport as the bulk sediment (Fig. 5). The hydraulic inequivalence of silty bulk sediment and 0.2 mm detrital zircon is significant enough for them to be transported in different modes and could cause preferential deposition of large detrital zircon. Given the catchment area of Earth's major rivers, such as in the Amazon and Orinoco rivers, it is likely that a wide range of zircon grain sizes would be incorporated to the river system at some point from the hinterland source regions, increasing chance of sorting zircon grains larger than 0.2 mm from silty deposits (Lawrence et al., 2011; Ibañez-Mejia et al., 2018).

2.7. Conclusions

I review paleohydraulic reconstruction methods in the context of detrital zircon provenance studies. I demonstrate methodology by applying it ancient Undifferentiated Cutler Formation deposits in the Paradox Basin, and compare these results against reconstructions using measurements from modern rivers. A comparison between the modern measurements and our calculations for the same gravel- and sand-bedded modern rivers indicate that the reconstruction methods yield slope and discharge values that are consistent with modern values. Using the proportionally weighted method of grain size estimation (D_{50}) yields more accurate paleohydraulic reconstruction results than using grain size from thin section (D_{50fine}), emphasizing the importance of accurately characterizing the median grain size measurement of fluvial channel deposits (Eq. 1). Flow depths reconstructed from the height of lateral accretion surfaces (Eq. 2), and the lower limits of α and γ used to reconstruct depth from t_{set} (Eq. 3, 4), result in

values of reconstructed slope (Eq. 8), particle Reynolds number (Eq. 6), and Shields

Stress (Eq. 7) that are most consistent with reported modern river values (Trampush et

al., 2014). These methods applied to the Paradox Basin Undifferentiated Cutler

Formation system are sensitive enough to reveal spatial variance in flow conditions

when D_{50} is calculated using Eq. 1 and flow depth is constrained with measurements of

LAS (Fig. 7, 10).

Flow velocity calculated using the Hayden et al. (2019) methods (Eq. 9) is

overestimated at locations that have the lowest reconstructed grain size and slope, and

deepest flow depths in the transect (Fig. 8). Ferguson (2007) methods for flow velocity

reconstruction (Eq. 11, 12) consistently result in overestimated flow velocities across the

transect, and reveal no clear spatial flow velocity trends as slope decreases away from

the uplift. The calculation of the skin friction component of Shields stress is interpreted

to be the likely cause of anomalous results for flow velocity and channel discharge. The

Hayden et al. (2019) methods yield inaccurate flow velocity and a skin friction

component that is greater than total Shields Stress when grain size is finer than 0.5 mm

or coarser than 74 mm. Ferguson (2007) methods work best in systems with a flow depth

to D_{50} ratio (d/D_{50}) < 30, but the Cutler Group has d/D_{50} > 55. Flow velocity calculation

shows the limitations of these methods for identifying spatial changes in flow velocity

that would affect provenance data.

Sediment transported in suspended and bed loads are predicted to be transported

at different rates, yet are often deposited together in fluvial channels, and observed

together in ancient strata (Slingerland, 1977, 1984; Ghosh et al., 1986; Singer, 2008;

70

Hajek et al., 2010; Lynds et al., 2014; Wysocki, 2015). Particle Reynolds number and

Shields stress of measured data plotted on a modified Shields diagram with Rouse curves

indicate that modern gravel- and sand-bedded rivers transport the bulk sediment in bed

load and mixed load and detrital zircon in suspended and mixed load, indicating zircon

gets winnowed from the bed load (Trampush et al., 2014). Hydraulic equivalence

methods applied to Undifferentiated Cutler Formation fluvial deposits indicate that the

system was capable of moving the largest zircons from the UU (0.160 mm) at all sample

locations, and Rouse curves indicate that zircon grains would be transported in

suspension at all locations (Table 11, 12; Fig. 9). Sorting across the hydraulic boundary

between Richardson Amphitheater in the proximal basin and Castle Valley in the medial,

salt-deformed basin identified by grain size and slope reconstructions was not identified

by settling equivalency and Rouse curve methods, and, despite transport in different

modes, detrital zircon and sand-sized bulk sediment is still deposited with the coarser

fraction of sediment on the sediment bed. Winnowing of the suspended load did not sort

detrital zircon from the bulk sediment in the Undifferentiated Cutler Formation. Our

results indicate sorting did not affect detrital zircon age spectra, instead spatial variance

in age spectra is likely related to differences in sediment provenance.

Typical zircon in igneous and sedimentary rocks have an ESD grain size of 0.03

– 0.31 mm, and zircon larger than 0.2 mm is sorted from silty rivers (Poldervaart, 1955,

1956). When the bulk sediment D_{50} is finer than 0.062 mm, hydraulic equivalence

methods predict zircon grains larger than 0.035 mm would not be transported with the

bulk sediment. In contrast, Rouse curves predict that the bulk sediment and zircon

smaller than 0.2 mm would be transported in suspension with the bulk sediment, and zircon larger than 0.2 mm would be transported in the mixed mode and preferentially deposited (Fig. 5). The hydraulic equivalence method sets a much smaller limit on the size of zircon that would be transported with the silty bulk sediment, but both methods agree that zircon grains larger than 0.2 mm could be sorted from a silty bulk sediment. Detrital zircon age datasets are strengthened when reported with bulk sample grain size, dune or bar set thicknesses, and detrital zircon grain size. The integration of these data sets allows for more complete reconstruction of the transport system and identification of autogenic hydraulic sorting signals in detrital zircon age signatures in systems where they are present, leading to more confident interpretations of allogenic signals in provenance data.

2.8. References

Aronoff, R.F., Andronicos, C.L., Vervoort, J.D., and Hunter, R.A., 2016, Redefining the metamorphic history of the oldest rocks in the southern Rocky Mountains: Bulletin of the Geological Society of America, v. 128, p. 1207–1227, doi: 10.1130/B31455.1.

Barbeau, D.L., 2003, A flexural model for the Paradox Basin: Implications for the tectonics of the Ancestral Rocky Mountains: Basin Research, v. 15, p. 97–115, doi: 10.1046/j.1365-2117.2003.00194.x.

Best, J.L., and Brayshaw, A.C., 1985, Minerals Within Alluvial Channels: v. 142, p. 747–755.

Bickford, M.E., and Cudzilo, T.F., 1975, U-Pb age of zircon from Vernal Mesa-type

quartz monzonite, Unaweep Canyon, west-central Colorado: Bulletin of the
Geological Society of America, v. 86, p. 1432–1434, doi: 10.1130/0016-
7606(1975)86<1432:UAOZFV>2.0.CO;2.

Bonich, M.B., Samson, S.D., and Fedo, C.M., 2017, Incongruity of detrital zircon ages
of granitic bedrock and its derived alluvium: An example from the stepladder
mountains, Southeastern California: The Journal of Geology, v. 125, p. 337–350,
doi: 10.1086/691146.

Bradley, R.W., and Venditti, J.G., 2017, Reevaluating dune scaling relations: Earth-
Science Reviews, v. 165, p. 356–376, doi: 10.1016/j.earscirev.2016.11.004.

Bridge, J.S., 2009, Rivers and Floodplains: Forms, Processes, and Sedimentary Record:
John Wiley & Sons, 504 p.

Campbell, J.A., 1980, Lower Permian depositional systems and Wolfcampian
paleogeography, Uncomphagre Basin, eastern Utah and southwestern Colorado:
Paleozoic Paleogeography of the West-Central United States: Rocky Mountain
Paleogeography Symposium 1, v. 6, p. 327–340.

Cawood, P.A., Nemchin, A.A., Freeman, M., and Sircombe, K., 2003, Linking source
and sedimentary basin: Detrital zircon record of sediment flux along a modern river
system and implications for provenance studies: Earth and Planetary Science
Letters, v. 210, p. 259–268, doi: 10.1016/S0012-821X(03)00122-5.

Cheng, N.-S., 1997, Simplified Settling Velocity Formula for Sediment Particle: Journal
of Hydraulic Engineering, v. 123, p. 149–152, doi: 10.1061/(ASCE)0733-
9429(1997)123:2(149).

Condon, S.M., 1997, Geology of the Pennsylvanian and Permian Cutler Group and

    Permian Kaibab Limestone in the Paradox Basin, Southeastern Utah and

    Southwestern Colorado: U.S. Geological Survey Bulletin, p. 46,

    http://pubs.usgs.gov/bul/b2000p/b2000p.pdf.

Daniel, C.G., Pfeifer, L.S., Jones, J. V., and McFarlane, C.M., 2013, Detrital zircon

    evidence for non-Laurentian provenance, Mesoproterozoic (ca. 1490-1450 Ma)

    deposition and orogenesis in a reconstructed orogenic belt, northern New Mexico,

    USA: Defining the Picuris orogeny: Geological Society of America Bulletin, v.

    125, p. 1423–1441, doi: 10.1130/B30804.1.

Dickinson, W.R., and Gehrels, G.E., 2003, U–Pb ages of detrital zircons from Permian

    and Jurassic eolian sandstones of the Colorado Plateau, USA: paleogeographic

    implications: Sedimentary Geology, v. 163, p. 29–66, doi: 10.1016/S0037-

    0738(03)00158-1.

Dubiel, R.F., Huntoon, J.E., Stanesco, J.D., and Condon, S.M., 2009, Cutler Group

    Alluvial, Eolian, and Marine Deposystems: Permian Facies Relations and Climatic

    Variability in the Paradox Basin: Rocky Mountain Geologist, p. 265–308.

Engelund, F., and Hansen, E., 1967, A monograph on sediment transport in alluvial

    streams: Technical University of Denmark 0stervoldgade 10, Copenhagen K.,.

Fedele, J.J., and Paola, C., 2007, Similarity solutions for fluvial sediment fining by

    selective deposition: Journal of Geophysical Research, v. 112, p. F02038, doi:

    10.1029/2005JF000409.

Ferguson, R.I., 2003, Emergence of abrupt gravel to sand transitions along rivers

through sorting processes: Geology, v. 31, p. 159, doi: 10.1130/0091-7613(2003)031<0159:EOAGTS>2.0.CO;2.

Ferguson, R., 2007, Flow resistance equations for gravel- and boulder-bed streams: Water Resources Research, v. 43, p. 1–12, doi: 10.1029/2006WR005422.

Findlay, C., 2020a, "Paradox Basin - Cutler Group - Fluvial Bulk Sediment Grain Size Data", Texas Data Repository Dataverse, V1, https://doi.org/10.18738/T8/QBCUGG.

Findlay, C., 2020b, "Paradox Basin - Cutler Group - Fluvial and Aeolian Cross-stratification Set Thickness Data", Texas Data Repository Dataverse, V1, https://doi.org/10.18738/T8/IS4QM3.

Findlay, C., 2020c, "Paradox Basin - Cutler Group, Moenkopi Formation, and Chinle Formation - Detrital Zircon ICP-MS U-Th-Pb Data", Texas Data Repository Dataverse, V1, https://doi.org/10.18738/T8/C13S4H.

Findlay, C., 2020d, "Paradox Basin - Cutler Group and Chinle Formation - Detrital Zircon Grain Size and Age Data", Texas Data Repository Dataverse, V1, https://doi.org/10.18738/T8/0VVUBO.

Garzanti, E., Andò, S., and Vezzoli, G., 2009, Grain-size dependence of sediment composition and environmental bias in provenance studies: Earth and Planetary Science Letters, v. 277, p. 422–432, doi: 10.1016/j.epsl.2008.11.007.

Garzanti, E., Andò, S., and Vezzoli, G., 2008, Settling equivalence of detrital minerals and grain-size dependence of sediment composition: Earth and Planetary Science Letters, v. 273, p. 138–151, doi: 10.1016/j.epsl.2008.06.020.

Gehrels, G.E., Butler, R.F., and Bazard, D.R., 1996, Detrital zircon geochronology of the

    Alexander terrane, southeastern Alaska: GSA Bulletin, v. 108, p. 722–734, doi:

    10.1130/0016-7606(1996)108<0722:DZGOTA>2.3.CO;2.

Ghosh, J.K., Mazumder, B.S., and Saha, M.R., 1986, Deposition of Sand by Suspension

    Currents: Experimental and Theoretical Studies: SEPM Journal of Sedimentary

    Research, v. Vol. 56, p. 57–66, doi: 10.1306/212F8882-2B24-11D7-

    8648000102C1865D.

Hajek, E.A., Heller, P.L., and Schur, E.L., 2012, Field test of autogenic control on

    alluvial stratigraphy (Ferris Formation, Upper Cretaceous-Paleogene, Wyoming):

    Bulletin of the Geological Society of America, v. 124, p. 1898–1912, doi:

    10.1130/B30526.1.

Hajek, E.A., Huzurbazar, S. V., Mohrig, D., Lynds, R.M., and Heller, P.L., 2010,

    Statistical Characterization of Grain-Size Distributions in Sandy Fluvial Systems:

    Journal of Sedimentary Research, v. 80, p. 184–192, doi: 10.2110/jsr.2010.020.

Hattingh, J., and Rust, I.C., 1993, Flood transport and deposition of tracer heavy

    minerals in a gravel- bed meander bend channel: Journal of Sedimentary Petrology,

    v. 63, p. 828–834, doi: 10.1306/D4267C17-2B26-11D7-8648000102C1865D.

Hayden, A.T., Lamb, M.P., Fischer, W.W., Ewing, R.C., McElroy, B.J., and Williams,

    R.M.E., 2019, Formation of sinuous ridges by inversion of river-channel belts in

    Utah, USA, with implications for Mars: Icarus, v. 332, p. 92–110, doi:

    10.1016/j.icarus.2019.04.019.

Hietpas, J., Samson, S., Moecher, D., and Chakraborty, S., 2011, Enhancing tectonic and

provenance information from detrital zircon studies: assessing terrane-scale

sampling and grain-scale characterization: Journal of the Geological Society, v.

168, p. 309–318, doi: 10.1144/0016-76492009-163.

Ibañez-Mejia, M., Pullen, A., Pepper, M., Urbani, F., Ghoshal, G., and Ibañez-Mejia,

J.C., 2018, Use and abuse of detrital zircon U-Pb geochronology—A case from the

Río Orinoco delta, eastern Venezuela: Geology, v. 46, p. 1019–1022, doi:

10.1130/G45596.1.

Ireland, T.R., Flöttmann, T., Fanning, C.M., Gibson, G.M., and Preiss, W. V., 1998,

Development of the early Paleozoic Pacific margin of Gondwana from detrital-

zircon ages across the Delamerian orogen: Geology, v. 26, p. 243, doi:

10.1130/0091-7613(1998)026<0243:DOTEPP>2.3.CO;2.

Jerolmack, D.J., and Brzinski, T.A., 2010, Equivalence of abrupt grain-size transitions in

alluvial rivers and eolian sand seas: A hypothesis: Geology, v. 38, p. 719–722, doi:

10.1130/G30922.1.

Jessup, M.J., Jones III, J. V., Karlstrom, K.E., Williams, M.L., Connelly, J.N., and

Heizler, M.T., 2006, Three Proterozoic Orogenic Episodes and an Intervening

Exhumation Event in the Black Canyon of the Gunnison Region, Colorado: The

Journal of Geology, v. 114, p. 555–576, doi: 10.1086/506160.

Jones, J. V., Connelly, J.N., Karlstrom, K.E., Williams, M.L., and Doe, M.F., 2009, Age,

provenance, and tectonic setting of Paleoproterozoic quartzite successions in the

southwestern United States: Bulletin of the Geological Society of America, v. 121,

p. 247–264, doi: 10.1130/B26351.1.

77

Kartashov, I., 1971, Geological features of alluvial placers: Economic Geology, v. 66, p. 879–885, doi: 10.2113/gsecongeo.66.6.879.

Knott, J.R., Fantozzi, J.M., Ferguson, K.M., Keller, S.E., Nadimi, K., Rath, C.A., Tarnowski, J.M., and Vitale, M.L., 2012, Paleowind velocity and paleocurrents of pluvial Lake Manly, Death Valley, USA: Quaternary Research (United States), v. 78, p. 363–372, doi: 10.1016/j.yqres.2012.06.007.

Kock, S., Martini, R., Reischmann, T., and Stampfli, G.M., 2007, Detrital zircon and micropalaeontological ages as new constraints for the lowermost tectonic unit (Talea Ori unit) of Crete, Greece: Palaeogeography, Palaeoclimatology, Palaeoecology, v. 243, p. 307–321, doi: 10.1016/j.palaeo.2006.08.006.

Komar, P.D., and Reimers, C.E., 1978, Grain Shape Effects on Settling Rates: The Journal of Geology, v. 86, p. 193–209, doi: 10.1086/649674.

Lamb, M.P., and Venditti, J.G., 2016, The grain size gap and abrupt gravel-sand transitions in rivers due to suspension fallout: Geophysical Research Letters, v. 43, p. 3777–3785, doi: 10.1002/2016GL068713.

Lawrence, R.L., Cox, R., Mapes, R.W., and Coleman, D.S., 2011, Hydrodynamic fractionation of zircon age populations: Geological Society of America Bulletin, v. 123, p. 295–305, doi: 10.1130/B30151.1.

Lawton, T.F., Buller, C.D., and Parr, T.R., 2015, Provenance of a Permian erg on the western margin of Pangea: Depositional system of the Kungurian (late Leonardian) Castle Valley and White Rim sandstones and subjacent Cutler Group, Paradox Basin, Utah, USA: Geosphere, v. 11, p. 1475–1506, doi: 10.1130/GES01174.1.

Leary, R.J., Umhoefer, P., Smith, M.E., Smith, T.M., Saylor, J.E., Riggs, N., Burr, G., Lodes, E., Foley, D., Licht, A., Mueller, M.A., and Baird, C., 2020, Provenance of Pennsylvanian–Permian sedimentary rocks associated with the Ancestral Rocky Mountains orogeny in southwestern Laurentia: Implications for continental-scale Laurentian sediment transport systems: Lithosphere, v. 12, p. 88–121, doi: 10.1130/L1115.1.

Leclair, S.F., and Bridge, J.S., 2001, Quantitative Interpretation of Sedimentary Structures Formed by River Dunes: Journal of Sedimentary Research, v. 71, p. 713–716, doi: 10.1306/2DC40962-0E47-11D7-8643000102C1865D.

Link, P.K., Fanning, C.M., and Beranek, L.P., 2005, Reliability and longitudinal change of detrital-zircon age spectra in the Snake River system, Idaho and Wyoming: An example of reproducing the bumpy barcode: Sedimentary Geology, v. 182, p. 101–142, doi: 10.1016/j.sedgeo.2005.07.012.

Livaccari, R., Bowring, T.J., Farmer, E.T., Garhart, K.S., Hosack, A.M., Scott, R.B., and Unruh, D., 2001, Proterozoic Rocks of the Uncompahgre Plateau , Western Colorado and Eastern Utah: Geological Society of America Abstracts with Programs, v. 33, p. 44.

Lynds, R.M., Mohrig, D., Hajek, E.A., and Heller, P.L., 2014, Paleoslope Reconstruction In Sandy Suspended-Load-Dominant Rivers: Journal of Sedimentary Research, v. 84, p. 825–836, doi: 10.2110/jsr.2014.60.

Mack, G.H., and Rasmussen, K.A., 1984, Alluvial- fan sedimentation of the Cutler Formation (Permo- Pennsylvanian) near Gateway, Colorado (USA).: Geological

Society of America Bulletin, v. 95, p. 109–116, doi: 10.1130/0016-7606(1984)95<109:ASOTCF>2.0.CO;2.

Malusà, M.G., Resentini, A., and Garzanti, E., 2016, Hydraulic sorting and mineral fertility bias in detrital geochronology: Gondwana Research, v. 31, p. 1–19, doi: 10.1016/j.gr.2015.09.002.

Markwitz, V., Kirkland, C.L., Mehnert, A., Gessner, K., and Shaw, J., 2017, 3-D Characterization of Detrital Zircon Grains and its Implications for Fluvial Transport, Mixing, and Preservation Bias: Geochemistry, Geophysics, Geosystems, v. 18, p. 4655–4673, doi: 10.1002/2017GC007278.

Martin, R.L., and Jerolmack, D.J., 2013, Origin of hysteresis in bed form response to unsteady flows: Water Resources Research, v. 49, p. 1314–1333, doi: 10.1002/wrcr.20093.

Miall, A.D., 1996, The Geology of Fluvial Deposits: Sedimentary Facies, Basin Analysis, and Petroleum Geology: 582 p.

Middleton, G. V., and Southard, J.B., 1984, Mechanics of sediment movement: SEPM Short Course, v. 3.

Miller, K.L., Szabó, T., Jerolmack, D.J., and Domokos, G., 2014, Quantifying the significance of abrasion and selective transport for downstream fluvial grain size evolution: Journal of Geophysical Research: Earth Surface, v. 119, p. 2412–2429, doi: 10.1002/2014JF003156.

Mohrig, D., Heller, P.L., and Lyons, W.J., 2000, Guadalope-Matarranya system (northern Spain) and Wasatch Formation (western Colorado): Geological Soceity of

America Bulletin, v. 112, p. 1787–1803, doi: 10.1130/0016-7606(2000)112<1787:IAPFAA>2.0.CO;2.

Mose, D.G., and Bickford, M.E., 1969, Precambrian geochronology in the Unaweep Canyon, west-central Colorado: Journal of Geophysical Research, v. 74, p. 1677–1687, doi: 10.1029/JB074i006p01677.

Nittrouer, J.A., Mohrig, D., Allison, M.A., and Peyret, A.P.B., 2011, The lowermost Mississippi River: A mixed bedrock-alluvial channel: Sedimentology, v. 58, p. 1914–1934, doi: 10.1111/j.1365-3091.2011.01245.x.

Olson, J.C.C., Marvin, R.F.F., Parker, R.L.L., and Mehnert, H.H.H., 1977, Age and tectonic setting of lower Paleozoic alkalic and mafic rocks, carbonatites, and thorium veins in south-central Colorado: US Geological Survey Journal of Research, v. 5, p. 673–687.

Paola, C., and Borgman, L., 1991, Reconstructing random topography from preserved stratification: Sedimentology, v. 38, p. 553–565, doi: 10.1111/j.1365-3091.1991.tb01008.x.

Paola, C., and Mohrig, D., 1996, Palaeohydraulics revisited: palaeoslope estimation in coarse-grained braided rivers: Basin Research, v. 8, p. 243–254, doi: 10.1046/j.1365-2117.1996.00253.x.

Parker, G., 1991a, Selective Sorting and Abrasion of River Gravel. I: Theory: Journal of Hydraulic Engineering, v. 117, p. 131–147, doi: 10.1061/(ASCE)0733-9429(1991)117:2(131).

Parker, G., 1991b, Selective Sorting and Abrasion of River Gravel. II: Applications:

Journal of Hydraulic Engineering, v. 117, p. 150–171, doi: 10.1061/(ASCE)0733-9429(1991)117:2(150).

Parker, G., Wilcock, P.R., Paola, C., Dietrich, W.E., and Pitlick, J., 2007, Physical basis for quasi-universal relations describing bankfull hydraulic geometry of single-thread gravel bed rivers: Journal of Geophysical Research: Earth Surface, v. 112, p. 1–21, doi: 10.1029/2006JF000549.

Pfeiffer, A.M., Finnegan, N.J., and Willenbring, J.K., 2017, Sediment supply controls equilibrium channel geometry in gravel rivers: Proceedings of the National Academy of Sciences, v. 114, p. 3346–3351, doi: 10.1073/pnas.1612907114.

Poldervaart, A., 1956, Zircon in rocks; Part 2, Igneous rocks: American Journal of Science, v. 254, p. 521–554, doi: 10.2475/ajs.254.9.521.

Poldervaart, A., 1955, Zircons in rocks; Part 1, Sedimentary rocks: American Journal of Science, v. 253, p. 433–461, doi: 10.2475/ajs.253.8.433.

Rainbird, R.H., Hearnan, L.M., and Young, G., 1992, Sampling Laurentia: Detrital zircon geochronology offers evidence for an extensive Neoproterozoic river system originating from the Grenville orogen: Geology, v. 20, p. 351, doi: 10.1130/0091-7613(1992)020<0351:SLDZGO>2.3.CO;2.

Rasmussen, D.L., 2009, Road Logs Across the Uncompahgre Uplift and the Deep Fold and Fault Belt, Northern Paradox Basin, Colorado and Utah: RMAG Special Publication, v. The Parado, p. 691–778.

Saylor, J.E., Jordan, J.C., Sundell, K.E., Wang, X., Wang, S., and Deng, T., 2018, Topographic growth of the Jishi Shan and its impact on basin and hydrology

evolution, NE Tibetan Plateau: Basin Research, v. 30, p. 544–563, doi:
10.1111/bre.12264.

Saylor, J.E., and Sundell, K.E., 2016, Quantifying comparison of large detrital
geochronology data sets: Geosphere, v. 12, p. 203–220, doi: 10.1130/GES01237.1.

Saylor, J.E., Sundell, K.E., and Sharman, G.R., 2019, Characterizing sediment sources
by non-negative matrix factorization of detrital geochronological data: Earth and
Planetary Science Letters, v. 512, p. 46–58, doi: 10.1016/j.epsl.2019.01.044.

Schindelin, J., Arganda-Carreras, I., Frise, E., Kaynig, V., Longair, M., Pietzsch, T.,
Preibisch, S., Rueden, C., Saalfeld, S., Schmid, B., Tinevez, J.-Y., White, D.J.,
Hartenstein, V., Eliceiri, K., et al., 2012, Fiji: an open-source platform for
biological-image analysis: Nature Methods, v. 9, p. 676–682, doi:
10.1038/nmeth.2019.

Schoene, B., and Bowring, S.A., 2006, U–Pb systematics of the McClure Mountain
syenite: thermochronological constraints on the age of the 40Ar/39Ar standard
MMhb: Contributions to Mineralogy and Petrology, v. 151, p. 615–630, doi:
10.1007/s00410-006-0077-4.

Sharman, G.R., Sharman, J.P., and Sylvester, Z., 2018, detritalPy: A Python-based
toolset for visualizing and analysing detrital geo-thermochronologic data: The
Depositional Record, v. 4, p. 202–215, doi: 10.1002/dep2.45.

Singer, M.B., 2008, Downstream patterns of bed material grain size in a large, lowland
alluvial river subject to low sediment supply: Water Resources Research, v. 44, p.
1–7, doi: 10.1029/2008WR007183.

Sircombe, K.N., Bleeker, W., and Stern, R.A., 2001, Detrital zircon geochronology and
grain-size analysis of a ~2800 Ma Mesoarchean proto-cratonic cover succession,
Slave Province, Canada: Earth and Planetary Science Letters, v. 189, p. 207–220,
doi: 10.1016/S0012-821X(01)00363-6.

Slingerland, R.L., 1984, Role of Hydraulic Sorting in the Origin of Fluvial Placers:
SEPM Journal of Sedimentary Research, v. Vol. 54, p. 137–150, doi:
10.1306/212F83C8-2B24-11D7-8648000102C1865D.

Slingerland, R.L., 1977, The Effects of Entrainment on the Hydraulic Equivalence
Relationships of Light and Heavy Minerals in Sands: SEPM Journal of Sedimentary
Research, v. Vol. 47, p. 753–770, doi: 10.1306/212F7243-2B24-11D7-
8648000102C1865D.

Soreghan, G.S., Soreghan, M.J., Sweet, D.E., and Moore, K.D., 2009, Hot Fan or Cold
Outwash? Hypothesized Proglacial Deposition in the Upper Paleozoic Cutler
Formation, Western Tropical Pangea: Journal of Sedimentary Research, v. 79, p.
495–522, doi: 10.2110/jsr.2009.055.

Stewart, J.H., Gehrels, G.E., Barth, A.P., Link, P.K., Christie-Blick, N., and Wrucke,
C.T., 2001, Detrital zircon provenance of Mesoproterozoic to Cambrian arenites in
the western United States and northwestern Mexico: Geological Society of America
Bulletin, v. 113, p. 1343–1356, doi: 10.1130/0016-
7606(2001)113<1343:DZPOMT>2.0.CO;2.

Trampush, S.M., Huzurbazar, S., and McElroy, B., 2014, Empirical assessment of theory
for bankfull characteristics of alluvial channels: Water Resources Research, v. 50,

p. 9211–9220, doi: 10.1002/2014WR015597.

Trudgill, B.D., 2011, Evolution of salt structures in the northern Paradox Basin: controls on evaporite deposition, salt wall growth and supra-salt stratigraphic architecture: Basin Research, v. 23, p. 208–238, doi: 10.1111/j.1365-2117.2010.00478.x.

Venus, J.H., Mountney, N.P., and Mccaffrey, W.D., 2015, Syn-sedimentary salt diapirism as a control on fluvial-system evolution: An example from the proximal Permian Cutler Group, SE Utah, USA: Basin Research, v. 27, p. 152–182, doi: 10.1111/bre.12066.

Vermeesch, P., and Garzanti, E., 2015, Making geological sense of "Big Data" in sedimentary provenance analysis: Chemical Geology, v. 409, p. 20–27, doi: 10.1016/j.chemgeo.2015.05.004.

Vermeesch, P., Resentini, A., and Garzanti, E., 2016, An R package for statistical provenance analysis: Sedimentary Geology, v. 336, p. 14–25, doi: 10.1016/j.sedgeo.2016.01.009.

Viparelli, E., Solari, L., and Hill, K.M., 2015, Downstream lightening and upward heavying: Experiments with sediments differing in density (D. Mohrig, Ed.): Sedimentology, v. 62, p. 1384–1407, doi: 10.1111/sed.12187.

Wentworth, C.K., 1922, A Scale of Grade and Class Terms for Clastic Sediments: The Journal of Geology, v. 30, p. 377–392, doi: 10.1086/622910.

Whitmeyer, S.J., and Karlstrom, K.E., 2007, Tectonic model for the Proterozoic growth of North America: Geosphere, v. 3, p. 220–259, doi: 10.1130/GES00055.1.

Wilkerson, G. V., and Parker, G., 2011, Physical Basis for Quasi-Universal

Relationships Describing Bankfull Hydraulic Geometry of Sand-Bed Rivers: Journal of Hydraulic Engineering, v. 137, p. 739–753, doi: 10.1061/(ASCE)HY.1943-7900.0000352.

Williams, R.M.E., Irwin, R.P., and Zimbelman, J.R., 2009, Evaluation of paleohydrologic models for terrestrial inverted channels: Implications for application to martian sinuous ridges: Geomorphology, v. 107, p. 300–315, doi: 10.1016/j.geomorph.2008.12.015.

Wissink, G.K., and Hoke, G.D., 2016, Eastern margin of Tibet supplies most sediment to the Yangtze River: Lithosphere, v. 8, p. 601–614, doi: 10.1130/L570.1.

Wissink, G.K., Hoke, G.D., Garzione, C.N., and Liu-Zeng, J., 2016, Temporal and spatial patterns of sediment routing across the southeast margin of the Tibetan Plateau: Insights from detrital zircon: Tectonics, v. 35, p. 2538–2563, doi: 10.1002/2016TC004252.

Wohl, E.E., Anthony, D.J., Madsen, S.W., and Thompson, D.M., 1996, A comparison of surface sampling methods for coarse fluvial sediments: Water Resources Research, v. 32, p. 3219–3226, doi: 10.1029/96WR01527.

Wolman, M.G., 1954, A method of sampling coarse river-bed material: Transactions, American Geophysical Union, v. 35, p. 951, doi: 10.1029/TR035i006p00951.

Wu, Y., and Zheng, Y., 2004, Genesis of zircon and its constraints on interpretation of U-Pb age: Chinese Science Bulletin, v. 49, p. 1554–1569, doi: 10.1007/BF03184122.

Wysocki, N.P., 2015, Fine Sediment Deposition and Storage in Sandy-Fluvial Systems:

The Pennsylvania State University, 1–74 p.

Yang, S., Zhang, F., and Wang, Z., 2012, Grain size distribution and age population of
detrital zircons from the Changjiang (Yangtze) River system, China: Chemical
Geology, v. 296–297, p. 26–38, doi: 10.1016/j.chemgeo.2011.12.016.

3. IDENTIFYING FRACTIONATION OF DETRITAL ZIRCON AGE GROUPS IN ANCIENT FLUVIAL DEPOSITS, PART II: ALLOGENIC AND AUTOGENIC INFLUENCES ON THE PERMIAN UNDIFFERENTIATED CUTLER FORMATION FLUVIAL SYSTEM – PARADOX BASIN, UT AND CO

3.1. Introduction

Understanding sediment dispersal patterns across basins and continents is essential to reconstructing the tectonic, depositional, and climate conditions that shape modern and ancient landscapes. Sediment provenance techniques, including detrital zircon U-Pb geochronology, are a primary means to identify the spatial and temporal shifts in dispersal patterns that may reflect changes in tectonic, depositional, and climate conditions. Shifts in sediment provenance results are typically associated with allogenic processes acting on sedimentary basins, including tectonic, climatic, and eustatic events (Ireland et al., 1998; Cawood et al., 2013; Gehrels et al., 2011; Gehrels and Pecha, 2014; Blum et al., 2018; Nair et al., 2018; Jackson et al., 2019; Mason et al., 2019; Sharman et al., 2019). Many sediment provenance shifts may also be linked to system boundary conditions, such as zircon fertility and exposure area of parent rocks in the catchment (Amidon et al., 2005a, 2005b; Moecher and Samson, 2006; Dickinson, 2008; Capaldi et al., 2017). Sediment provenance can also be affected by autogenic processes, such as fractionation by hydraulic sorting during transport in fluvial systems (Hietpas et al., 2011; Lawrence et al., 2011; Yang et al., 2012; Bonich et al., 2017; Ibañez-Mejia et al., 2018). Recognizing the interplay between allogenic and autogenic processes in

sedimentary basin development remains challenging but has implications for sediment routing in ancient and modern systems, paleogeographic reconstructions, and can improve tools for characterization and correlation of subsurface petroleum and water reservoirs.

Combining detrital zircon geochronology with paleohydraulic reconstruction helps distinguish signals of hydraulic sorting and changes in sediment provenance in ancient fluvial systems. Paleocurrent direction depth, slope, velocity, discharge, settling equivalence, particle Reynolds number, and Shields number calculations can be used to characterize spatial changes in transport conditions and identify sites along ancient fluvial systems where hydraulic sorting of detrital zircon may have occurred (Ferguson, 2007; Garzanti et al., 2008; Trampush et al., 2014; Hayden et al., 2019).(Paola and Borgman, 1991; Leclair and Bridge, 2001; Mohrig et al., 2000; Hajek and Heller, 2012; Bradley and Venditti, 2017; Hayden et al., 2019; Paola and Mohrig, 1996; Lynds et al., 2014; Ferguson, 2007; Garzanti et al., 2008)(Paola and Borgman, 1991; Leclair and Bridge, 2001; Mohrig et al., 2000; Hajek and Heller, 2012; Bradley and Venditti, 2017; Hayden et al., 2019; Paola and Mohrig, 1996; Lynds et al., 2014; Ferguson, 2007; Garzanti et al., 2008) Paleohydraulic reconstruction techniques synthesized in Findlay et al. (in review) were applied to the Undifferentiated Cutler Formation fluvial system in the foredeep of the Paradox Basin of UT and CO. That paper demonstrates that the observed spatial and vertical variations in fluvial detrital zircon U-Pb geochronologic results (Lawton et al., 2015; Leary et al., 2020) cannot be attributed by hydraulic sorting. This study integrates detrital zircon grain size, detrital zircon U-Pb geochronologic

89

results, multidimensional scaling (MDS) statistical analysis, and paleocurrent direction analysis to investigate how those spatial and vertical patterns of detrital zircon age spectra from the Undifferentiated Cutler Formation instead reflect contributions from fluvial processes, active salt deformation, and catchment evolution.

3.2. Background

3.2.1. Tectonic Setting

The Pennsylvanian–Permian Paradox Basin subsided as a broken plate foreland basin adjacent to the Uncompahgre Uplift (UU), a reverse fault-bounded basement block uplifted approximately 5 km during Late Paleozoic Ancestral Rocky Mountain (ARM) deformation (Fig. 14) (Yang and Dorobek, 1995; Hoy and Ridgway, 2002; Barbeau, 2003; Condon, 1997; Kluth and Duchene, 2009). The ARM created a series of Pennsylvanian–Permian basement uplifts adjacent to intracontinental flexural basins in western USA that deformed coeval with other significant deformational events in Laurentia: the compressional Marathon-Ouachita orogeny on the eastern and southeastern margins of Laurentia (Kluth and Coney, 1981; Hatcher, 1987; Keller and Hatcher, 1999); transpressional deformation on the southwestern margin (Leary et al., 2017); and possibly, shortening along the western margin of Laurentia shortly after the Late Mississippian termination of the Antler orogeny (Speed and Sleep, 1982; Ye et al., 1996). Proterozoic metasedimentary and granite basement zircon U-Pb ages of the UU and the greater Utah, Colorado and New Mexico region reflect 503–583 Ma alkali intrusions, 1300–1500 Ma magmatism of the Granite–Rhyolite province, 1400–1490 Ma deformation during the Picuris orogeny, and 1600–1860 Ma deformation during the

Yavapai–Mazatzal orogeny (Mose and Bickford, 1969; Bickford and Cudzilo, 1975;

Olson et al., 1977; Livaccari et al., 2001; Jessup et al., 2006; Schoene and Bowring,

2006; Whitmeyer and Karlstrom, 2007; Jones et al., 2009; Daniel et al., 2013; Aronoff et

al., 2016).
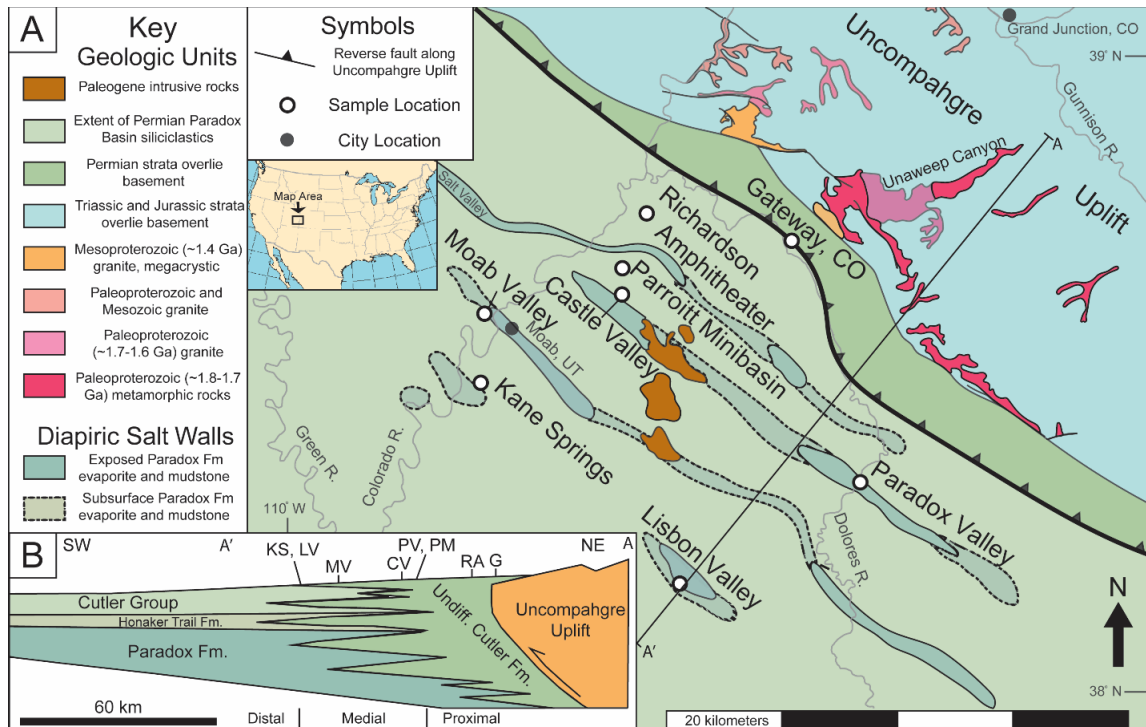
Figure 14: Geologic map and schematic cross-section of the study area shows the Paradox Basin in southeast UT and southwest CO. A) Map of the Permian Paradox Basin with modern rivers, towns, and Triassic cover on Uncompahgre Uplift basement (UU). Anticlines in the medial basin are salt walls created by movement of the Paradox salt and expose the Undifferentiated Cutler Formation on their flanks and along their axis where the salt core has been eroded (after Lawton et al., 2015). B) Schematic cross-section (A – A') of the Paradox Basin showing the proximal, medial, and distal regions of the foredeep (after Barbeau, 2003). Sample locations: G – Gateway, CO; PV – Paradox Valley; PM – Parroitt Minibasin; RA – Richardson Amphitheater; CV – Castle Valley; MV – Moab Valley; LV – Lisbon Valley; KS – Kane Springs.

3.2.2. Stratigraphic And Depositional Overview

Sedimentation in the Paradox Basin began in the Pennsylvanian. Deposition of marine and coastal carbonate, shale, and evaporite successions that comprise the Paradox Formation was followed by deposition of carbonate, siliciclastic mudstone, and calcarenite of the Honaker Trail Formation. In the proximal foredeep, up to ca. 5 km of fluvial deposits are preserved as the Undifferentiated Cutler Formation (Condon, 1997; Barbeau, 2003; Trudgill, 2011). The 50–530 m thick early Permian Cutler Group overlies the Honaker Trail Formation in the medial–distal foredeep and forebulge, and interfingers with the Undifferentiated Cutler in the proximal foredeep (Condon, 1997; Dubiel et al., 2009; Lawton et al., 2015). In stratigraphic order, the Cutler Group is divided into the Lower Cutler, fluvial-aeolian Cedar Mesa, fluvial-aeolian Organ Rock, and aeolian White Rim formations (Condon, 1997; Dubiel et al., 2009; Lawton et al., 2015). The Undifferentiated Cutler Formation fluvial system has been variably described as either three megafans draining the Uncompahgre Uplift (UU), or as an axial transport system fed by a line source of fans exiting the UU and directed and partitioned by salt-cored anticlines (Campbell and Steele-Mallory, 1979; Campbell, 1980; Mack and Rasmussen, 1984; Cain and Mountney, 2009; Trudgill, 2011; Lawton et al., 2015; Venus et al., 2015).

In most of the basin, the Cutler Group and Undifferentiated Cutler Formation are unconformably overlain by the Early–Middle Triassic Moenkopi Formation, but is overlain by the Late Triassic Chinle Formation where the Moenkopi is not present (Condon, 1997; Dubiel et al., 2009; Rasmussen, 2009). The base of the Moenkopi is

defined by a conglomerate dominated by chert or carbonate clasts across much of the basin, a gypsum bed (1–2 meters) at Castle Valley, Utah, and a gypsiferous unit with abundant gypsum veins at Gateway, Colorado (Condon, 1997; Rasmussen, 2009). Pre-existing basement structures in the Paradox Basin caused variation in thickness of Pennsylvanian Paradox Formation salt, and guided the position of salt walls and associated mini-basins above and adjacent to the structures during Permian or Triassic deposition (Trudgill, 2011; Banham and Mountney, 2013).

In salt-walled mini-basins, subsidence is accelerated by salt withdrawal caused by sediment loading in the mini-basin depocenters, which can create surface topography on the flanks of the mini-basins that affect sedimentation by rerouting fluvial systems (Hudec et al., 2009; Trudgill, 2011; Banham and Mountney, 2013; Venus et al., 2015). The Permian Undifferentiated Cutler Formation fluvial system flowed over a mobile substrate of the evaporite-rich Paradox Formation, resulting in development of salt walls that breached the surface during deposition (Trudgill and Paz, 2009; Trudgill, 2011; Venus et al., 2015). Varying paleocurrent directions and thickness variations of the Undifferentiated Cutler Formation in the salt-deformed region of the basin suggest that halokinesis influenced the fluvial system (Venus et al., 2015).

3.3. Methods

3.3.1. Experiment Design

The Paradox Basin and the Undifferentiated Cutler Formation are an ideal setting to assess the potential contributions from autogenic and allogenic processes on resulting sediment composition across a basin and through time. Previous detrital zircon U-Pb

geochronologic studies on the Cutler Group demonstrate the prominence of two age

peaks at 1440 Ma and 1721 Ma across the basin. In select sites, such as near Durango

and Ouray, CO, a third age peak at 520 Ma is observed in the western basin at Castle

Valley and Gateway, CO (Lawton et al., 2015; Leary et al., 2020) (Fig. 14). These 3 age

groups are present in the UU and ARM uplifts that are the dominant sediment source for

the Paradox Basin. However, subtle variations in presence and abundance of age modes

are observed spatially across the basin, and vertically through successions at some sites.

This study leverages the known diagnostic age signals from the UU with recent results

from paleohydraulic reconstructions as tools to unravel how two contrasting proposed

models for the depositional environment, and changes in fluvial catchments draining the

UU are expressed in strata of the Paradox Basin. This design tests the role of autogenic

and allogenic processes in basin development and fluvial deposition.

Contrasting interpretations of fluvial style of the Undifferentiated Cutler

Formation set up two hypotheses regarding spatial variations in sediment provenance

that can be tested with detrital zircon U-Pb geochronology. Detrital zircon age signatures

in the basin can vary spatially in both fluvial models, but for different reasons. In the fan

model, sediment is derived from a single watershed and delivered to the basin via point

source. Although the fan has a single sediment source, downstream changes in sediment

provenance datasets, if they occur, would be attributed to autogenic sorting, rather than

true shifts in sediment provenance. In the axial model, spatial variance in sediment

provenance datasets could be linked to autogenic sorting, but can also be driven by a

combination of allogenic processes, including salt deformation that can partition mini-

94

basins and redirect different fluvial systems (and sediment derived from their respective

catchments) into different depocenters, as well as changed to the configuration and

exposure of rock units within the catchments. This study tests these hypotheses using

integrated sediment provenance and paleohydraulic reconstruction approaches and

evaluates the paleogeographic implications of the models.

The study area is in the western Paradox Basin and extends from proximal

deposits at Gateway, CO where the Undifferentiated Cutler Formation overlies UU

basement rock, to the salt-deformed medial basin where the Undifferentiated Cutler

Formation is exposed on the flanks of salt-cored (Paradox Formation) anticlines at

Paradox Valley, Castle Valley, Moab Valley, Kane Springs, and Lisbon Valley (Fig. 14).

Sample locations cover an area of Undifferentiated Cutler deposits described as both

megafan and axial deposits (Campbell and Steele-Mallory, 1979; Campbell, 1980; Mack

and Rasmussen, 1984; Cain and Mountney, 2009; Trudgill, 2011; Lawton et al., 2015;

Venus et al., 2015). The proximity to salt-cored anticlines provides an opportunity to test

how halokinesis influenced the fluvial system. Three stratigraphic markers are used

across the basin to identify a relatively time-correlative spatial transect in this study. The

fluvial and aeolian rocks in this study are situated below the contact with the White Rim

and Moenkopi Formations and above the Lower Cutler Formation. The contact with the

Moenkopi Formation is an erosional unconformity and is not strictly time-correlative

and represents the most distinctive lithostratigraphic marker available. Our measured

sections and samples are chronostratigraphically correlative with the Cedar Mesa and

Organ Rock formations according to seismic interpretations and outcrop interpretations (Cain and Mountney, 2009; Trudgill, 2011; Venus et al., 2015; Allred, 2016).

3.3.2. Sampling

Samples were collected at sites situated along a NE-SW transect across the Paradox Basin, and discussed in detail in a companion manuscript . This transect spanned proximal deposits at Gateway, CO to medial deposits at Kane Springs and Lisbon Valley, UT. These sites were selected to capture a range of grain sizes, including gravel- and sand-bedded channels. Eight measured stratigraphic sections (25 m to 300 m thick) and 13 samples (10 for paleohydraulic reconstruction, 9 of which were also used for Undifferentiated Cutler Formation detrital zircon U-Pb geochronology, and 3 for detrital zircon U-Pb geochronology correlation of the Organ Rock and Moenkopi formations) were collected from outcrops proximal to the sediment source and both between and on the flanks of salt-cored anticlines (Fig. 14). Detrital zircon sample sites were located at Gateway, CO, Paradox Valley, UT, and Richardson Amphitheater in Undifferentiated Cutler Formation fluvial facies proximal to the UU ($n_{outcrop}$=3, $n_{samples}$=4) and at Castle Valley, Moab Valley, Kane Springs, and Lisbon Valley in Undifferentiated Cutler Formation fluvial deposits in the medial salt deformed basin ($n_{outcrop}$=4, $n_{samples}$=5). Additional detrital zircon samples from fluvial facies in the Organ Rock, Moenkopi, and Chinle formations ($n_{outcrop}$=3, $n_{samples}$=3) at Hite, UT, Richardson Amphitheater, and Moab Valley, respectively, were used to confirm that primary samples are from the Undifferentiated Cutler Formation (Fig. 14 and 15). At each site, I observed and interpreted decimeter scale stratigraphic thickness, lithology, grain size,

sedimentary structures, facies interpretations, paleocurrent direction rose diagrams, and stratigraphic level of detrital zircon samples (Fig. 15). Facies analysis (see Appendix A) shows that all samples were taken from dune trough or low-angle cross-stratified pebbly sandstone or sandstone contained within channel forms observed in the outcrops (Fig. 15).

Figure 15: Measured sections of Undifferentiated Cutler Formation sample locations with detrital zircon sample locations and paleocurrent measurement arrows. Paleocurrent direction data shown here was measured from dune and bar cross-stratification and is divided stratigraphically to show vertical changes in flow direction, and no paleocurrent direction measurements from previous authors is included. See Appendix A for facies descriptions.

99
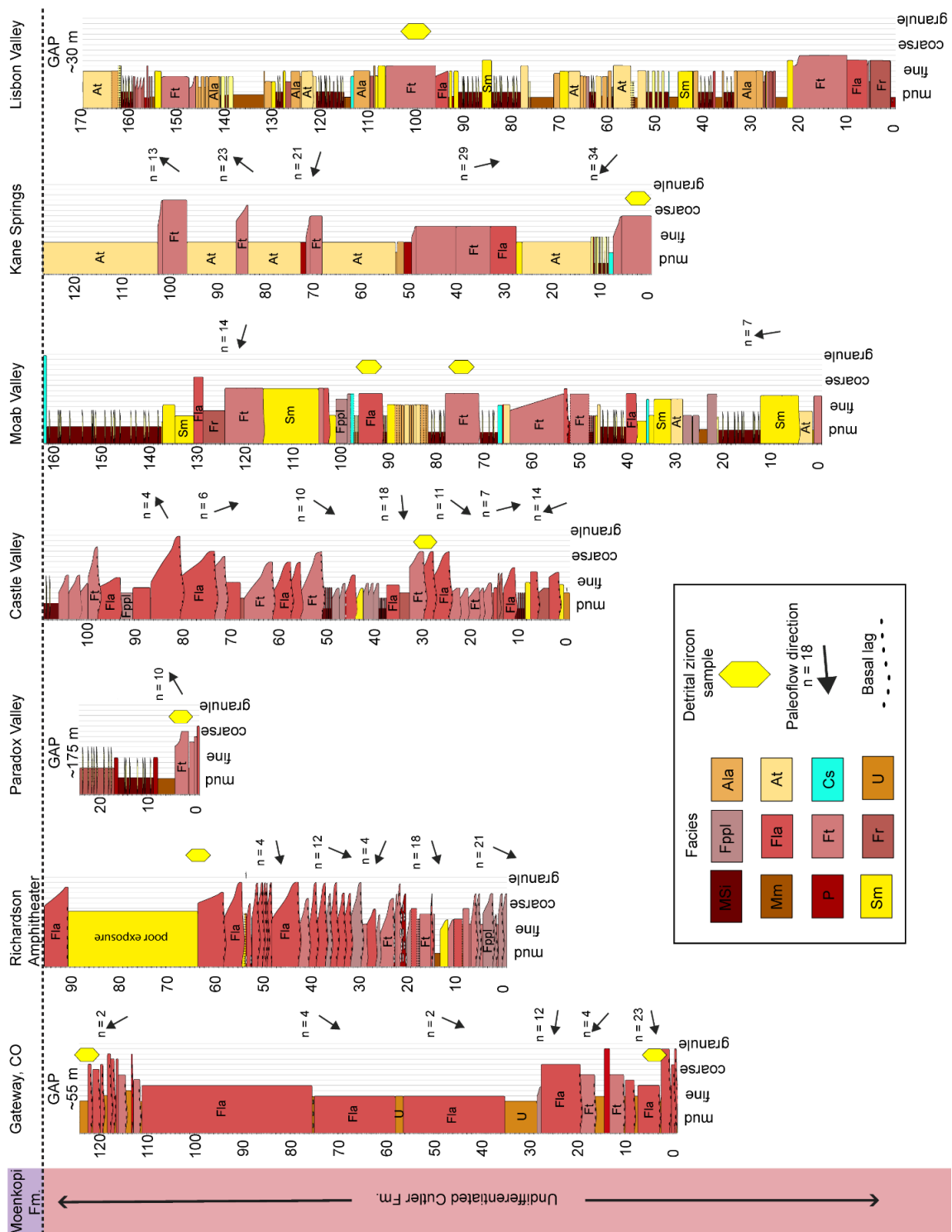
3.3.3. Paleocurrent Direction Analysis

Paleocurrent directions were determined from orientations of dune trough and channel scour axes, the dip direction of bar and dune trough cross-stratification limbs after correcting for regional tectonic dip at each locale (Decelles et al., 1983). Trough axis orientations reflect primary flow direction most accurately, and the average of trough limb dip directions reflect axis orientations when $15 - 30$ measurements are made per outcrop (Decelles et al., 1983). Where exposed in 3D, measurements of the trough axis orientation, and the attitude of the left and right limb, were made using a Brunton compass. Stereonet 10 software was used to correct for regional dip by rotating paleocurrent direction data around the axis of regional strike by the magnitude of regional dip measured in the field and calculating Von Mises distribution statistics (Allmendinger et al., 2011). Von Mises distribution analysis of directional data yields two parameters that describe uncertainty, the mean vector direction (μ) with standard error and the concentration variable (κ) which is the inverse of the dispersion of values around the mean. Relatively high κ ($\kappa > 5$) and a greater number of measurements ($n > 15$) yields low uncertainty. Rotation of individual measurements for local bedding dip at each location results in over-rotation and polar-switching of many dip directions of dune and bar dip angles that are < 10, so dune and bar measurements with dip angle < 10 after rotation were deleted to remove over-rotated measurements.

3.3.4. Detrital Zircon Geochronology And Statistics

Approximately 5 to 10 kilograms of sandstone from each fluvial sample location was collected for detrital zircon U-Pb age analysis. Mineral separation was conducted by ZirChron LLC and at Texas A&M University. Detrital zircons were separated from samples using standard mechanical, density, and magnetic methods (Gehrels et al., 2006). High purity zircon separates were mounted in epoxy, polished to approximately the middle section of grains, and imaged by backscatter SEM to confirm mineralogy. Detrital zircon separates were analyzed for U-Th-Pb age using laser ablation and an inductively coupled plasma mass spectrometer (LA-ICP-MS) at Texas A&M University and the University of Houston (Supplementary Table 1). A minimum of 117 grains are analyzed for each sample in order to ensure all age groups that make up at least 5% of the zircons in the sample are identified at the 95% confidence level (Vermeesch, 2004). Ages more than 10% discordant are filtered from the data to avoid zircon ages skewed by lead loss or inheritance, and 1σ uncertainty is reported. Probability density functions (PDPs) of age spectra were plotted using the Isoplot excel add-in.

Cross-correlation and MDS statistical tests were used to compare the presence and abundance of age groups and the grain size of age groups between samples to determine whether they share similar sediment sources. Cross-correlation coefficient values (R^2) of detrital zircon age PDPs were calculated using DZstats to quantify similarity of age spectra (Saylor and Sundell, 2016). Grain size data was used to bolster detrital zircon age data for provenance. Detrital zircon median grain size (D_{50}) calculated

from measurements of equivalent spherical diameter (ESD), e.g. nominal diameter ($D_n = (D_{long} * D_{intermediate} * D_{short})^{1/3}$), of zircon grains mounted in epoxy (Komar and Reimers, 1978). To visualize quantitative comparisons between the detrital zircon age and size signatures of the samples, multidimensional scaling (MDS) and 3-way MDS, i.e. individual dissimilarity scaling (INDSCAL), figures were plotted using the Provenance R-package (Vermeesch and Garzanti, 2015; Vermeesch et al., 2016). MDS plots the distance between samples according to their statistical similarity. In MDS and 3-way MDS, samples that are most similar plot closest to each other, and samples most dissimilar plot further apart.

3.3.5. Grain Size Measurement For Paleohydraulic Reconstruction

Physics-based methods were used to reconstruct channel flow depth, slope, particle Reynolds number, Shields stress, and basal shear stress of the paleo fluvial system in the Paradox Basin, and discussed in detail with regard to detrital zircon U-Pb geochronologic provenance methods in Findlay et al. (in review) (Bridge and Best, 1997; Paola and Mohrig, 1996; Cheng, 1997; Leclair and Bridge, 2001; Mohrig et al., 2000; Garzanti et al., 2008; Wilkerson and Parker, 2011; Hajek and Heller, 2012; Lynds et al., 2014; Trampush et al., 2014; Vermeesch et al., 2016; Bradley and Venditti, 2017; Hayden et al., 2019). To determine median grain size (D_{50}) of mixed gravel and sand deposits a proportionately weighted method was used (Eq. 1) . The long and intermediate axes of gravel-size clasts in outcrop ($D_{50\ coarse}$) were measured using a measuring stick. The fine fraction of grains was measured in outcrop with a grain card or by point counts in thin section ($D_{50\ fine}$) (Bunte and Abt, 2001). The approximate

proportions of the coarse and fine fractions were determined by point counting 100 random points overlain on an image of a representative channel deposit for each location. The coarse and fine grain sizes were weighted by their respective proportions (Eq. 1), providing the median grain size that reflects the volume of gravel and sand present at each location.

$$D_{50} = \frac{D_{50\,coarse}(\%\ gravel) + D_{50\,fine}(\%\ fines)}{100} \tag{1}$$

3.3.6. Paleohydraulic Reconstruction

Paleohydraulic reconstruction of flow depth, particle Reynolds number, Shields stress, and basal shear stress from grain size and dune and LAS cross-stratification set thickness were used to support previous in-depth analysis of the effects of hydraulic sorting on detrital zircon provenance data . Minimum values of flow depths calculated from dune cross-stratification thickness are roughly equal to flow depth calculated from thickness of LAS in the Undifferentiated Cutler Formation. An empirical relationship was used to relate Shields Stress to particle Reynolds number (Trampush et al., 2014; Hayden et al., 2019), and basal shear stress was calculated from Shields stress, grain size, and density of quartz and zircon grains (Wilkerson and Parker, 2011).

3.4. Results

3.4.1. Paleocurrent Direction

Paleocurrent direction is used to discriminate between a generally SW flowing megafan and NW flowing axial system. Undifferentiated Cutler Formation fluvial paleocurrent directions in the proximal basin are generally SW and SE. Paleocurrent directions in the medial basin are generally SW and NW, but measurements at Kane Springs are dominantly NE (Table 13, 14; Fig. 15, 16). At proximal basin site Gateway, dune and bar dip directions vary stratigraphically in different beds, shifting between SW and NW mean directions. At Castle Valley, mean dune and bar dip directions of different beds vary upsection between NW, S - SW, to SE. At Kane Springs, mean dune and bar dip directions of different beds vary upsection between NW, SE, back to NW, and NE, but all beds have NE and NW measurements. NW - NE directions support a generally NW flowing axial system in the medial basin, and the stratigraphic variation between SW-SE and NW - NE directions indicates temporal change in fluvial style. Dune and bar dip directions show similar dispersion and mean dip direction and were combined for statistical calculation and are reported as one dataset (Table 14).

Table 13: Dune trough and channel scour axis orientations.

Location	Axis n=	Mean Direction (u)	Uncertainty (+-)	Concentration (k)
Gateway	3	155.4º	35.2º	1.48
Richardson				
Amphitheater	13	205.4º	13.4º	2.01
Paradox Valley	0			
Parriott Minibasin	5	244.4º	20.1º	2.21
Castle Valley	11	296.2º	15.9º	1.79
Moab Valley	5	317.9º	11.1º	5.85
Lisbon Valley	8	249.3º	10.2º	4.49
Kane Springs	14	41.7º	13º	1.9

Table 14: Dune and bar cross-stratification dip directions.

Location	Dunes and Bars n=	Mean Direction (u)	Uncertainty (+-)	Concentration (k)
Gateway	44	260.6º	10.1º	1.33
Richardson				
Amphitheater	60	226º	10.1º	1.1
Paradox Valley	9	69º	30.4º	0.98
Parriott Minibasin	7	317º	285.7º	0.1
Castle Valley	113	216.1º	9.3º	0.85
Moab Valley	24	313.2º	17.6º	0.98
Lisbon Valley	0			
Kane Springs	120	13.1º	22.7º	0.32
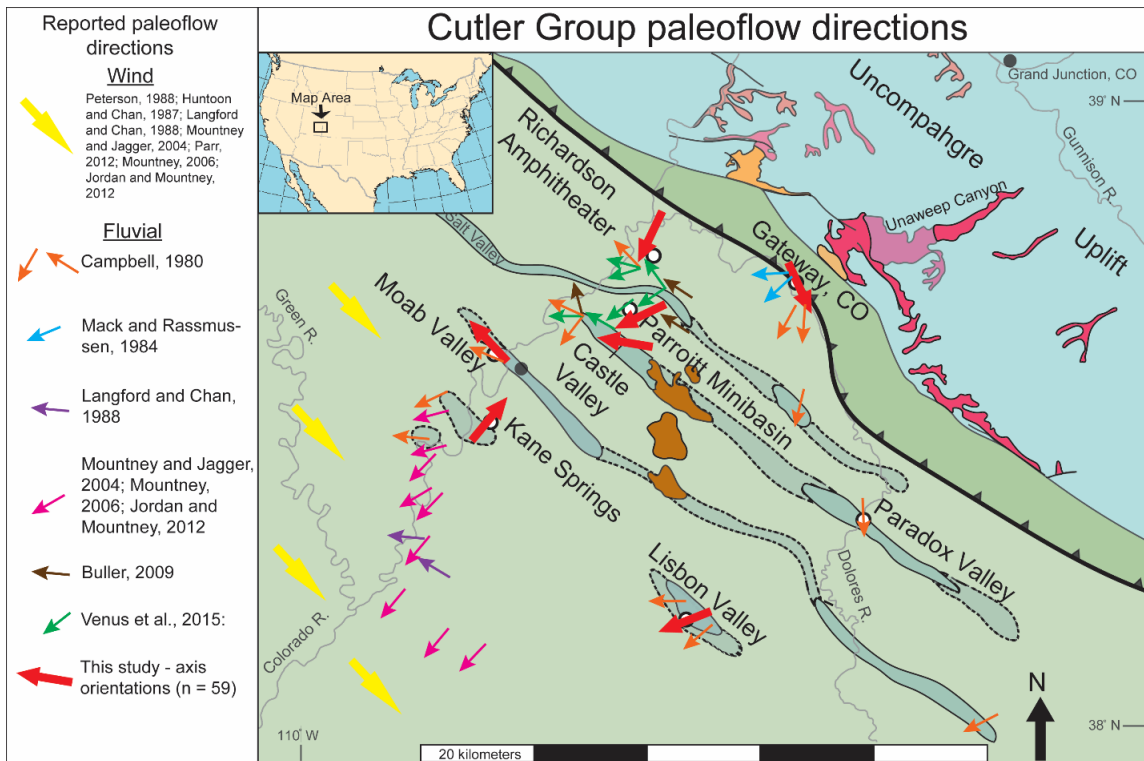
Figure 16: Cutler Group paleocurrent directions from previous authors (data cited in legend) and trough axis orientation measurements of this study (red arrows). Aeolian wind directions are interpreted from the Cedar Mesa and White Rim formations, fluvial directions are from the Undifferentiated Cutler, Cedar Mesa, and Organ Rock formations. Data locations were visually approximated from map figures in the studies cited.

3.4.2. Detrital Zircon Geochronology

Two detrital zircon age groups, broad peaks centered on 1440 Ma and 1727 Ma, dominate the spectra of Undifferentiated Cutler Formation fluvial deposits in the Paradox Basin, and are consistent with sediment derived from the UU (Fig. 17, 18) (Lawton et al., 2015; Leary et al., 2020; Findlay, 2020c). Two broad groups of samples are observed, those dominated by a bimodal signature (samples from Richardson

Amphitheater, Castle Valley, and Kane Springs, and the lower sample at Moab Valley),

and those dominated by a unimodal signal (samples from Gateway, Paradox Valley, and

the upper sample at Moab Valley). Lisbon Valley is the only sample that shows three

age groups, with peaks an additional peak at 526 Ma, consistent with sediment derived

from the eastern UU (Leary et al., 2020). However, the presence and proportions of the

1440 Ma and 1727 Ma groups vary between sites.

The two samples at Gateway are dominated by a mode centered at 1440 Ma with

a low percentage of grains from the 1727 Ma mode (90 – 94 % and 3 - 4 %,

respectively). Statistical comparison of the Gateway samples yields an R^2 value of 0.63

(Table 15), likely decreased by higher analytical error in the older sample and 0.7 % of

grains in the upper sample with ages of 557 Ma, 1058 Ma, and 2769 Ma. Medial basin

samples from Richardson Amphitheater, Castle Valley, and Kane Springs, and the lower

sample at Moab Valley are dominated by two age peaks at 1440 Ma and 1727 Ma, but

the proportions of these age groups varies spatially resulting in R^2 values of 0.15 – 0.85

(Table 15). Paradox Valley and the stratigraphically youngest sample from Moab Valley

have > 95 % 1720 Ma grains and have an R^2 value of 0.98, indicating they are nearly

identical (Table 15). High analytical uncertainty in Kane Springs and Lisbon Valley

samples resulted in a broad group of ages from 1300 – 2000 Ma when 2 sigma error is

plotted in PDPs, so I report 1 sigma error for all samples to show that the wide peak is an

artifact of analytical uncertainty (Fig. 17).

The Moab Valley section highlights upsection variation in detrital zircon age signature. Whereas the stratigraphically oldest sample has both 1440 Ma and 1727 Ma, the youngest sample lacks zircons from the 1440 Ma group, and instead is dominated by the 1727 Ma age group. Statistical comparison of the Moab Valley samples yields an R^2 value of 0.02, indicating they are very different. These samples are separated stratigraphically by ca. 30 m (Fig. 15). See Appendix B for minor age groups.

Statistical comparison between the Organ Rock, Moenkopi, and Chinle age signatures and other samples yields R^2 values of 0 – 0.29, indicating they are distinct from the Undifferentiated Cutler Formation samples and each other (Fig. 17, 18). The Organ Rock sample (CPF_070) from Hite, UT, where the contact between the Cedar Mesa formation and overlying Organ Rock formation is clear, has broad peaks of ages between 1300 – 1500 Ma and 1600 – 1860 Ma that are consistent with derivation from local basement sources. This sample also has several age groups between 291 – 490 Ma and 497 – 682 Ma, which are rare in our samples from the Undifferentiated Cutler Formation. At Richardson Amphitheater, the Moenkopi Formation overlies our section above an angular unconformity (Allred, 2016). The Moenkopi sample (CPF_068) has 520 – 530 Ma, 928 – 1299 Ma, 1300 – 1500 Ma, and 1600 – 1860 Ma, as well as 291 – 490 Ma and 497 – 682 Ma age groups similar to the Organ Rock. Overlying the Moenkopi, the Chinle Formation sample (18PX02) from Moab Valley is dominated the 291 – 490 Ma, 497 – 682 Ma, and 928 – 1299 Ma age groups, as well as a Late Triassic age group with a peak at 214 Ma defining a maximum depositional age, thus confirming Norian depositional age (Irmis et al., 2011).

Figure 17: Probability density plots (PDPs) and histograms of detrital zircon U-Pb age results with 1σ uncertainty. Undifferentiated Cutler fluvial samples are dominantly bimodal, but presence and abundance of age peaks change spatially. In PDPs, wide, short peaks either cover a wide range of ages or represent a narrow range of ages with high uncertainty. Dominant age groups for Cutler Group fluvial samples are 1440 Ma and 1727 Ma, as seen in the Castle Valley data from Lawton et al. (2015). A single sample at Lisbon Valley has a dominant peak at 526 Ma. Organ Rock, Moenkopi, and Chinle samples have different age signatures than the Undifferentiated Cutler Group.

Cutler Group Fluvial Detrital Zircon Geochronology
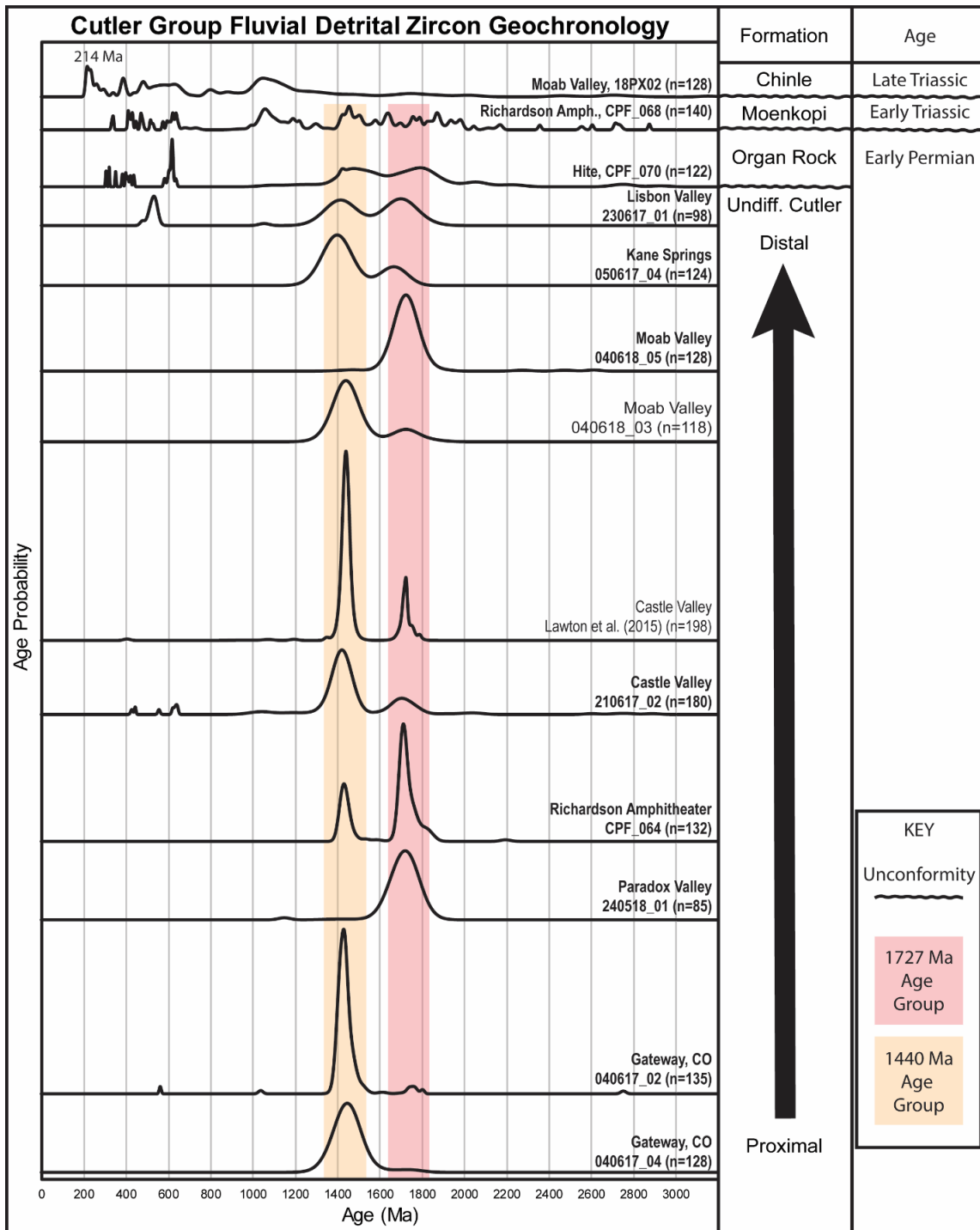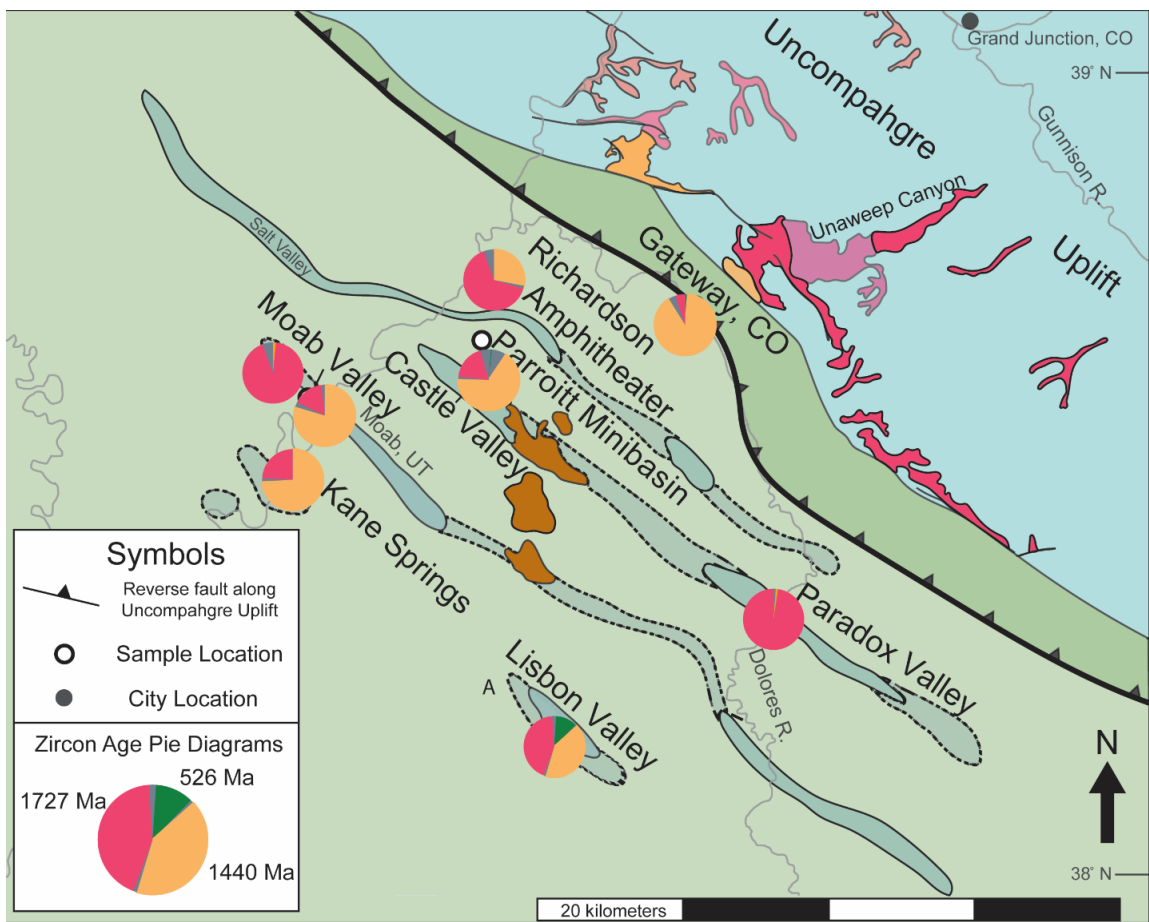
Figure 18: Pie graphs of age spectra illustrate spatial variability in the abundance of age groups and the presence of the 526 Ma age group at Lisbon Valley. Map and pie chart colors are the same as in Figure 1.

Table 15: Cross-correlation coefficient values (R^2) from statistical comparison of detrital zircon age PDPs, highest values (most similar samples) are darkest red. Calculated using DZstats (Saylor and Sundell, 2016). Samples: 1 – Gateway, 040617_04; 2 - Gateway, 040617_02; 3 – Paradox Valley, 240518_01; 4 – Richardson Amphitheater, CPF_064; 5 – Castle Valley, 210617_02; 6 – Castle Valley, data from Lawton et al. (2015); 7 – Moab Valley Lower, 040618_03; 8 - Moab Valley upper, 040618_03; 9 – Kane Springs, 050617_04; 10 – Lisbon Valley, 230617_01; 11 – Organ Rock, CPF_070; 12 – Moenkopi, CPF_068; 13 – Chinle – 18PX02.

	1	2	3	4	5	6	7	8	9	10	11	12	13
1	1.00	0.63	0.00	0.09	0.76	0.49	0.96	0.00	0.71	0.35	0.22	0.09	0.00
2	0.63	1.00	0.00	0.13	0.68	0.70	0.65	0.00	0.43	0.18	0.10	0.06	0.00
3	0.00	0.00	1.00	0.64	0.08	0.03	0.02	0.98	0.06	0.46	0.17	0.05	0.01
4	0.09	0.13	0.64	1.00	0.27	0.28	0.16	0.67	0.15	0.42	0.16	0.03	0.01
5	0.76	0.68	0.08	0.27	1.00	0.53	0.85	0.07	0.73	0.43	0.17	0.07	0.00
6	0.49	0.70	0.03	0.28	0.53	1.00	0.50	0.04	0.31	0.21	0.12	0.11	0.00
7	0.96	0.65	0.02	0.16	0.85	0.50	1.00	0.02	0.79	0.44	0.23	0.08	0.00
8	0.00	0.00	0.98	0.67	0.07	0.04	0.02	1.00	0.04	0.43	0.16	0.05	0.01
9	0.71	0.43	0.06	0.15	0.73	0.31	0.79	0.04	1.00	0.49	0.14	0.04	0.00
10	0.35	0.18	0.46	0.42	0.43	0.21	0.44	0.43	0.49	1.00	0.29	0.08	0.01
11	0.22	0.10	0.17	0.16	0.17	0.12	0.23	0.16	0.14	0.29	1.00	0.07	0.02
12	0.09	0.06	0.05	0.03	0.07	0.11	0.08	0.05	0.04	0.08	0.07	1.00	0.05
13	0.00	0.00	0.01	0.01	0.00	0.00	0.00	0.01	0.00	0.01	0.02	0.05	1.00

3.4.3. Detrital Zircon Grain Size

Detrital zircon size was used to supplement age data for provenance interpretation and to determine spatial sorting in the fluvial system (Table 16) (Findlay, 2020d). The median grain sizes of both 1440 Ma and 1727 Ma age groups are 0.062 – 0.1 mm at Gateway, Richardson Amphitheater, Castle Valley, Kane Springs, and Lisbon Valley. The smallest detrital zircon median grain sizes are at locations furthest from the UU, Kane Springs and Lisbon Valley, which have different bulk grain sizes (Table 16). Median grain size of the 1727 Ma age group at Paradox Valley and Moab Valley is 0.124 – 0.160 mm, which is larger than median grain sizes from all other locations and

highlights another similarity between Paradox Valley and Moab Valley alongside

unimodal 1727 Ma age signatures (Fig. 17, 18).

Table 16: Bulk sediment grain size, detrital zircon grain size, and calculated basal shear stress (Eq. 8) from the Undifferentiated Cutler Formation.

Location	Bulk D_{50fine} (mm)	Bulk D_{50} (mm)	1440 Ma Measured Zircon D_{50} (mm)	1720 Ma Measured Zircon D_{50} (mm)	520 Ma Measured Zircon D_{50} (mm)	Calculated Basal Shear Stress
G Base	1.410	5.803	0.085±0.024	0.089±0.021		0.038
G Top	3.732	7.937	0.100±0.023	0.095±0.036		0.041
RA	0.692	4.072	0.082±0.026	0.082±0.027		0.035
PV	0.732	6.831	0.094	0.160±0.046		0.039
PM	0.350	2.657				0.031
CV	0.217	1.309	0.087±0.022	0.088±0.020		0.026
MV Lower	0.353	1.693	0.115±0.027	0.133±0.040		0.028
MV Upper	0.210	1.595	0.094±0.018	0.124±0.042		0.027
LV	0.350	0.418	0.067±0.021	0.068±0.019	0.087±0.035	0.016
KS	0.659	2.373	0.062±0.022	0.077±0.038		0.030

3.4.4. Bulk Sediment Grain Size and Basal Shear Stress

Pebble-sized particles constitute the median grain size (D_{50}) (Eq. 1) at the

proximal locations of Gateway, Richardson Amphitheater, and Paradox Valley (Findlay,

2020a, 2020b). At the medial basin locations Castle Valley, Moab Valley, Kane Springs,

and Lisbon Valley the grainsizes range from granule to sand sized. The median grain

diameter decreases away from the uplift from a maximum of 7.94 mm at Gateway to a

minimum of 0.42 mm at Lisbon Valley (Table 16). Notably, the median grain size

transitioned from gravel (i.e., pebble) to sand between Richardson Amphitheater and

Castle Valley. Richardson Amphitheater is 20 km from the base of the uplift and 29 km from the apex of the putative megafan at Gateway, CO. Calculated basal shear stress is least where bulk sediment grain size is smallest, mirroring spatial patterns in bulk sediment grain size measurements (Table 16).

3.5. Discussion

The results provide a means to assess the role of hydraulics in determining the detrital zircon distribution across the basin and reveal new insights into the type of fluvial system draining the UU and in the Paradox Basin. The Undifferentiated Cutler Formation fluvial system has been paradoxically described as a megafan and as an axial system (Campbell and Steele-Mallory, 1979; Campbell, 1980; Mack and Rasmussen, 1984; Cain and Mountney, 2009; Trudgill, 2011; Lawton et al., 2015; Venus et al., 2015). Transport in a single fluvial megafan should not introduce or mix age groups downstream, and paleocurrent directions should generally radiate outward from the highland sediment source. These characteristics contrast with transport direction patterns parallel to the uplift and the confluence of multiple rivers transporting sediment from a mix of source rocks expected from axial fluvial systems. Detrital zircon age, detrital zircon grain size, paleocurrent direction, and paleohydraulics data in the Undifferentiated Cutler Formation vary spatially from the Uncompahgre Uplift (UU) to the medial, salt deformed basin . Here I explore the role of autogenic and allogenic drivers that may contribute to vertical and lateral variability of data, including spatial sorting of the zircon grains related to downstream change in fluvial slope and shear

114

stress, confluence of tributaries sourcing discretely aged basement rocks, and sediment routing by salt wall fluctuations.

3.5.1. Multidimensional Scaling Applied To Integration Of Provenance And Paleohydraulic Results

Paleohydraulic analysis shows that the Undifferentiated Cutler Formation fluvial system has the competence to transport all detrital zircon grain sizes that were present in the system . Findlay et al (in review) also used a global compilation of flow conditions of modern rivers (Trampush et al., 2014) to show that silty rivers can sort detrital zircon larger than 0.2 mm from the bulk sediment load. Samples of this study have median bulk sediment grain size values of 0.42 – 7.94 mm, which indicates, based on modern river data, sorting should not affect the detrital zircon age or size distribution. To further investigate whether detrital zircon age populations may have been impacted by sorting and grain size variations, 3-way MDS plots were used to compare the similarity among samples based on detrital zircon grain ages, the measured ESD D_{50} of detrital zircon age groups, and reconstructed basal shear stress data (Fig. 17; Table 16).

3-way MDS plots show that distinct detrital zircon age groupings (here, samples dominated by either 1440 Ma or 1727 Ma ages) are not linked with specific grain sizes, and instead display a range of detrital zircon grain sizes and bulk sediment grain sizes. Grain age and size determine the scale (weight) of the first 3-way MDS plot, so the age and size dissimilarity between samples plot along the x- and y-axis of the plot, respectively (Fig. 19). The resulting map groups samples that have the most similar age

115

spectra along the x-axis and the samples with most similar detrital zircon size along the y-axis (Fig. 19). Age spectra that share similarities in the presence and abundance of 520 Ma, 1440 Ma, and 1727 Ma age groups based on visual inspection remain clustered by 3-way MDS analysis when zircon grain size was also considered. Paradox Valley and Moab Valley plot with Richardson Amphitheater along the x-axis because they have more 1727 Ma ages than other locations. However, these three samples spread along the y-axis because they have different detrital zircon grain sizes, indicating that age does not have a strong correlation with grain size for the 1727 Ma age group. The remaining samples from Gateway, Castle Valley, the lower sample from Moab Valley, Kane Springs, and Lisbon Valley cluster together because they have more 1440 Ma grains and have a smaller range of detrital zircon grain sizes than the other cluster of samples (Fig. 19; Table 16).
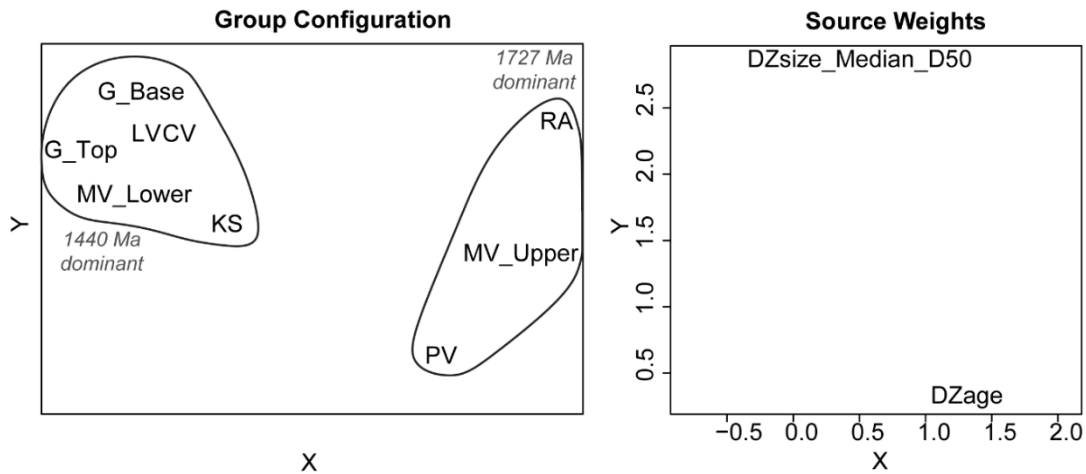
Figure 19: 3-way MDS plot of Undifferentiated Cutler Formation detrital zircon U-Pb age KDEs and detrital zircon median ESD grain size. Richardson Amphitheater, Paradox Valley, and the upper sample from Moab Valley plot separately from the rest of the samples along the x-axis because they have more 1727 Ma zircon, but Richardson Amphitheater plots even with the rest of the samples along the y-axis because it has similar detrital zircon grain size. Plotted using Provenance (Vermeesch et al., 2016). Source weights of 3-way MDS analysis show that Cutler Group detrital zircon U-Pb age KDEs and detrital zircon median ESD grain size not strongly related. Sample locations: G – Gateway, CO; PV – Paradox Valley; RA – Richardson Amphitheater; CV – Castle Valley; MV – Moab Valley; LV – Lisbon Valley; KS – Kane Springs.

A final dataset of calculated shear stress from Findlay et al. (in review) was added to 3-way MDS to interpret the effect of paleohydraulics and sorting on detrital zircon grain size and age (Fig. 20; Table 16). Shear stress and age spectra are weighted heavier than detrital zircon grain size, showing greater utility of paleohydraulic reconstruction than zircon grain size in discerning effects of sorting on detrital zircon age data. Results are similar to the previous 3-way MDS analysis in that Richardson Amphitheater, Paradox Valley, and the upper sample from Moab Valley are separated from the rest of the samples along the x-axis. However, these three samples are not

117

separated from the other samples along the y-axis. Proximal sites with gravel bulk grain size at Gateway, Paradox Valley, and Richardson Amphitheater plot lowest on the y-axis, and medial basin sites with finer bulk grain size at Castle Valley, Moab Valley, Kane Springs, and Lisbon Valley plot higher on the y-axis. This reinforces Findlay et al., (in review) results showing that different paleohydraulic conditions in the proximal and medial basin did not control age signatures. Lisbon Valley and Castle Valley plot furthest up on the y-axis because they have the finest bulk sediment and smallest calculated shear stress. Lisbon Valley has the smallest shear stress but has a measured detrital zircon age spectrum and grain size similar to other samples, indicating that the low shear stress did not control the size or age of zircon transported to Lisbon Valley. Paradox Valley has the largest zircon grain size, but shear stress values are similar to those calculated for Gateway samples, indicating shear stress did not control measured detrital zircon size. The age groups are similar in both 3-way MDS plots, but clustering along the y-axis changes according to detrital zircon grain size and calculated shear stress, indicating that similarity of age, measured zircon size, and shear stress between samples are not strongly linked. These maps support findings from Findlay et al., (in review), which show that detrital zircon results were unlikely to have been affected by preferential deposition or winnowing of zircon size fractions during transport.
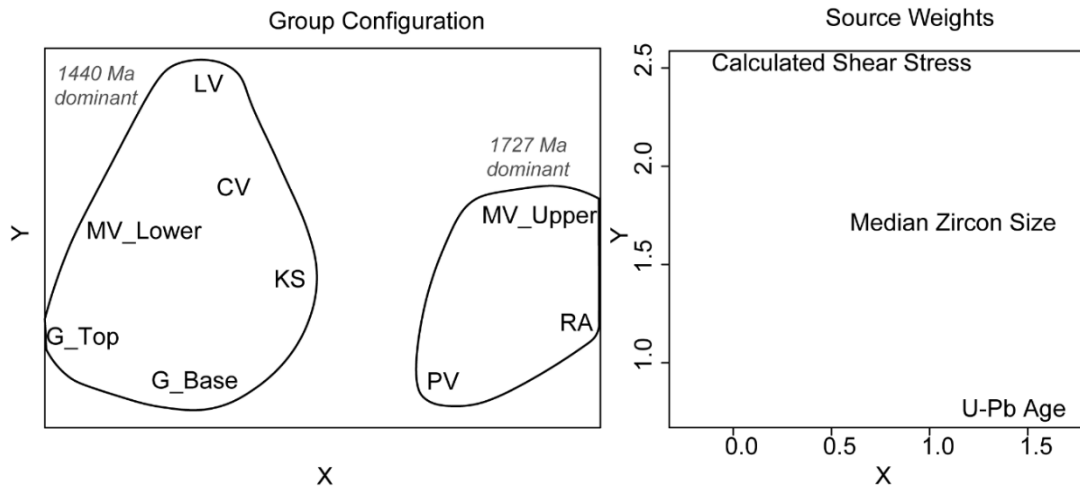
Figure 20: 3-way MDS plot of detrital zircon age and size data and calculated shear stress values show a wide spread of paleohydraulic values in the data and separation of proximal and medial basin samples along the y-axis, and dissimilarity in detrital zircon age of Richardson Amphitheater, Paradox Valley, and the upper sample from Moab Valley samples along the x-axis. Plotted using Provenance _(Vermeesch et al., 2016)_. Source weights of 3-way MDS analysis show that Undifferentiated Cutler Formation detrital zircon U-Pb age KDEs are weighted along the x-axis, and they are not similar to bulk sediment shear stress and detrital zircon median ESD grain size that are weighted along the y-axis. Sample locations: G – Gateway, CO; PV – Paradox Valley; RA – Richardson Amphitheater; CV – Castle Valley; MV – Moab Valley; LV – Lisbon Valley; KS – Kane Springs.

3.5.2. Reconstructing Fluvial Style And Explaining Provenance Dataset Variations

The simplicity of the well-defined Uncompahgre Uplift source material and previously interpretted megafan fluvial style for the Undifferentiated Cutler Formation bely the complexity shown by the coupled detrital zircon and paleohydraulic approach (Fig. 17 - 20). The megafan model suggests that time-correlative distributary fans prograded from the UU to the distal basin, aligning with typical foreland basin sedimentation models that invoke a clastic wedge prograding out from the adjacent topographic load (e.g. Allen and Heller, 2012) (Campbell, 1980; Mack and Rasmussen,

119

1984; Cain and Mountney, 2009). Prograding megafans create coarsening upward stratigraphic patterns as amalgamated channel deposits of the proximal fan migrate over isolated channel deposits separated by abundant fine-grained overbank deposits of the medial and distal fan (Owen et al., 2017). Such stratigraphic patterns are not observed in measured sections of this study, amalgamated channels deposits are present throughout our sections and their abundance does not increase upsection (Fig. 15). However, the abundance of fine-grained floodplain deposits increases and grain size decreases away from the uplift in accordance with fan models (Owen et al., 2017). In the gravel reaches of fans, slope and grain size decrease exponentially downstream, and there is a sharp decrease in grain size across a gravel-sand transition (Hack, 1973; Flint, 1974; Slingerland, 1977, 1984; Best and Brayshaw, 1985; Parker, 1991a, 1991b; Ferguson, 2003, 2007; Fedele and Paola, 2007; Jerolmack and Brzinski, 2010; Miller et al., 2014; Lamb and Venditti, 2016).

Though not widely described in the studies of ancient fluvial systems, identifying the gravel-sand transition in this study provided a new tool to aid detailed spatial reconstructions. Consistent with a fan model, Findlay et al. (in review) show grain size and slope decrease exponentially from Gateway to Richardson Amphitheater, and the sharp decrease in grain size between Richardson Amphitheater and Castle Valley could be a gravel-sand transition in a fan system. Gravel-sand transitions typically begin at a distance from the apex 60% of the total length of the gravel reaches of a fluvial fan (Miller et al., 2014). In our transect, based on the contact of the Cutler Group boulder conglomerates with the UU, the apex of the fan was a few km toward the UU from

120

Gateway, CO. The absence of pebbles and cobbles at locations basinward from Castle

Valley indicate that Castle Valley is the point along the fluvial system at which no more

gravel reaches existed. Thus, I use the distance of 35 km from Castle Valley to a few km

updip of Gateway, CO as the maximum length of the gravel reaches of a putative fan.

Based on the analysis of modern fans, the gravel-sand transition would have started ca.

20 km from Gateway, CO. Richardson Amphitheater is ca. 20 km from the UU and 29

km from Gateway, CO, indicating the sharp decrease basinward of Richardson

Amphitheater may be a gravel-sand transition in a fan, but not in a megafan with an apex

at Gateway, CO. This interpretation and unimodal age spectra in the proximal basin are

consistent with bajada style fans localized to the proximal basin and draining unique

catchments within the UU, but paleocurrent directions and provenance data in the medial

basin indicate a megafan model is not representative of the basin-wide system.

Although some elements of the drainage system indicate fans were part of the

fluvial system in the proximal basin, paleocurrent directions do not show a radial pattern

centered at an apex and detrital zircon samples do not have the same bimodal age

signature that defines the western Uncompahgre Uplift, 1440 Ma and 1727 Ma, as is

expected in the megafan model (Fig. 15 - 18) (Lawton et al., 2015; Owen et al., 2015,

2017; Leary et al., 2020). Paleocurrent direction analyses conducted by previous authors

at various locations in the basin yield varied interpretations of sediment routing patterns

during deposition of the Cutler Group. Near Gateway, CO and Paradox Valley,

paleocurrent directions are SE-, S- and SW-directed (Campbell, 1980; Mack and

Rasmussen, 1984). In contrast, NW, SW, SE, and NE paleocurrent directions are

observed in the salt-deformed foredeep region (Campbell and Steele-Mallory, 1979; Campbell, 1980; Buller, 2009; Cain and Mountney, 2009; Parr, 2012; Lawton et al., 2015; Venus et al., 2015). SW and W fluvial paleocurrent directions are also reported further from the uplift near the Needles district of Canyonlands National Park where aeolian paleoflow direction was SE (Huntoon and Chan, 1987; Peterson, 1988; Langford and Chan, 1988; Mountney and Jagger, 2004; Mountney, 2006; Jordan and Mountney, 2012). The greatest spatial and temporal variations in paleocurrent directions are observed in fluvial deposits flanking and between salt-cored anticlines, but combining all measurements yields an average SW-directed paleocurrent direction that has led previous authors to infer transverse flow in prograding megafans and sediment provenance from the UU (Campbell and Steele-Mallory, 1979; Campbell, 1980; Cain and Mountney, 2009). Although SW-SE paleocurrent direction results and the position of the gravel-sand transition are consistent with fan-type fluvial deposition in the proximal basin, NW directed paleocurrent directions and variable detrital zircon age, detrital zircon size, reconstructed slope, and reconstructed discharge in the salt-deformed medial region suggest interaction with an axial fluvial network that could have transported sediment from the eastern basin (Lawton et al., 2015; Venus et al., 2015; Leary et al., 2020).

Unimodal and bimodal age signatures with varying proportions of 1440 Ma and 1726 Ma grains and the differences in detrital zircon grain size allows for detailed reconstruction of unique catchments draining the western UU. Undifferentiated Cutler Formation samples of this study are derived from the western UU except for the Lisbon

Valley sample, which has 526 Ma grains consistent with derivation from the eastern UU (Leary et al., 2020). Remarkably, Paradox Valley and the stratigraphically youngest sample from Moab Valley share similar unimodal 1727 Ma age spectra, zircon grain size, reconstructed slope, and reconstructed channel discharge values, and NW paleocurrent direction at Moab Valley supports transport from Paradox Valley to Moab Valley . These observations are consistent with the axial fluvial system scenario that predicts NW directed sediment transport and that distal mini-basins were filled with a mixture of sediment from catchments that supplied sediment to proximal mini-basin locations (Fig. 17 - 20; Table 15, 16) (Leary et al., 2020).

Given the constrained zircon source and the fluvial outcrop exposure from the source into the basin, the boundary conditions of the UU and the Undifferentiated Cutler Formation are ideal to implement a simple mixing model. If different catchments within the UU have distinct parent compositions, then detrital zircon age signatures could vary spatially across a transect from the UU to the distal basin. Sorting is expected to remove detrital zircon age groups from a sediment load or reduce their abundance, and sediment mixing by channel confluence is expected to add age groups in abundance proportionate to the volume of sediment from each source (Amidon et al., 2005a, 2005b; Saylor et al., 2018; Sharman and Johnstone, 2017).

A qualitative mixing model is especially simple if each daughter distribution is treated as a mixture of sediment from the unimodal detrital distributions at Gateway (1440 Ma, 0.085 – 0.1 mm) and Paradox Valley (1727 Ma, 0.124 – 0.16 mm), and the trimodal age signature of the eastern Paradox Basin (520 Ma, 1430 Ma, and 1730 Ma)

(Fig. 17, 18; Table 16) (Leary et al., 2020). A catchment upstream of Gateway was a primary source of 1440 Ma zircons, and similarly, that the catchment upstream of Paradox Valley supplied only 1727 Ma zircons that have a larger grain size than zircons from Gateway. A catchment in the eastern UU near Durango, CO supplied the only 526 Ma zircons to the western basin (Leary et al., 2020). The downstream changes in detrital zircon spectra are explained by mixing varying proportion of these three proximal age groups in the medial salt deformed region of the basin due to the confluence of rivers draining those unique catchments within the UU. Samples from Castle Valley, the oldest Moab Valley sample, and Kane Springs received relatively more sediment from the catchment upstream of Gateway, because they have higher proportions of 1440 Ma zircons and have detrital zircon median grain sizes smaller than 0.1 mm. 1727 Ma grains in these samples were not observed at our Gateway location, which doesn't preclude them from the Gateway catchment, but indicates contribution from the Paradox Valley catchment. In contrast, other sites received relatively more sediment from the catchment upstream of Paradox Valley. The relatively large (0.124 mm) 1727 Ma detrital zircons observed in the youngest sample from Moab Valley are consistent with increased sediment contribution from the catchment upstream from Paradox Valley, a sample that also has relatively larger zircons of 1727 Ma age. Richardson Amphitheater may have also received more sediment from the catchment upstream of Paradox Valley because it has a higher proportion of 1727 Ma detrital zircon, but detrital zircon median grain size is smaller than 0.1 mm at Richardson Amphitheater and reconstruction of the gravel-sand transition indicates it might have been part of a separate fan, which increases

uncertainty in the mixing model. The simple UU mixing model can be applied by invoking confluence of rivers from the catchments upstream of Gateway and Paradox Valley, and is a model that explains bimodal age signatures with varying peak heights for all locations, except at Lisbon Valley. Lisbon Valley has an additional age group of 526 Ma, which I interpret was sourced from a third catchment located in the eastern UU (Leary et al., 2020). Because Lisbon Valley lacks many of the other grain ages observed in Cedar Mesa Formation aeolian strata, I do not interpret that it was recycled from earlier aeolian deposits (Dickinson and Gehrels, 2003).

At least three distinct catchments and fluvial belts drained the UU upstream of Gateway, Paradox Valley, and the eastern basin, and sediment from these catchments were variably mixed in the medial basin. Furthermore, the temporal variation in sediment provenance at Moab Valley, situated on the flank of a salt wall, suggests that the catchments and/or transport pathways were rearranged through time. Detrital zircon age and grain size, paleocurrent directions, and paleohydaulic conditions display the most variance in the salt-deformed region of the Paradox Basin. Topography created by salt deformation in the medial basin is a mechanism that could have controlled dispersal patterns (Trudgill et al., 2011; Venus et al., 2015; Banham and Mountney, 2016). Although the time frame and spatial dimension of reorganization of Undifferentiated Cutler Formation fluvial belts remain poorly constrained, the role of active salt wall deformation likely played a role in reconfiguration of the transport system.

The emerging picture of the Undifferentiated Cutler Formation fluvial system is one of multiple alluvial fans draining the UU at proximal locations (Fig. 7). These fans

extended into the medial basin but may have been intercepted by an axial fluvial system that was routed and variably mixed as it traversed the mobile substrate of the Paradox Formation and interacted with actively uplifting salt walls. The change of detrital zircon spectra from bimodal to unimodal upsection suggests fluvial style changed through time (Fig. 17). The spatial and vertical variations in the detrital zircon age signatures from fluvial strata of the Undifferentiated Cutler Formation largely reflects allogenic processes (catchment variability; salt mobility) with limited influence from hydrodynamic sorting of zircon grains.
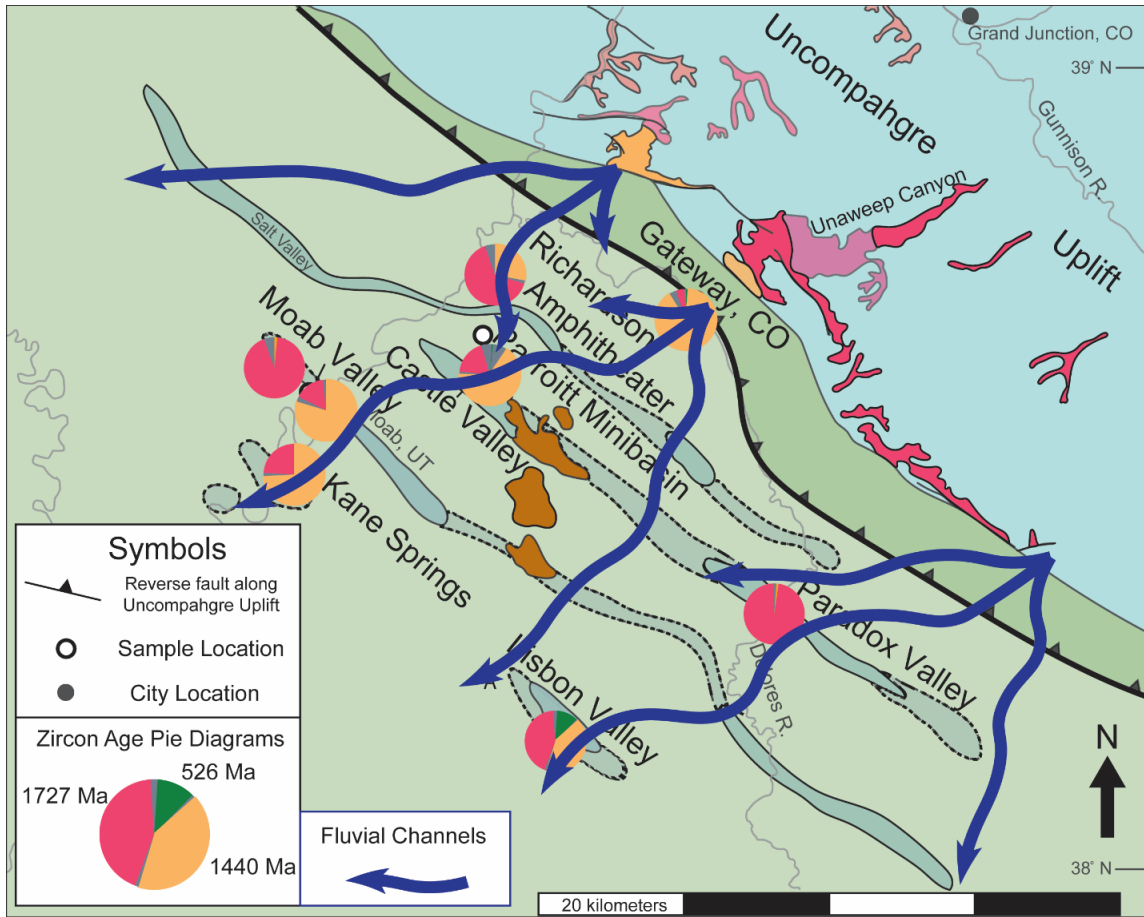
Figure 21: At least three distinct fans drained the UU, each with unique detrital zircon age signatures (Lawton et al., 2015; Leary et al., 2020). Fans extended into the medial basin, as shown by similar age spectra, detrital zircon size, and trends in bulk grain size, slope, and discharge between Gateway, Castle Valley, and Kane Springs.
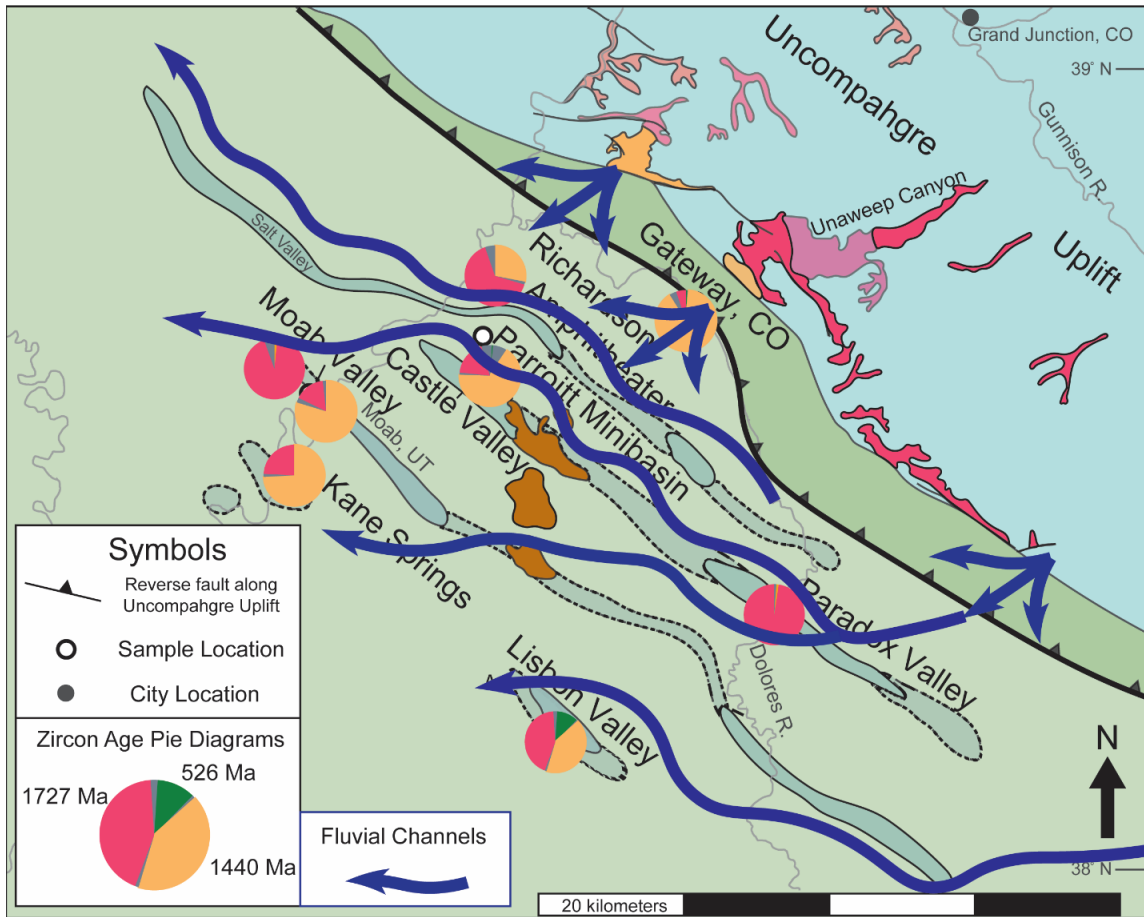
Figure 22: Axial NW transport from Paradox Valley to Moab Valley and from the eastern basin to Lisbon Valley is interpreted from detrital zircon age and size data and trends in paleohydraulic reconstructions.

3.6. Conclusions

A basinward transect of the Undifferentiated Cutler Formation fluvial system reveals spatial variation in detrital zircon age signatures, detrital zircon grain size, paleocurrent directions, bulk sediment grain size, and reconstructed slope, discharge, and basal shear stress across salt walls . 3-way MDS analysis using detrital zircon age,

detrital zircon grain size, and bulk sediment shear stress support conclusions that paleohydraulic conditions were sufficient to transport all detrital zircon grain sizes derived from the UU downstream (Fig. 19, 20) . Based on this, it is unlikely that paleohydraulic conditions were sufficient to explain spatial variability in detrital zircon age signatures.

Our data indicates that gravel- and sand-bedded fluvial depositional environments may not fractionate zircon groups by hydraulic sorting during transport, and possibly reveal an ancient gravel-sand transition at Richardson Amphitheater. Spatial variation in detrital zircon age signatures of the Undifferentiated Cutler Formation can be explained by changes in sediment provenance between multiple fans draining the UU and between salt-walled minibasins that divided the fluvial system into multiple channel belts that drained distinct catchments. Next to the Moab Valley salt wall, I observe an upsection switch from a bimodal (1440 Ma and 1727 Ma) to unimodal (1727 Ma) detrital zircon age signature, and a decrease in bulk sediment grain size accompanied by an increase in the abundance of the 1727 Ma detrital zircon age group, which has a larger grain size (Fig. 17; Table 16). The unimodal (1727 Ma) age signature and large detrital zircon grain size in the upper sample at Moab Valley is most similar to the age and grain size signature at Paradox Valley. The age groups at Lisbon Valley (526 Ma, 1440 Ma, 1727 Ma) are most consistent with Undifferentiated Cutler Formation samples in the eastern Paradox Basin near Durango and Ouray, CO (Leary et al., 2020). This spatial variation in detrital zircon U-Pb geochronologic age signatures show that the Early Permian Cutler Group in the Paradox Basin received sediment from at least three

distinct catchments in the adjacent Uncompahgre Uplift (Fig. 17, 18). The catchment

upstream from Gateway has a unimodal 1440 Ma detrital zircon group that has a median

grain size of 0.085 – 0.1 mm, and the catchment upstream from Paradox Valley supplied

a unimodal 1727 Ma detrital zircon group that has a median grain size of 0.124 – 0.16

mm (Table 16). A third sediment source supplied 526 Ma detrital zircon to Lisbon

Valley and was likely situated to the SE in the eastern UU (Leary et al., 2020).

Transport of sediment from Paradox Valley to Moab Valley, and the eastern

Paradox Basin to Lisbon Valley, requires axial NW directed transport. The proximity of

variations in provenance signatures to salt walls, and the absence of evidence for sorting,

indicate that the changes in sediment provenance signatures observed across the Cutler

Formation likely reflect the impact of actively deforming salt walls on rerouting of

upstream fluvial channels with distinct catchments into downstream depocenters through

time (Fig. 21, 22). Our results emphasize the role of surface topography created by salt

deformation and minibasins on by spatial and temporal variations in sediment

provenance and composition.

The Undifferentiated Cutler Formation transect in this study is gravelly or sandy

at all locations and only ~ 60 kilometers from the UU, but transport from the eastern

basin to Lisbon Valley is considerably further. In longer systems, where hydraulic

conditions and grain size decrease more than observed here, sorting may become more

impactful toward provenance signatures at distal positions further downstream . This

study demonstrates how detrital zircon provenance analysis, paleocurrent direction

analysis, and fluvial paleohydraulic reconstruction can be integrated along a spatial

transect of a basin, and enhances the confidence in depositional environment and sediment provenance interpretations, and helps differentiate between the impacts of autogenic and allogenic processes on basin development and sediment composition.

3.7. References

Abati, J., Gerdes, A., Suárez, J.F., Arenas, R., Whitehouse, M.J., and Fernández, R.D., 2010, Magmatism and early-Variscan continental subduction in the northern Gondwana margin recorded in zircons from the basal units of Galicia, NW Spain: Bulletin of the Geological Society of America, v. 122, p. 219–235, doi: 10.1130/B26572.1.

Allen, P.A., and Heller, P.L., 2012, Dispersal and Preservation of Tectonically Generated Alluvial Gravels in Sedimentary Basins, *in* Tectonics of Sedimentary Basins, Chichester, UK, John Wiley & Sons, Ltd, p. 111–130, doi: 10.1002/9781444347166.ch6.

Allmendinger, R.W., Cardozo, N., and Fisher, D.M., 2011, Structural geology algorithms: Vectors and tensors: v. 9781107012, 1–289 p., doi: 10.1017/CBO9780511920202.

Allred, I.J., 2016, Spatial Trends and Facies Distribution of the High- Energy Alluvial Cutler Formation , Southeastern Utah: Brigham Young University, 104 p.

Amidon, W.H., Burbank, D.W., and Gehrels, G.E., 2005a, Construction of detrital mineral populations: Insights from mixing of U-Pb zircon ages in Himalayan rivers: Basin Research, v. 17, p. 463–485, doi: 10.1111/j.1365-2117.2005.00279.x.

Amidon, W.H., Burbank, D.W., and Gehrels, G.E., 2005b, U-Pb zircon ages as a

sediment mixing tracer in the Nepal Himalaya: Earth and Planetary Science Letters, v. 235, p. 244–260, doi: 10.1016/j.epsl.2005.03.019.

Aronoff, R.F., Andronicos, C.L., Vervoort, J.D., and Hunter, R.A., 2016, Redefining the metamorphic history of the oldest rocks in the southern Rocky Mountains: Bulletin of the Geological Society of America, v. 128, p. 1207–1227, doi: 10.1130/B31455.1.

Banham, S.G., and Mountney, N.P., 2013, Evolution of fluvial systems in salt-walled mini- basins: a review and new insights: Sedimentary Geology, v. 296, p. 142–166.

Barbeau, D.L., 2003, A flexural model for the Paradox Basin: Implications for the tectonics of the Ancestral Rocky Mountains: Basin Research, v. 15, p. 97–115, doi: 10.1046/j.1365-2117.2003.00194.x.

Best, J.L., and Brayshaw, A.C., 1985, Flow separation - a physical process for the concentration of heavy minerals within alluvial channels.: Journal - Geological Society (London), v. 142, p. 747–755, doi: 10.1144/gsjgs.142.5.0747.

Bickford, M.E., and Cudzilo, T.F., 1975, U-Pb age of zircon from Vernal Mesa-type quartz monzonite, Unaweep Canyon, west-central Colorado: Bulletin of the Geological Society of America, v. 86, p. 1432–1434, doi: 10.1130/0016-7606(1975)86<1432:UAOZFV>2.0.CO;2.

Blum, M., Rogers, K., Gleason, J., Najman, Y., Cruz, J., and Fox, L., 2018, Allogenic and Autogenic Signals in the Stratigraphic Record of the Deep-Sea Bengal Fan: Scientific Reports, v. 8, p. 1–13, doi: 10.1038/s41598-018-25819-5.

Bonich, M.B., Samson, S.D., and Fedo, C.M., 2017, Incongruity of detrital zircon ages

of granitic bedrock and its derived alluvium: An example from the stepladder

    mountains, Southeastern California: The Journal of Geology, v. 125, p. 337–350,

    doi: 10.1086/691146.

Bradley, R.W., and Venditti, J.G., 2017, Reevaluating dune scaling relations: Earth-

    Science Reviews, v. 165, p. 356–376, doi: 10.1016/j.earscirev.2016.11.004.

Bridge, J., and Best, J., 1997, Preservation of planar laminae due to migration of low-

    relief bed waves over aggrading upper-stage plane beds: Comparison of

    experimental data with theory: Sedimentology, v. 44, p. 253–262, doi:

    10.1111/j.1365-3091.1997.tb01523.x.

Buller, C.D., 2009, The Influence of Salt on Stratigraphy and Depositional

    Environments in the Pennsylvanian-Permian Honaker Trail and Cutler Formations,

    Paradox Basin: New Mexico State University, 91 p.

Bunte, K., and Abt, S.R., 2001, Sampling Surface and Subsurface Particle-Size

    Distributions in Wadable Gravel- and Cobble-Bed Streams for Analyses in

    Sediment Transport , Hydraulics , and Streambed Monitoring: U.S. Department of

    Agriculture, Forest Service, Rocky Mountain Research Station, v. Gen. Tech., p.

    428, doi: 10.1017/CBO9781107415324.004.

Cain, S.A., and Mountney, N.P., 2009, Spatial and temporal evolution of a terminal

    fluvial fan system: The permian organ rock formation, South-east Utah, USA:

    Sedimentology, v. 56, p. 1774–1800, doi: 10.1111/j.1365-3091.2009.01057.x.

Campbell, J.A., 1980, Lower Permian depositional systems and Wolfcampian

    paleogeography, Uncomphagre Basin, eastern Utah and southwestern Colorado:

Paleozoic Paleogeography of the West-Central United States: Rocky Mountain
Paleogeography Symposium 1, v. 6, p. 327–340.

Campbell, J.A., and Steele-Mallory, B.A., 1979, Depositional Environments of the
Uranium bearing Cutler Formations , Lisbon Valley , Utah: United States
Department of the Interior Geologic Survey, v. Open-File.

Capaldi, T.N., Horton, B.K., McKenzie, N.R., Stockli, D.F., and Odlum, M.L., 2017,
Sediment provenance in contractional orogens: The detrital zircon record from
modern rivers in the Andean fold-thrust belt and foreland basin of western
Argentina: Earth and Planetary Science Letters, v. 479, p. 83–97, doi:
10.1016/j.epsl.2017.09.001.

Cawood, P.A., Hawkesworth, C.J., and Dhuime, B., 2013, The continental record and
the generation of continental crust: Bulletin of the Geological Society of America,
v. 125, p. 14–32, doi: 10.1130/B30722.1.

Cheng, N.-S., 1997, Simplified Settling Velocity Formula for Sediment Particle: Journal
of Hydraulic Engineering, v. 123, p. 149–152, doi: 10.1061/(ASCE)0733-
9429(1997)123:2(149).

Condon, S.M., 1997, Geology of the Pennsylvanian and Permian Cutler Group and
Permian Kaibab Limestone in the Paradox Basin, Southeastern Utah and
Southwestern Colorado: U.S. Geological Survey Bulletin, p. 46,
http://pubs.usgs.gov/bul/b2000p/b2000p.pdf.

Daniel, C.G., Pfeifer, L.S., Jones, J. V., and McFarlane, C.M., 2013, Detrital zircon
evidence for non-Laurentian provenance, Mesoproterozoic (ca. 1490-1450 Ma)

deposition and orogenesis in a reconstructed orogenic belt, northern New Mexico, USA: Defining the Picuris orogeny: Geological Society of America Bulletin, v. 125, p. 1423–1441, doi: 10.1130/B30804.1.

Decelles, P.G., Langford, R.P., and Schwartz, R.K., 1983, Two new methods of paleocurrent determination from trough cross- stratification.: Journal of Sedimentary Petrology, v. 53, p. 629–642, doi: 10.1306/212f824c-2b24-11d7-8648000102c1865d.

Dickinson, W.R., 2008, Impact of differential zircon fertility of granitoid basement rocks in North America on age populations of detrital zircons and implications for granite petrogenesis: Earth and Planetary Science Letters, v. 275, p. 80–92, doi: 10.1016/j.epsl.2008.08.003.

Dickinson, W.R., and Gehrels, G.E., 2009, U-Pb ages of detrital zircons in Jurassic eolian and associated sandstones of the Colorado plateau: Evidence for transcontinental dispersal and intraregional recycling of sediment: Bulletin of the Geological Society of America, v. 121, p. 408–433, doi: 10.1130/B26406.1.

Dickinson, W.R., and Gehrels, G.E., 2003, U–Pb ages of detrital zircons from Permian and Jurassic eolian sandstones of the Colorado Plateau, USA: paleogeographic implications: Sedimentary Geology, v. 163, p. 29–66, doi: 10.1016/S0037-0738(03)00158-1.

Dubiel, R.F., Huntoon, J.E., Stanesco, J.D., and Condon, S.M., 2009, Cutler Group Alluvial, Eolian, and Marine Deposystems: Permian Facies Relations and Climatic Variability in the Paradox Basin: RMAG Special Publication, p. 265–308.

Eberth, D.A., and Miall, A.D., 1991, Stratigraphy, sedimentology and evolution of a
vertebrate-bearing, braided to anastomosed fluvial system, Cutler Formation
(Permian-Pennsylvanian), north-central New Mexico: Sedimentary Geology, v. 72,
p. 225–252, doi: 10.1016/0037-0738(91)90013-4.

Fedele, J.J., and Paola, C., 2007, Similarity solutions for fluvial sediment fining by
selective deposition: Journal of Geophysical Research, v. 112, p. F02038, doi:
10.1029/2005JF000409.

Ferguson, R.I., 2003, Emergence of abrupt gravel to sand transitions along rivers
through sorting processes: Geology, v. 31, p. 159, doi: 10.1130/0091-
7613(2003)031<0159:EOAGTS>2.0.CO;2.

Ferguson, R., 2007, Flow resistance equations for gravel- and boulder-bed streams:
Water Resources Research, v. 43, p. 1–12, doi: 10.1029/2006WR005422.

Findlay, C., 2020a, "Paradox Basin - Cutler Group - Fluvial Bulk Sediment Grain Size
Data", Texas Data Repository Dataverse, V1,
https://doi.org/10.18738/T8/QBCUGG.

Findlay, C., 2020b, "Paradox Basin - Cutler Group - Fluvial and Aeolian Cross-
stratification Set Thickness Data", Texas Data Repository Dataverse, V1,
https://doi.org/10.18738/T8/IS4QM3.

Findlay, C., 2020c, "Paradox Basin - Cutler Group, Moenkopi Formation, and Chinle
Formation - Detrital Zircon ICP-MS U-Th-Pb Data", Texas Data Repository
Dataverse, V1, https://doi.org/10.18738/T8/C13S4H.

Findlay, C., 2020d, "Paradox Basin - Cutler Group and Chinle Formation - Detrital

Zircon Grain Size and Age Data", Texas Data Repository Dataverse, V1,
https://doi.org/10.18738/T8/0VVUBO.

Flint, J.J., 1974, Stream gradient as a function of order, magnitude, and discharge: Water
Resources Research, v. 10, p. 969–973, doi: 10.1029/WR010i005p00969.

Garzanti, E., Andò, S., and Vezzoli, G., 2008, Settling equivalence of detrital minerals
and grain-size dependence of sediment composition: Earth and Planetary Science
Letters, v. 273, p. 138–151, doi: 10.1016/j.epsl.2008.06.020.

Gehrels, G.E., Blakey, R., Karlstrom, K.E., Timmons, J.M., Dickinson, B., and Pecha,
M., 2011, Detrital zircon U-Pb geochronology of Paleozoic strata in the Grand
Canyon, Arizona: Lithosphere, v. 3, p. 183–200, doi: 10.1130/L121.1.

Gehrels, G., and Pecha, M., 2014, Detrital zircon U-Pb geochronology and Hf isotope
geochemistry of Paleozoic and Triassic passive margin strata of western North
America: Geosphere, v. 10, p. 49–65, doi: 10.1130/GES00889.1.

Gehrels, G., Valencia, V., and Pullen, A., 2006, Detrital Zircon Geochronology by
Laser-Ablation Multicollector ICPMS at the Arizona LaserChron Center: The
Paleontological Society Papers, v. 12, p. 67–76, doi: 10.1017/s1089332600001352.

Hack, J.T., 1973, Stream-Profile Analysis and Stream-Gradient Index: Journal Research
of United States Geological Survey, p. 421–429,
https://www.scirp.org/(S(lz5mqp453edsnp55rrgjct55))/reference/ReferencesPapers.
aspx?ReferenceID=1320012 (accessed April 2020).

Hajek, E.A., and Heller, P.L., 2012, Flow-Depth Scaling In Alluvial Architecture and
Nonmarine Sequence Stratigraphy: Example from the Castlegate Sandstone,

Central Utah, U.S.A: Journal of Sedimentary Research, v. 82, p. 121–130, doi: 10.2110/jsr.2012.8.

Hatcher, R., 1987, Tectonics Of The Southern And Central Appalachian Internides: Annual Review of Earth and Planetary Sciences, v. 15, p. 337–362, doi: 10.1146/annurev.earth.15.1.337.

Hayden, A.T., Lamb, M.P., Fischer, W.W., Ewing, R.C., McElroy, B.J., and Williams, R.M.E., 2019, Formation of sinuous ridges by inversion of river-channel belts in Utah, USA, with implications for Mars: Icarus, v. 332, p. 92–110, doi: 10.1016/j.icarus.2019.04.019.

Hietpas, J., Samson, S., Moecher, D., and Chakraborty, S., 2011, Enhancing tectonic and provenance information from detrital zircon studies: assessing terrane-scale sampling and grain-scale characterization: Journal of the Geological Society, v. 168, p. 309–318, doi: 10.1144/0016-76492009-163.

Hoy, R.G., and Ridgway, K.D., 2002, Syndepositional thrust-related deformation and sedimentation in an Ancestral Rocky Mountains basin, Central Colorado trough, Colorado, USA: Bulletin of the Geological Society of America, v. 114, p. 804–828, doi: 10.1130/0016-7606(2002)114<0804:STRDAS>2.0.CO;2.

Hudec, M.R., Jackson, M.P.A., and Schultz-Ela, D.D., 2009, The paradox of minibasin subsidence into salt: Clues to the evolution of crustal basins: Bulletin of the Geological Society of America, v. 121, p. 201–221, doi: 10.1130/B26275.1.

Hunter, R.E., 1977, Terminology of Cross-Stratified Sedimentary Layers and Climbing-Ripple Structures: SEPM Journal of Sedimentary Research, v. Vol. 47, p. 697–706,

doi: 10.1306/212f7225-2b24-11d7-8648000102c1865d.

Huntoon, J.E., and Chan, M.A., 1987, Marine origin of paleotopographic relief on eolian White Rim Sandstone (Permian), Elaterite Basin, Utah: American Association of Petroleum Geologists Bulletin, v. 71, p. 1035–1045, doi: 10.1306/703c7def-1707-11d7-8645000102c1865d.

Ibañez-Mejia, M., Pullen, A., Pepper, M., Urbani, F., Ghoshal, G., and Ibañez-Mejia, J.C., 2018, Use and abuse of detrital zircon U-Pb geochronology—A case from the Río Orinoco delta, eastern Venezuela: Geology, v. 46, p. 1019–1022, doi: 10.1130/G45596.1.

Ireland, T.R., Flöttmann, T., Fanning, C.M., Gibson, G.M., and Preiss, W. V., 1998, Development of the early Paleozoic Pacific margin of Gondwana from detrital-zircon ages across the Delamerian orogen: Geology, v. 26, p. 243, doi: 10.1130/0091-7613(1998)026<0243:DOTEPP>2.3.CO;2.

Irmis, R.B., Mundil, R., Martz, J.W., and Parker, W.G., 2011, High-resolution U-Pb ages from the Upper Triassic Chinle Formation (New Mexico, USA) support a diachronous rise of dinosaurs: Earth and Planetary Science Letters, v. 309, p. 258–267, doi: 10.1016/j.epsl.2011.07.015.

Jackson, L.J., Horton, B.K., and Vallejo, C., 2019, Detrital zircon U-Pb geochronology of modern Andean rivers in Ecuador: Fingerprinting tectonic provinces and assessing downstream propagation of provenance signals: Geosphere, v. 15, p. 1943–1957, doi: 10.1130/GES02126.1.

Jerolmack, D.J., and Brzinski, T.A., 2010, Equivalence of abrupt grain-size transitions in

alluvial rivers and eolian sand seas: A hypothesis: Geology, v. 38, p. 719–722, doi: 10.1130/G30922.1.

Jessup, M.J., Jones III, J. V., Karlstrom, K.E., Williams, M.L., Connelly, J.N., and Heizler, M.T., 2006, Three Proterozoic Orogenic Episodes and an Intervening Exhumation Event in the Black Canyon of the Gunnison Region, Colorado: The Journal of Geology, v. 114, p. 555–576, doi: 10.1086/506160.

Jones, J. V., Connelly, J.N., Karlstrom, K.E., Williams, M.L., and Doe, M.F., 2009, Age, provenance, and tectonic setting of Paleoproterozoic quartzite successions in the southwestern United States: Bulletin of the Geological Society of America, v. 121, p. 247–264, doi: 10.1130/B26351.1.

Jordan, O.D., and Mountney, N.P., 2012, Sequence Stratigraphic Evolution and Cyclicity of An Ancient Coastal Desert System: The Pennsylvanian-Permian Lower Cutler Beds, Paradox Basin, Utah, U.S.A: Journal of Sedimentary Research, v. 82, p. 755–780, doi: 10.2110/jsr.2012.54.

Keller, G.R., and Hatcher, R.D., 1999, Some comparisons of the structure and evolution of the southern Appalachian-Ouachita orogen and portions of the Trans-European suture zone region, *in* Tectonophysics, v. 314, p. 43–68, doi: 10.1016/S0040-1951(99)00236-X.

Kluth, C.F., and Coney, P.J., 1981, Plate tectonics of the Ancestral Rocky Mountains: Geology, v. 9, p. 10–15, doi: 10.1130/0091-7613(1981)9<10:PTOTAR>2.0.CO;2.

Kluth, C.F., and Duchene, H.R., 2009, Late Pennsylvanian and Early Permian Structural Geology and Tectonic History of the Paradox Basin and Uncompahgre Uplift,

Colorado and Utah: RMAG Special Publication, p. 178–197.

Kocurek, G., 1991, Interpretation of ancient eolian sand dunes: Annual review of Earth
and planetary sciences, 19, p. 43–75, doi: 10.1146/annurev.ea.19.050191.000355.

Komar, P.D., and Reimers, C.E., 1978, Grain Shape Effects on Settling Rates: The
Journal of Geology, v. 86, p. 193–209, doi: 10.1086/649674.

Lamb, M.P., and Venditti, J.G., 2016, The grain size gap and abrupt gravel-sand
transitions in rivers due to suspension fallout: Geophysical Research Letters, v. 43,
p. 3777–3785, doi: 10.1002/2016GL068713.

Langford, R., and Chan, M.A., 1988, Flood surfaces and deflation surfaces within the
Cutler Formation and Cedar Mesa Sandstone (Permian), southeastern Utah:
Bulletin of the Geological Society of America, v. 100, p. 1541–1549, doi:
10.1130/0016-7606(1988)100<1541:FSADSW>2.3.CO;2.

Langford, R.P., and Chan, M.A., 1989, Fluvial-aeolian interactions: Part II, ancient
systems: Sedimentology, v. 36, p. 1037–1051, doi: 10.1111/j.1365-
3091.1989.tb01541.x.

Lawrence, R.L., Cox, R., Mapes, R.W., and Coleman, D.S., 2011, Hydrodynamic
fractionation of zircon age populations: Geological Society of America Bulletin, v.
123, p. 295–305, doi: 10.1130/B30151.1.

Lawton, T.F., Buller, C.D., and Parr, T.R., 2015, Provenance of a Permian erg on the
western margin of Pangea: Depositional system of the Kungurian (late Leonardian)
Castle Valley and White Rim sandstones and subjacent Cutler Group, Paradox
Basin, Utah, USA: Geosphere, v. 11, p. 1475–1506, doi: 10.1130/GES01174.1.

Leary, R.J., Umhoefer, P., Smith, M.E., and Riggs, N., 2017, A three-sided orogen: A new tectonic model for Ancestral Rocky Mountain uplift and basin development: Geology, v. 45, p. 735–738, doi: 10.1130/G39041.1.

Leary, R.J., Umhoefer, P., Smith, M.E., Smith, T.M., Saylor, J.E., Riggs, N., Burr, G., Lodes, E., Foley, D., Licht, A., Mueller, M.A., and Baird, C., 2020, Provenance of Pennsylvanian–Permian sedimentary rocks associated with the Ancestral Rocky Mountains orogeny in southwestern Laurentia: Implications for continental-scale Laurentian sediment transport systems: Lithosphere, v. 12, p. 88–121, doi: 10.1130/L1115.1.

Leclair, S.F., and Bridge, J.S., 2001, Quantitative Interpretation of Sedimentary Structures Formed by River Dunes: Journal of Sedimentary Research, v. 71, p. 713–716, doi: 10.1306/2DC40962-0E47-11D7-8643000102C1865D.

Link, P.K., Mahon, R.C., Beranek, L.P., Campbell-Stone, E.A., and Lynds, R., 2014, Detrital zircon provenance of Pennsylvanian to Permian sandstones from the Wyoming craton and Wood River Basin, Idaho, U.S.A.: Rocky Mountain Geology, v. 49, p. 115–136, doi: 10.2113/gsrocky.49.2.115.

Livaccari, R., Bowring, T.J., Farmer, E.T., Garhart, K.S., Hosack, A.M., Scott, R.B., and Unruh, D., 2001, Proterozoic Rocks of the Uncompahgre Plateau , Western Colorado and Eastern Utah: Geological Society of America Abstracts with Programs, v. 33, p. 44.

Lynds, R.M., Mohrig, D., Hajek, E.A., and Heller, P.L., 2014, Paleoslope Reconstruction In Sandy Suspended-Load-Dominant Rivers: Journal of

Sedimentary Research, v. 84, p. 825–836, doi: 10.2110/jsr.2014.60.

Mack, G.H., and Rasmussen, K.A., 1984, Alluvial- fan sedimentation of the Cutler

Formation (Permo- Pennsylvanian) near Gateway, Colorado (USA).: Geological

Society of America Bulletin, v. 95, p. 109–116, doi: 10.1130/0016-

7606(1984)95<109:ASOTCF>2.0.CO;2.

Mason, C.C., Romans, B.W., Stockli, D.F., Mapes, R.W., and Fildani, A., 2019, Detrital

zircons reveal sea-level and hydroclimate controls on Amazon River to deep-sea

fan sediment transfer: Geology, v. 47, p. 563–567, doi: 10.1130/G45852.1.

May, S.R., Gray, G.G., Summa, L.L., Stewart, N.R., Gehrels, G.E., and Pecha, M.E.,

2013, Detrital zircon geochronology from the bighorn basin, wyoming, usa:

Implications for tectonostratigraphic evolution and paleogeography: Bulletin of the

Geological Society of America, v. 125, p. 1403–1422, doi: 10.1130/B30824.1.

Miller, K.L., Reitz, M.D., and Jerolmack, D.J., 2014, Generalized sorting profile of

alluvial fans: Geophysical Research Letters, v. 41, p. 7191–7199, doi:

10.1002/2014GL060991.

Moecher, D.P., and Samson, S.D., 2006, Differential zircon fertility of source terranes

and natural bias in the detrital zircon record: Implications for sedimentary

provenance analysis: Earth and Planetary Science Letters, v. 247, p. 252–266, doi:

10.1016/j.epsl.2006.04.035.

Mohrig, D., Heller, P.L., Paola, C., and Lyons, W.J., 2000, Interpreting avulsion process

from ancient alluvial sequences: Guadalope-Matarranya system (Northern Spain)

and Wasatch formation (Western Colorado): Bulletin of the Geological Society of

America, v. 112, p. 1787–1803, doi: 10.1130/0016-
7606(2000)112<1787:IAPFAA>2.0.CO;2.

Mose, D.G., and Bickford, M.E., 1969, Precambrian geochronology in the Unaweep
Canyon, west-central Colorado: Journal of Geophysical Research, v. 74, p. 1677–
1687, doi: 10.1029/JB074i006p01677.

Mountney, N.P., 2006, Periodic accumulation and destruction of aeolian erg sequences
in the Permian Cedar Mesa Sandstone, White Canyon, southern Utah, USA:
Sedimentology, v. 53, p. 789–823, doi: 10.1111/j.1365-3091.2006.00793.x.

Mountney, N.P., and Jagger, A., 2004, Stratigraphic evolution of an aeolian erg margin
system: The Permian Cedar Mesa Sandstone, SE Utah, USA: Sedimentology, v. 51,
p. 713–743, doi: 10.1111/j.1365-3091.2004.00646.x.

Nair, K., Singleton, J., Holm-Denoma, C., and Egenhoff, S., 2018, Detrital Zircon
Geochronology of Pennsylvanian-Permian Strata in Colorado: Evidence for
Appalachian-Derived Sediment and Implications for the Timing of Ancestral Rocky
Mountains Uplift: The Mountain Geologist, v. 55, p. 119–140, doi:
10.31582/rmag.mg.55.3.119.

Olson, J.C.C., Marvin, R.F.F., Parker, R.L.L., and Mehnert, H.H.H., 1977, Age and
tectonic setting of lower Paleozoic alkalic and mafic rocks, carbonatites, and
thorium veins in south-central Colorado: US Geological Survey Journal of
Research, v. 5, p. 673–687.

Owen, A., Jupp, P.E., Nichols, G.J., Hartley, A.J., Weissmann, G.S., and Sadykova, D.,
2015, Statistical Estimation of the Position of An Apex: Application To the

Geological Record: Journal of Sedimentary Research, v. 85, p. 142–152, doi: 10.2110/jsr.2015.16.

Owen, A., Nichols, G.J., Hartley, A.J., and Weissmann, G.S., 2017, Vertical trends within the prograding Salt Wash distributive fluvial system, SW United States: Basin Research, v. 29, p. 64–80, doi: 10.1111/bre.12165.

Paola, C., and Borgman, L., 1991, Reconstructing random topography from preserved stratification: Sedimentology, v. 38, p. 553–565, doi: 10.1111/j.1365-3091.1991.tb01008.x.

Paola, C., and Mohrig, D., 1996, Palaeohydraulics revisited: palaeoslope estimation in coarse-grained braided rivers: Basin Research, v. 8, p. 243–254, doi: 10.1046/j.1365-2117.1996.00253.x.

Parker, G., 1991a, Selective Sorting and Abrasion of River Gravel. I: Theory: Journal of Hydraulic Engineering, v. 117, p. 131–147, doi: 10.1061/(ASCE)0733-9429(1991)117:2(131).

Parker, G., 1991b, Selective Sorting and Abrasion of River Gravel. II: Applications: Journal of Hydraulic Engineering, v. 117, p. 150–171, doi: 10.1061/(ASCE)0733-9429(1991)117:2(150).

Parr, T.R., 2012, Correlation of the Castle Valley Eolianite, Castle Valley, Utah, and the influence of the Castle Valley salt diapir on depositional setting and stratigraphic geometry: Las Cruces, New Mexico State University, 125 p. p.

Peterson, F., 1988, Pennsylvanian to Jurassic eolian transportation systems in the western United States: Sedimentary Geology, v. 56, p. 207–260, doi: 10.1016/0037-

0738(88)90055-3.

Rasmussen, D.L., 2009, Road Logs Across the Uncompahgre Uplift and the Deep Fold
and Fault Belt, Northern Paradox Basin, Colorado and Utah: RMAG Special
Publication, p. 691–778.

Saylor, J.E., Jordan, J.C., Sundell, K.E., Wang, X., Wang, S., and Deng, T., 2018,
Topographic growth of the Jishi Shan and its impact on basin and hydrology
evolution, NE Tibetan Plateau: Basin Research, v. 30, p. 544–563, doi:
10.1111/bre.12264.

Saylor, J.E., and Sundell, K.E., 2016, Quantifying comparison of large detrital
geochronology data sets: Geosphere, v. 12, p. 203–220, doi: 10.1130/GES01237.1.

Schoene, B., and Bowring, S.A., 2006, U–Pb systematics of the McClure Mountain
syenite: thermochronological constraints on the age of the 40Ar/39Ar standard
MMhb: Contributions to Mineralogy and Petrology, v. 151, p. 615–630, doi:
10.1007/s00410-006-0077-4.

Sharman, G.R., and Johnstone, S.A., 2017, Sediment unmixing using detrital
geochronology: Earth and Planetary Science Letters, v. 477, p. 183–194, doi:
10.1016/j.epsl.2017.07.044.

Sharman, G.R., Sylvester, Z., and Covault, J.A., 2019, Conversion of tectonic and
climatic forcings into records of sediment supply and provenance: Scientific
Reports, v. 9, p. 4115, doi: 10.1038/s41598-019-39754-6.

Slingerland, R.L., 1984, Role of Hydraulic Sorting in the Origin of Fluvial Placers:
SEPM Journal of Sedimentary Research, v. Vol. 54, p. 137–150, doi:

10.1306/212F83C8-2B24-11D7-8648000102C1865D.

Slingerland, R.L., 1977, The Effects of Entrainment on the Hydraulic Equivalence
Relationships of Light and Heavy Minerals in Sands: SEPM Journal of Sedimentary
Research, v. Vol. 47, p. 753–770, doi: 10.1306/212F7243-2B24-11D7-
8648000102C1865D.

Soreghan, G.S.L.L., Elmore, R.D., and Lewchuck, M.T., 2002, Sedimentologic-
magnetic record of western Pangean climate in upper Paleozoic loessite (lower
Cutler beds, Utah): Bulletin of the Geological Society of America, v. 114, p. 1019–
1035, doi: 10.1130/0016-7606(2002)114<1019:SMROWP>2.0.CO;2.

Soreghan, G.S., Soreghan, M.J., and Hamilton, M.A., 2008, Origin and significance of
loess in late Paleozoic western Pangaea: A record of tropical cold?
Palaeogeography, Palaeoclimatology, Palaeoecology, v. 268, p. 234–259, doi:
10.1016/j.palaeo.2008.03.050.

Soreghan, G.S., Soreghan, M.J., Sweet, D.E., and Moore, K.D., 2009, Hot Fan or Cold
Outwash? Hypothesized Proglacial Deposition in the Upper Paleozoic Cutler
Formation, Western Tropical Pangea: Journal of Sedimentary Research, v. 79, p.
495–522, doi: 10.2110/jsr.2009.055.

Speed, R.C., and Sleep, N.H., 1982, Antler orogeny and foreland basin: a model (
Nevada, Idaho).: Geological Society of America Bulletin, v. 93, p. 815–828, doi:
10.1130/0016-7606(1982)93<815:AOAFBA>2.0.CO;2.

Sweet, A.C., Soreghan, G.S., Sweet, D.E., Soreghan, M.J., and Madden, A.S., 2013,
Permian dust in Oklahoma: Source and origin for Middle Permian (Flowerpot-

Blaine) redbeds in Western Tropical Pangaea: Sedimentary Geology, v. 284–285, p. 181–196, doi: 10.1016/j.sedgeo.2012.12.006.

Thomas, W.A., Gehrels, G.E., and Romero, M.C., 2016, Detrital zircons from crystalline rocks along the Southern Oklahoma fault system, Wichita and Arbuckle Mountains, USA: Geosphere, v. 12, p. 1224–1234, doi: 10.1130/GES01316.1.

Trampush, S.M., Huzurbazar, S., and McElroy, B., 2014, Empirical assessment of theory for bankfull characteristics of alluvial channels: Water Resources Research, v. 50, p. 9211–9220, doi: 10.1002/2014WR015597.

Trudgill, B.D., 2011, Evolution of salt structures in the northern Paradox Basin: controls on evaporite deposition, salt wall growth and supra-salt stratigraphic architecture: Basin Research, v. 23, p. 208–238, doi: 10.1111/j.1365-2117.2010.00478.x.

Trudgill, B.D., and Paz, M., 2009, Restoration of Mountain Front and Salt Structures in the northern Paradox Basin, SE Utah: RMAG Special Publication, p. 132–177.

Venus, J.H., Mountney, N.P., and Mccaffrey, W.D., 2015, Syn-sedimentary salt diapirism as a control on fluvial-system evolution: An example from the proximal Permian Cutler Group, SE Utah, USA: Basin Research, v. 27, p. 152–182, doi: 10.1111/bre.12066.

Vermeesch, P., 2004, How many grains are needed for a provenance study? Earth and Planetary Science Letters, v. 224, p. 441–451, doi: 10.1016/j.epsl.2004.05.037.

Vermeesch, P., and Garzanti, E., 2015, Making geological sense of 'Big Data' in sedimentary provenance analysis: Chemical Geology, v. 409, p. 20–27, doi: 10.1016/j.chemgeo.2015.05.004.

Vermeesch, P., Resentini, A., and Garzanti, E., 2016, An R package for statistical provenance analysis: Sedimentary Geology, v. 336, p. 14–25, doi: 10.1016/j.sedgeo.2016.01.009.

Whitmeyer, S.J., and Karlstrom, K.E., 2007, Tectonic model for the Proterozoic growth of North America: Geosphere, v. 3, p. 220–259, doi: 10.1130/GES00055.1.

Wilkerson, G. V., and Parker, G., 2011, Physical Basis for Quasi-Universal Relationships Describing Bankfull Hydraulic Geometry of Sand-Bed Rivers: Journal of Hydraulic Engineering, v. 137, p. 739–753, doi: 10.1061/(ASCE)HY.1943-7900.0000352.

Wortman, G.L., Samson, S.D., and Hibbard, J.P., 2000, Precise U-Pb zircon constraints on the earliest magmatic history of the Carolina terrane: Journal of Geology, v. 108, p. 321–338, doi: 10.1086/314401.

Yang, K.-M., and Dorobek, S.L., 1995, The Permian Basin of West Texas and New Mexico: flexural modeling and evidence for lithospheric heterogeneity across the Marathon Foreland, *in* Stratigraphic Evolution of Foreland Basins, p. 37–50, doi: 10.2110/pec.95.52.0037.

Yang, S., Zhang, F., and Wang, Z., 2012, Grain size distribution and age population of detrital zircons from the Changjiang (Yangtze) River system, China: Chemical Geology, v. 296–297, p. 26–38, doi: 10.1016/j.chemgeo.2011.12.016.

Ye, H., Royden, L., Burchfiel, C., and Schuepbach, M., 1996, Late Paleozoic Deformation of Interior North America : The Greater Ancestral Rocky Mountains 1: v. 9, p. 1397–1432.

4. ALLOGENIC CONTROLS ON ANCIENT FLUVIAL AND AEOLIAN INTERACTIONS – PERMIAN CUTLER GROUP

4.1. Introduction

Fluvial and aeolian systems erode, transport, and deposit sand and silt across planetary surfaces. Typically, fluvial systems supply most of the sand for aeolian systems, but interactions between these two systems occur where sediment is reciprocally recycled from one to the other typically due to spatial and temporal changes in climate, tectonics, and sedimentation (Langford and Chan, 1989; Bullard and McTainsh, 2003; Field et al., 2009; Al-Masrahy and Mountney, 2015; Liu and Coulthard, 2015). Fluvial-aeolian interactions are well demonstrated in modern settings, such as the Namib-Orange river (Bluck et al., 2007; Garzanti et al., 2012, 2014), however detecting and unraveling such interactions in ancient deposits remains challenging because the processes that promote accumulation and preservation in these terrestrial system inherently bias environmental signals in the detrital record (Swanson et al., 2019; Cardenas et al., 2019). The extent to which reciprocal recycling from fluvial-aeolian interactions that leads to interbedded fluvial–aeolian deposits erase, obfuscate, or modulate the signals of autogenic and allogenic processes that act across time and space in a transport system remains poorly constrained (Langford and Chan, 1989; Jerolmack and Paola, 2010; Romans et al., 2016; Capaldi et al., 2019; Sharman et al., 2019). There is an opportunity to integrate approaches from paleohydraulics, sediment provenance, and mixing models to investigate how fluvial and aeolian systems interact and

150

disentangle the contributions from allogenic and autogenic processes, with implications for reconstructing ancient and modern environments on multiple planetary surfaces.

To better constrain the controls on fluvial-eolian interactions in ancient settings, I use detrital zircon geochronology paired with fluvial and aeolian paleohydraulic reconstruction to examine the effects of spatial sorting and sediment recycling on basinwide accumulation of interbedded fluvial-aeolian deposits in the Pennsylvanian–Permian Paradox Basin of UT and CO (Fig. 23). The Paradox Basin was flanked by the basement-cored Uncompahgre Uplift, one of multiple intraplate depocenters that developed during the Late Paleozoic Ancestral Rocky Mountains. The Virgilian–Wolfcampian foredeep fluvial and forebulge aeolian deposits in the Paradox Basin display unique provenance signature end members. In the Paradox Basin foredeep, the Cutler Group fluvial sediment displays detrital zircon U-Pb age modes of 526 Ma, 1440 Ma, and 1727 Ma, characteristic of sediment derived from the Uncompahgre Uplift (Lawton et al., 2015; Leary et al., 2020). On the forebulge, detrital zircon results demonstrate that equivalent aeolian dune field and loess sediment from the Cedar Mesa erg was derived predominantly from extrabasinal sources (Soreghan et al., 2002; Dickinson and Gehrels, 2003). However, in the foredeep and forebulge, fluvial and aeolian deposits are observed as interbedded and interfingering and influenced by variable subsidence and salt wall uplift that created topographic obstacles (Langford and Chan, 1989; Cain and Mountney, 2011; Venus et al., 2015). This paleogeography allows us to assess the extent to which sediment was recycled between the two systems, and how allogenic processes may have impacted fluvial–aeolian interactions.
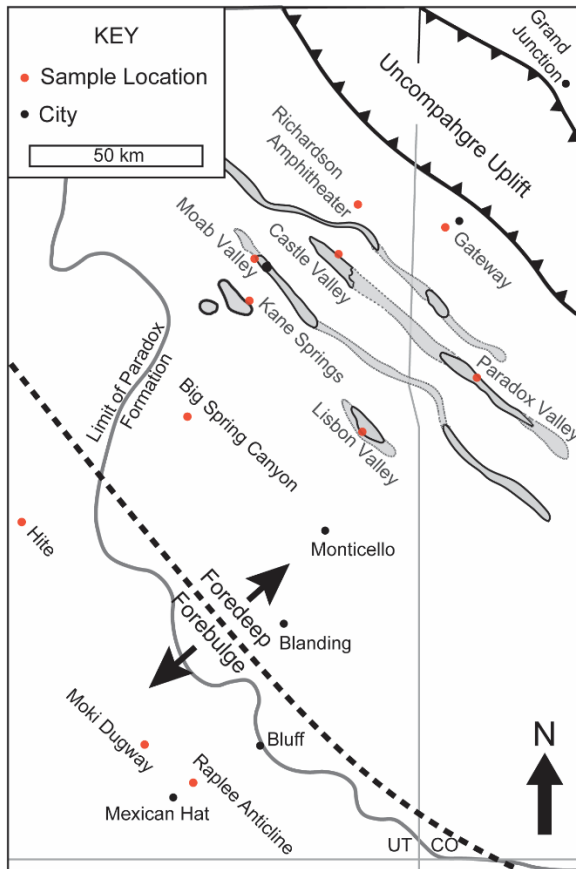
Figure 23: A schematic map of sample locations and the boundary between the foredeep and forebulge in the Paradox Basin (Adapted from Barbeau 2003 and Lawton et al., 2015). The Pennsylvanian – Permian Paradox Basin of UT and CO is a broken plate foreland basin adjacent to the Uncompahgre Uplift (UU) that subsided during deformation of the Ancestral Rocky Mountains (ARM). The Cutler Group is well exposed from source to sink, and grey shapes with black outlines in the foredeep represent aerially exposed salt-cored anticlines and grey outlines represent subsurface salt.

4.2. Methods Used In This Study

Detrital zircon geochronology is a commonly used tool to identify patterns of sediment provenance and mixing, and often implicates allogenic and transport processes as the main controls on the basin fill composition (Blum et al., 2018; Capaldi et al., 2019; Jackson et al., 2019; Mason et al., 2019). Samples (n = 16) were collected for detrital zircon age and size analysis from fluvial channel, aeolian dune, and loess deposits to investigate controls on sediment mixing in the Paradox Basin (Fig. 23) (Soreghan et al., 2002). Detrital zircons were separated from samples using standard mechanical, density, and magnetic methods and analyzed for U-Th-Pb age using an LA-ICP-MS (Gehrels et al., 2006). A minimum of 100–120 individual grains were analyzed in each sample, ages more than 10% discordant were discarded, and 1σ uncertainty is reported. Cross-correlation coefficients (R^2) of probability density functions were used to quantitatively compare similarity of age spectra (Saylor and Sundell, 2016).

Application of statistical mixing models to detrital geochronologic datasets has increased the capability to assess sediment mixing, but assumes that the presence and abundance of detrital zircon age groups in samples are not impacted by hydraulic sorting, which may alter age spectra and obscure evidence of sediment mixing if age groups are unevenly distributed across sediment size fractions (Garzanti et al., 2008; Lawrence et al., 2011; Vermeesch and Garzanti, 2015; Saylor and Sundell, 2016; Sundell and Saylor, 2017; Ibañez-Mejia et al., 2018; Sharman et al., 2018; Saylor et al., 2019). To identify effects of sorting in the ancient fluvial deposits, paleohydraulic reconstruction of fluvial channels was accomplished using grain size, dune cross-

153

stratification thickness (t_{set}), and lateral accretion surface height (h_{LAS}) measurements according to methods thoroughly described in Findlay et al. (in review a) (Ferguson, 2007; Hayden et al., 2019). The coefficient of variation of t_{set} was used to qualitatively determine the effect of aggradation rate on sediment mixing and detrital zircon age signatures in the fluvial and aeolian systems (Jerolmack and Mohrig, 2005; Cardenas et al., 2019). Equivalent spherical grain size (ESD = $(D_{long} * D_{intermediate} * D_{short})^{1/3}$) of detrital zircon was measured from loose grains, or grains mounted in epoxy pucks using a stereoscope. Fluvial bulk sediment median grain size (D_{50}) was calculated from proportionately weighted gravel clast counts and point counts of fine grains according to methods described in Findlay et al. (in review). Aeolian bulk sediment D_{50} was measured with a grain size card on outcrops, and Cedar Mesa D_{50} and D_{97} grain sizes were collected from previous studies (Eastwood, 2011).

To identify effects of sorting in the ancient aeolian deposits, paleowind velocity was reconstructed to determine if the wind could transport detrital zircon observed in fluvial deposits. Ratios of threshold shear velocity ($\boldsymbol{u_{*t}}$) needed to initiate movement of quartz and zircon grains (Shao and Lu, 2000), the impact shear velocity ($\boldsymbol{u_{*i}}$), which is the minimum bound needed to keep grains in motion once they have been initially moved (Bagnold, 1941), and settling velocity of quartz and zircon grains in air (Ferguson and Church, 2004) were related to transport mode of grains and calculate the competency of the ancient wind (Bagnold, 1941; Jerolmack et al., 2006; Eastwood et al., 2012). Particles transported in creep have a $\boldsymbol{u_*}/\boldsymbol{u_{*t}}$ ratio between 0.7 and 1, and in saltation have a ratio between 1 and 1.5 (Eastwood et al., 2012). The ratio of settling

154

velocity w_{sed} to the reconstructed $\boldsymbol{u}_*$ reliably predicts suspension (Eastwood et al., 2012).

Particles transported in suspension have a $w_{sed}/\boldsymbol{u}_*$ ratio of less than 1, in saltation have a

ratio greater than 2.5, and in creep have a ratio greater than ca. 8 (Jerolmack et al., 2006;

Eastwood et al., 2012). The $\boldsymbol{u}_{*t}$ of the D_{50} of aeolian deposits at each location was used

as a minimum estimate of shear velocity at the bed ($\boldsymbol{u}_*$), and $\boldsymbol{u}_{*i}$ of the D_{97} of grainflow

strata in the Cedar Mesa was used as a maximum value of $\boldsymbol{u}_*$ for the entire Paradox

Basin (i.e. Jerolmack et al., 2006; Fedo et al., 2015). If the wind and fluvial channels

could transport all zircon observed in the Cutler Group, hydraulic sorting likely did not

affect detrital zircon age spectra and variability in age spectra can be attributed to spatial

variation in sediment mixing.

4.3. Mixed Provenance Signatures

The flexural profile of the Paradox Basin likely controlled the degree to which

the fluvial system reworked local aeolian deposits. In the foredeep, the fluvial system did

not recycle a large volume of aeolian zircon, and instead received 91 – 98% of detrital

zircons from UU basement rock. Unimodal, bimodal, and trimodal age signatures with

peaks at 526 Ma, 1440 Ma, and 1727 Ma in foredeep Undifferentiated Cutler Formation

fluvial samples are consistent with previous results, and relatively uniform sediment

provenance in the proximal - medial foredeep (Fig. 24, Appendix C) (Lawton et al.,

2015; Leary et al., 2020; Findlay, 2020a). In the distal foredeep (ca. 60 – 125 km

distance from the UU), the UU age signature remains dominant in the Virgilian–

Wolfcampian the fluvial samples of the Lower Cutler Formation. I detect increased

recycling of aeolian deposits in the Lower Cutler Formation relative to proximal and

medial foredeep samples, as evidenced by more aeolian zircon (19%) (Fig. 23, Appendix

C). On the forebulge, the Raplee Anticline sample was deposited in a fluvial

environment but contains at least 59% aeolian zircon, indicating the fluvial channels on

the forebulge mixed sediment from the foredeep fluvial system and recycled aeolian

sediment, unlike channels in the foredeep (Appendix C).
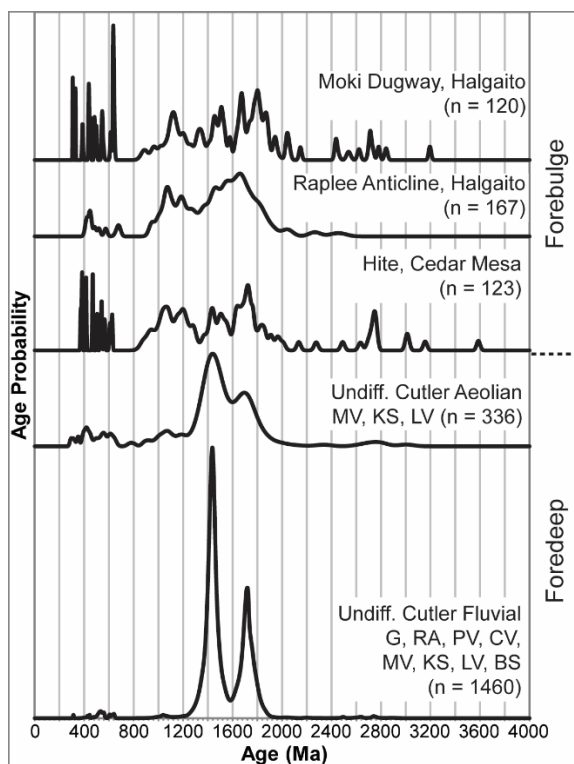
Figure 24: Probability density plots of detrital zircon U-Pb age data. Age spectra of fluvial deposits in the foredeep have age peaks at 526 Ma, 1440 Ma, and 1727 Ma that reflect basement ages of the UU. Interbedded aeolian deposits are more complex but have abundant UU basement ages. Halgaito Formation aeolian loess (Moki Dugway) and fluvial (Raplee Anticline) samples from the forebulge have more complex age signatures but contain UU basement ages. See Appendix C for statistical comparisons.

Variable contribution of the aeolian multimodal detrital zircon signature to fluvial samples across the foredeep to forebulge begs the question: did sorting effectively remove evidence of aeolian recycling in the foredeep or did accumulation controlled by tectonic or autogenic sedimentation affect the recycling? Previous results from settling equivalency and Rouse curves methods show that the fluvial system had sufficient competency to transport all detrital zircon grains derived from the UU and the Cedar Mesa, indicating sorting did not remove aeolian zircon from the fluvial sediment (Appendix D) . Measurements of zircon grains show that zircons with ESD grain size of 30 - 222 μm were deposited with the gravel and sand bed load sediment (Findlay, 2020b), and aeolian detrital zircon have D_{50} and D_{97} ESD grain sizes within that range, 52–153 μm. Thus, the fluvial system was capable of recycling detrital zircon from aeolian deposits, and the multimodal aeolian signal would have been deposited with fluvial sand bed load. However, the diagnostic multimodal detrital age signature consistently observed in aeolian strata is nearly absent in the foredeep fluvial age signatures, suggesting the foredeep fluvial system minimally reworked local aeolian deposits (Fig. 24; Appendix C, D). Reworking of aeolian strata by the Cutler Formation rivers was most prevalent on the forebulge, and somewhat on the distal foredeep, where subsidence rate and sediment supply from the UU were likely lower than in the proximal – medial foredeep.
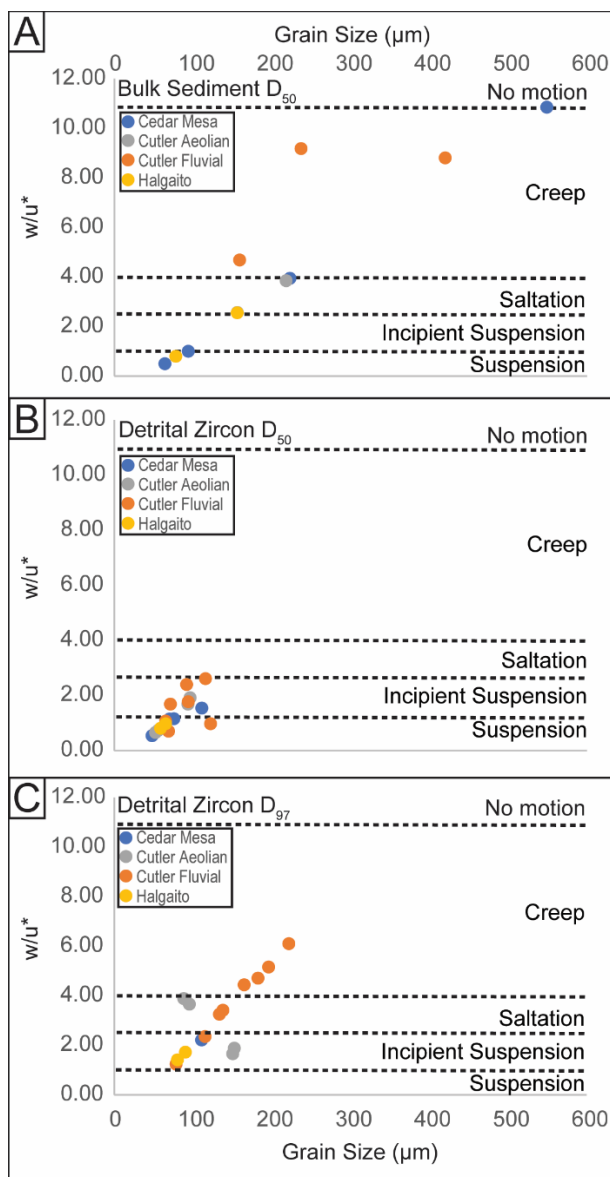
Figure 25: Aeolian paleohydraulic reconstruction of settling velocity (w) and shear velocity at the bed (u*). Threshold shear velocity of the aeolian bulk sediment D$_{50}$ is used for u* at each location to show spatial variation in wind speed. See Table 1 for Cedar Mesa values. A) w/u*values of the bulk sediment D$_{50}$ show that sand sized fluvial sediment could have been transported in creep, but most plots off of the graph and would not be transported. Aeolian an Raplee Anticline Halgaito sediment could be moved in saltation, and Moki Dugway Halgaito sediment in suspension. B) w/u*values of detrital zircon D$_{50}$ show fluvial and aeolian zircon could be transported in suspension, and Halgaito zircon in suspension. C) w/u*values of detrital zircon D$_{97}$ show that the largest zircon from all samples could be recycled and transported in saltation or creep by the wind.

Age spectra from aeolian samples suggest varying amounts of recycling fluvial deposits across the foredeep to forebulge, but, opposite the fluvial system, show more recycling in the foredeep. In the proximal - medial foredeep and near the UU (i.e. Moab Valley, Kane Springs, and Lisbon Valley), Cutler Group aeolian deposits contain UU age zircon, but retain some extrabasinal zircon signal (13 – 46%), and cross-correlation statistical values show foredeep aeolian deposits have more similar age spectra to foredeep fluvial samples than to the Cedar Mesa on the forebulge (Appendix C) (Findlay, 2020a). The proportion of detrital zircon reworked from fluvial deposits decreases away from the UU (toward the forebulge). Aeolian strata are completely composed of extrabasinal sediment (100%) in the forebulge portion of the basin (i.e. aeolian and loess samples from Hite and Moki Dugway, respectively; Fig. 24) (Dickinson and Gehrels, 2003).

Reconstructed wind velocity shows that the wind had the capacity to recycle fluvial zircon across the basin. (Figs. 23, 24). The D_{50} and D_{97} of fluvial zircon are hydraulically smaller than the D_{97} of grainflow deposits in the Cedar Mesa, and u_*/u_{*t} and w_{sed}/u_* ratios show that fluvial zircon could have been moved in suspension, saltation, or creep by the wind, depending on the location (Table 1; Fig. 25B and 25C) (Findlay, 2020b). Further, the abundance of the coarsest fluvial zircon age group (1727 Ma) increases in the foredeep aeolian samples, indicating sorting did not decrease the abundance of the largest grains (Appendix C). The Moki Dugway sample is from a structureless, silty bed, has the same amount of UU age zircon but is statistically dissimilar to the aeolian Cedar Mesa age signature, and was partially transported in

incipient suspension by the wind. The majority of sediment in the Moki Dugway sample is likely loess carried in suspension from the Cedar Mesa mixed with dust from sources further afield, and, like the Cedar Mesa Formation at Hite, did not recycle Cutler Group fluvial zircon (Soreghan et al., 2002). The abundance of UU-derived detrital zircons in the foredeep aeolian strata, but the lack of UU-derived detrital zircons on the forebulge, show that aeolian processes preferentially recycled local fluvial strata in the foredeep compared to the forebulge. More aeolian recycling and less fluvial recycling in the foredeep, where subsidence rate was higher, indicates that different drivers controlled recycling in the two systems but that recycling in both systems is likely tied to basin geometry.

Table 17: Aeolian paleohydraulic reconstruction of maximum size of quartz and zircon grains that could be transported in suspension, saltation, and creep. ($u^* = u^*i$ Cedar Mesa D_{97} (549 μm) = 0.27)

Criteria	Transport Mode	Maximum grain size of transport modes - Cedar Mesa		Quartz		Zircon	
		Quartz (μm)	**Zircon (μm)**	w/u*	u*/u*t	w/u*	u*/u*t
w/u* = 0.5	Pure Suspension	**64**	**48**	0.5	1.1	0.5	0.9
w/u* = 1	Suspension	**94**	**70**	1.0	1.1	1.0	1.0
w/u* = 2.5	Incipient Suspension	**163**	**120**	2.5	1.1	2.5	1.0
w/u* = 4 and u*/u*t = 1	Saltation	**229**	**170**	4.1	1.0	4.0	0.9
u*/u*t = 0.7	Max Creep	**550**	**300**	10.8	0.7	8.6	0.7

160

4.4. Spatially Variable Recycling Linked To Flexural Basin Dynamics

Our results show that fluvial samples become progressively more cosmopolitan away from the uplift as more extrabasinal material, which was delivered by aeolian processes, was reworked by Cutler Group rivers. In contrast, aeolian samples become more homogenized with interbedded fluvial systems closer to the UU, preserving less evidence of extrabasinal signals. Hydraulic sorting can be ruled out as a driver of the observed differences between fluvial and aeolian detrital zircon age signatures because both systems had sufficient hydraulic competency to move grains between the two environments. The degree of recycling by both the Cutler Group rivers and Cutler Group/Cedar Mesa erg generally tracks with spatial position along the flexural foreland basin profile.

I propose that the ability of the fluvial system to rework local aeolian deposits was in part driven by spatial variations in fluvial aggradation rate controlled by variation in basin subsidence rate and sediment supply and is directly tied to the lateral position within the flexural foreland basin system (Fig. 4). Our measurements of dune cross-stratification thickness (t_{set}) can be directly tied to aggradation rate (Jerolmack and Mohrig, 2005; Cardenas et al., 2019). If aggradation rate is zero, climb angle is zero, and dunes become erosive and recycle previous deposits. When aggradation rate is zero, the coefficient of variance of cross-stratification set thickness (C_v) is equal to 0.88 (Jerolmack and Mohrig, 2005; Cardenas et al., 2019). A C_v lower than 0.88 indicates aggradation was greater than 0, which causes a greater proportion of the dune height to be preserved. The C_v of from the foredeep Cutler Group fluvial system is 0.64,

consistent with a high aggradation rate. I also calculate a t_{set} / h_{dune} ratio of ca. 0.45,

higher than the average of modern rivers (avg = 0.34), and similar to aggradational

fluvial systems in ancient (Oligocene Guadalope-Mantarranya system) and modern

(North Loup River, Nebraska) settings (Appendix E) (Jerolmack and Mohrig, 2005). In

the forebulge region, fluvial deposits in the Halgaito Formation preserved few dune

cross-stratification sets (only three were measured in a 120 m measured section)

consistent with a low aggradation rate, increased erosion and greater mixing than in the

foredeep. However, the lack of preserved cross-stratification prohibits calculation of C_v

(Jerolmack and Mohrig, 2005). High aggradation can be driven by high sediment supply

and high subsidence, both of which were likely promoted in the proximal foredeep and

prohibited on the forebulge.

In the foredeep of flexural foreland basins, river systems exhibit high sediment

discharge (Q_s) and channel discharge (Q_w) accompanied by relatively rapid subsidence

attributed to proximity to the topographic load and position in the foredeep. In such

conditions, aggradation is rapid and sediment recycling is inhibited, consistent with the

lack of mixing observed between fluvial and aeolian settings in the proximal-medial

basin positions (as interpreted from detrital zircon age signatures) despite paleohydraulic

reconstructions suggesting that the river system would have been capable of reworking

aeolian deposits (Fig. 4). Approaching more distal reaches, river systems shift to lower

Q_s (driven by autogenic sediment extraction) and lower subsidence associated with the

distal foredeep, and possibly no subsidence or subtle uplift near the forebulge. This

results in a downstream decrease in Q_s/Q_w, which decreases aggradation and increases

channel stability, erosion/incision, and sediment recycling downstream (Armitage et al., 2011; Whittaker et al., 2011; Allen et al., 2013; Wang et al., 2020). This is consistent with detrital zircon age results from the Raplee Anticline Halgaito Formation fluvial sample that shows a high degree of recycling, consistent with low aggradation, low subsidence rate, and low sediment supply in the fluvial system on the forebulge (Fig. 24; Appendix C) (Fig. 26). The aeolian system does not show the same trend of less recycling and high aggradation where subsidence rate was greatest.
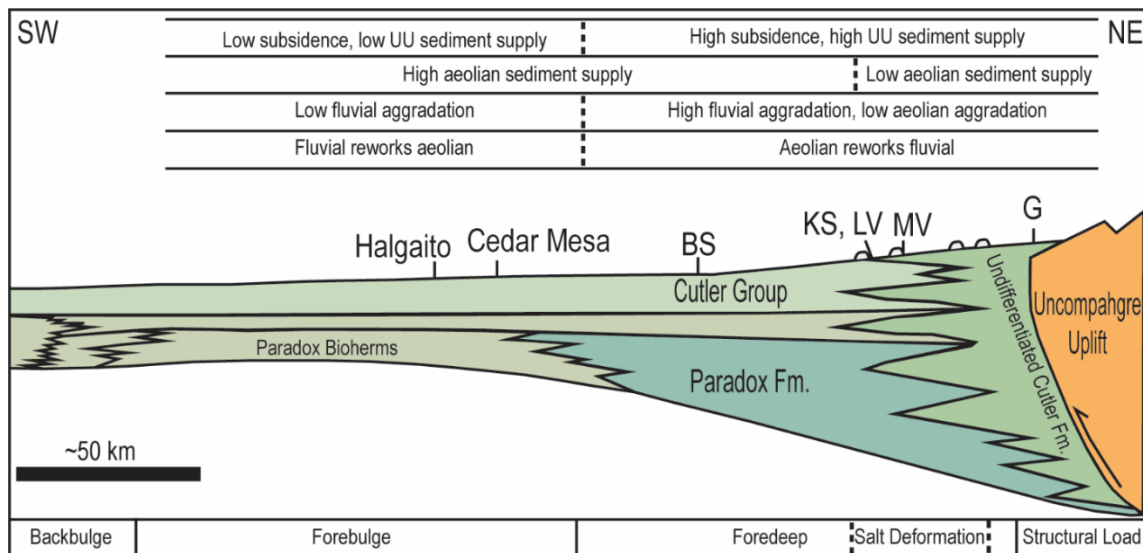
Figure 26: Schematic cross-section of the Paradox Basin with foreland basin structures labelled below and allogenic drivers of fluvial-aeolian interaction labelled above (Adapted from Barbeau, 2003).

Recycling by fluvial and aeolian processes have different spatial patterns across the basin. Sediment recycling by both systems was controlled by aggradation rate, but aggradation was driven by different mechanisms (Fig. 26). In the foredeep, C_v of 0.84

163

for aeolian strata interbedded with fluvial strata in the foredeep indicate aeolian aggradation rate was low, despite being situated where subsidence rate was likely highest and sediment supply from the UU was greatest (Appendix E). In the medial basin, I propose that low aggradation and more recycling of fluvial deposits in the aeolian system was driven by either coeval deformation of salt walls that acted as obstacles to the flow and decreased sediment supply from the Cedar Mesa dune field. The salt walls were likely low topographic features that did not greatly modify the wind, but caused more sand to be deposited on the windward side of the salt walls and decreased aeolian sediment supply to the minibasins on the lee sides of salt walls (e.g. Evans, 1962). On the forebulge, high sediment supply from the Cedar Mesa dune field and other dust sources caused minimal reworking of the UU-derived signature in distal fluvial deposits, consistent with the extrabasinal detrital zircon spectrum in the Cedar Mesa Formation dune field sample from Hite and the Halgaito Formation loess sample from Moki Dugway (Fig. 24). Increased sediment recycling and mixing by the fluvial system is driven by a downstream allogenic decrease in accommodation associated with foreland basin position. Increased sediment recycling and mixing by the aeolian system is unaffected by subsidence rate, and instead caused by a decrease in sediment supply downwind of allogenic salt wall deformation.

4.5. Conclusions

Our data from ancient deposits show that spatial variation in detrital zircon age spectra is not explained by variation in river or wind competency, instead, fluvial – aeolian interactions and the degree of sediment recycling between the two appear to be

164

strongly influenced by basin geometry. The fluvial system progressively incorporated and recycled more aeolian sediment from the foredeep to the forebulge, while the aeolian system displays the opposite trend, and progressively recycled greater proportions of fluvial sediment from the forebulge to the foredeep. In this example, mixing between the systems was directly tied to lateral changes in aggradation attributed to subsidence and sediment supply patterns within the active flexural basin system. Generally, fluvial and aeolian sediment mixing is promoted where aggradation rate is low, but aggradation rate in fluvial systems is driven by proximity to the sediment source and structural load of the foreland basin, and in aeolian systems is driven by low sediment supply downwind of salt-deformed topographic obstacles. These results demonstrate how the integration of provenance and paleohydraulic methods disentangle the interactions between autogenic and allogenic processes, and emphasize variable controls on the fidelity of signal transfer between interacting fluvial and aeolian systems.

4.6. References

Al-Masrahy, M.A., and Mountney, N.P., 2015, A classification scheme for fluvial-aeolian system interaction in desert-margin settings: Aeolian Research, v. 17, p. 67–88, doi: 10.1016/j.aeolia.2015.01.010.

Allen, P.A., Armitage, J.J., Carter, A., Duller, R.A., Michael, N.A., Sinclair, H.D., Whitchurch, A.L., and Whittaker, A.C., 2013, The Qs problem: Sediment volumetric balance of proximal foreland basin systems: Sedimentology, v. 60, p. 102–130, doi: 10.1111/sed.12015.

Armitage, J.J., Duller, R.A., Whittaker, A.C., and Allen, P.A., 2011, Transformation of

tectonic and climatic signals from source to sedimentary archive: Nature

Geoscience, v. 4, p. 231–235, doi: 10.1038/ngeo1087.

Bagnold, R.A., 1941, The Physics of Blown Sand and Desert Dunes: Nature, v. 148, p.
480–481, doi: 10.1038/148480a0.

Bluck, B.J., Ward, J.D., Cartwright, J., and Swart, R., 2007, The Orange River, southern
Africa: An extreme example of a wave-dominated sediment dispersal system in the
South Atlantic Ocean: Journal of the Geological Society, v. 164, p. 341–351, doi:
10.1144/0016-76492005-189.

Blum, M., Rogers, K., Gleason, J., Najman, Y., Cruz, J., and Fox, L., 2018, Allogenic
and Autogenic Signals in the Stratigraphic Record of the Deep-Sea Bengal Fan:
Scientific Reports, v. 8, p. 1–13, doi: 10.1038/s41598-018-25819-5.

Bullard, J.E., and McTainsh, G.H., 2003, Aeolian-fluvial interactions in dryland
environments: examples, concepts and Australia case study: Progress in Physical
Geography, v. 27, p. 471–501, doi: 10.1191/0309133303pp386ra.

Cain, S., and Mountney, N.P., 2011, Downstream changes and associated fluvial-eolian
interactions in an ancient terminal fluvial system: the Permian Organ Rock
Formation, SE Utah, U.S.A, *in* From River to Rock Record, SEPM Special
Publication, 97, p. 167–185.

Capaldi, T.N., George, S.W.M., Hirtz, J.A., Horton, B.K., and Stockli, D.F., 2019,
Fluvial and Eolian Sediment Mixing During Changing Climate Conditions
Recorded in Holocene Andean Foreland Deposits From Argentina (31–33°S):
Frontiers in Earth Science, v. 7, doi: 10.3389/feart.2019.00298.

Cardenas, B.T., Kocurek, G., Mohrig, D., Swanson, T., Hughes, C.M., and Brothers,

    S.C., 2019, Preservation of Autogenic Processes and Allogenic Forcings in Set-

    Scale Aeolian Architecture II: The Scour-and-Fill Dominated Jurassic Page

    Sandstone, Arizona, U.S.A.: Journal of Sedimentary Research, v. 89, p. 741–760,

    doi: 10.2110/jsr.2019.41.

Dickinson, W.R., and Gehrels, G.E., 2003, U–Pb ages of detrital zircons from Permian

    and Jurassic eolian sandstones of the Colorado Plateau, USA: paleogeographic

    implications: Sedimentary Geology, v. 163, p. 29–66, doi: 10.1016/S0037-

    0738(03)00158-1.

Eastwood, E.N., 2011, Reconstructing Environmental Forcings on Aeolian Dune Fields :

    Results From Modern, Ancient, and Numerically-simulated Dunes: The University

    of Texas, 177 p.

Eastwood, E.N., Kocurek, G., Mohrig, D., and Swanson, T., 2012, Methodology for

    reconstructing wind direction, wind speed and duration of wind events from aeolian

    cross-strata: Journal of Geophysical Research: Earth Surface, doi:

    10.1029/2012JF002368.

Evans, J.R., 1962, Falling and Climbing Sand Dunes in the Cronese (“Cat”) Mountain

    Area, San Bernardino County, California: The Journal of Geology, v. 70, p. 107–

    113, doi: 10.1086/626798.

Fedo, C.M., McGlynn, I.O., and McSween, H.Y., 2015, Grain size and hydrodynamic

    sorting controls on the composition of basaltic sediments: Implications for

    interpreting martian soils: Earth and Planetary Science Letters, v. 423, p. 67–77,

doi: 10.1016/j.epsl.2015.03.052.

Ferguson, R., 2007, Flow resistance equations for gravel- and boulder-bed streams: Water Resources Research, v. 43, p. 1–12, doi: 10.1029/2006WR005422.

Ferguson, R.I., and Church, M., 2004, A Simple Universal Equation for Grain Settling Velocity: Journal of Sedimentary Research, v. 74, p. 933–937, doi: 10.1306/051204740933.

Field, J.P., Breshears, D.D., and Whicker, J.J., 2009, Toward a more holistic perspective of soil erosion: Why aeolian research needs to explicitly consider fluvial processes and interactions: Aeolian Research, doi: 10.1016/j.aeolia.2009.04.002.

Findlay, C., 2020a, "Paradox Basin - Cutler Group, Moenkopi Formation, and Chinle Formation - Detrital Zircon ICP-MS U-Th-Pb Data", Texas Data Repository Dataverse, V1, https://doi.org/10.18738/T8/C13S4H.

Findlay, C., 2020b, "Paradox Basin - Cutler Group and Chinle Formation - Detrital Zircon Grain Size and Age Data", Texas Data Repository Dataverse, V1, https://doi.org/10.18738/T8/0VVUBO.

Garzanti, E., Andò, S., and Vezzoli, G., 2008, Settling equivalence of detrital minerals and grain-size dependence of sediment composition: Earth and Planetary Science Letters, v. 273, p. 138–151, doi: 10.1016/j.epsl.2008.06.020.

Garzanti, E., Andò, S., Vezzoli, G., Lustrino, M., Boni, M., and Vermeesch, P., 2012, Petrology of the Namib Sand Sea: Long-distance transport and compositional variability in the wind-displaced Orange Delta: Earth-Science Reviews, v. 112, p. 173–189, doi: 10.1016/j.earscirev.2012.02.008.

Garzanti, E., Vermeesch, P., Andò, S., Lustrino, M., Padoan, M., and Vezzoli, G., 2014, Ultra-long distance littoral transport of Orange sand and provenance of the Skeleton Coast Erg (Namibia): Marine Geology, v. 357, p. 25–36, doi: 10.1016/j.margeo.2014.07.005.

Gehrels, G., Valencia, V., and Pullen, A., 2006, Detrital Zircon Geochronology by Laser-Ablation Multicollector ICPMS at the Arizona LaserChron Center: The Paleontological Society Papers, v. 12, p. 67–76, doi: 10.1017/s1089332600001352.

Hayden, A.T., Lamb, M.P., Fischer, W.W., Ewing, R.C., McElroy, B.J., and Williams, R.M.E., 2019, Formation of sinuous ridges by inversion of river-channel belts in Utah, USA, with implications for Mars: Icarus, v. 332, p. 92–110, doi: 10.1016/j.icarus.2019.04.019.

Ibañez-Mejia, M., Pullen, A., Pepper, M., Urbani, F., Ghoshal, G., and Ibañez-Mejia, J.C., 2018, Use and abuse of detrital zircon U-Pb geochronology—A case from the Río Orinoco delta, eastern Venezuela: Geology, v. 46, p. 1019–1022, doi: 10.1130/G45596.1.

Jackson, L.J., Horton, B.K., and Vallejo, C., 2019, Detrital zircon U-Pb geochronology of modern Andean rivers in Ecuador: Fingerprinting tectonic provinces and assessing downstream propagation of provenance signals: Geosphere, v. 15, p. 1943–1957, doi: 10.1130/GES02126.1.

Jerolmack, D.J., and Mohrig, D., 2005, Frozen dynamics of migrating bedforms: Geology, v. 33, p. 57–60, doi: 10.1130/G20897.1.

Jerolmack, D.J., Mohrig, D., Grotzinger, J.P., Fike, D.A., and Watters, W.A., 2006,

Spatial grain size sorting in eolian ripples and estimation of wind conditions on planetary surfaces: Application to Meridiani Planum, Mars: Journal of Geophysical Research E: Planets, v. 111, doi: 10.1029/2005JE002544.

Jerolmack, D.J., and Paola, C., 2010, Shredding of environmental signals by sediment transport: Geophysical Research Letters, v. 37, p. 1–5, doi: 10.1029/2010GL044638.

Langford, R.P., and Chan, M.A., 1989, Fluvial-aeolian interactions: Part II, ancient systems: Sedimentology, v. 36, p. 1037–1051, doi: 10.1111/j.1365-3091.1989.tb01541.x.

Lawrence, R.L., Cox, R., Mapes, R.W., and Coleman, D.S., 2011, Hydrodynamic fractionation of zircon age populations: Geological Society of America Bulletin, v. 123, p. 295–305, doi: 10.1130/B30151.1.

Lawton, T.F., Buller, C.D., and Parr, T.R., 2015, Provenance of a Permian erg on the western margin of Pangea: Depositional system of the Kungurian (late Leonardian) Castle Valley and White Rim sandstones and subjacent Cutler Group, Paradox Basin, Utah, USA: Geosphere, v. 11, p. 1475–1506, doi: 10.1130/GES01174.1.

Leary, R.J., Umhoefer, P., Smith, M.E., Smith, T.M., Saylor, J.E., Riggs, N., Burr, G., Lodes, E., Foley, D., Licht, A., Mueller, M.A., and Baird, C., 2020, Provenance of Pennsylvanian–Permian sedimentary rocks associated with the Ancestral Rocky Mountains orogeny in southwestern Laurentia: Implications for continental-scale Laurentian sediment transport systems: Lithosphere, v. 12, p. 88–121, doi: 10.1130/L1115.1.

Liu, B., and Coulthard, T.J., 2015, Mapping the interactions between rivers and sand

    dunes: Implications for fluvial and aeolian geomorphology: Geomorphology, v.

    231, p. 246–257, doi: 10.1016/j.geomorph.2014.12.011.

Mason, C.C., Romans, B.W., Stockli, D.F., Mapes, R.W., and Fildani, A., 2019, Detrital

    zircons reveal sea-level and hydroclimate controls on Amazon River to deep-sea

    fan sediment transfer: Geology, v. 47, p. 563–567, doi: 10.1130/G45852.1.

Romans, B.W., Castelltort, S., Covault, J.A., Fildani, A., and Walsh, J.P., 2016,

    Environmental signal propagation in sedimentary systems across timescales: Earth-

    Science Reviews, v. 153, p. 7–29, doi: 10.1016/j.earscirev.2015.07.012.

Saylor, J.E., and Sundell, K.E., 2016, Quantifying comparison of large detrital

    geochronology data sets: Geosphere, v. 12, p. 203–220, doi: 10.1130/GES01237.1.

Saylor, J.E., Sundell, K.E., and Sharman, G.R., 2019, Characterizing sediment sources

    by non-negative matrix factorization of detrital geochronological data: Earth and

    Planetary Science Letters, v. 512, p. 46–58, doi: 10.1016/j.epsl.2019.01.044.

Shao, Y., and Lu, H., 2000, A simple expression for wind erosion threshold friction

    velocity: Journal of Geophysical Research: Atmospheres, v. 105, p. 22437–22443,

    doi: 10.1029/2000JD900304.

Sharman, G.R., Sharman, J.P., and Sylvester, Z., 2018, detritalPy: A Python-based

    toolset for visualizing and analysing detrital geo-thermochronologic data: The

    Depositional Record, v. 4, p. 202–215, doi: 10.1002/dep2.45.

Sharman, G.R., Sylvester, Z., and Covault, J.A., 2019, Conversion of tectonic and

    climatic forcings into records of sediment supply and provenance: Scientific

171

Reports, v. 9, p. 4115, doi: 10.1038/s41598-019-39754-6.

Soreghan, M.J., Soreghan, G.S.L.L., and Hamilton, M.A., 2002, Paleowinds inferred from detrital-zircon geochronology of upper Paleozoic loessite, western equatorial Pangea: Geology, v. 30, p. 695–698, doi: 10.1130/0091-7613(2002)030<0695:PIFDZG>2.0.CO;2.

Sundell, K.E., and Saylor, J.E., 2017, Unmixing detrital geochronology age distributions: Geochemistry, Geophysics, Geosystems, v. 18, p. 2872–2886, doi: 10.1002/2016GC006774.

Swanson, T., Mohrig, D., Kocurek, G., Cardenas, B.T., and Wolinsky, M.A., 2019, Preservation of Autogenic Processes and Allogenic Forcings in Set-Scale Aeolian Architecture I: Numerical Experiments: Journal of Sedimentary Research, v. 89, p. 728–740, doi: 10.2110/jsr.2019.42.

Venus, J.H., Mountney, N.P., and Mccaffrey, W.D., 2015, Syn-sedimentary salt diapirism as a control on fluvial-system evolution: An example from the proximal Permian Cutler Group, SE Utah, USA: Basin Research, v. 27, p. 152–182, doi: 10.1111/bre.12066.

Vermeesch, P., and Garzanti, E., 2015, Making geological sense of "Big Data" in sedimentary provenance analysis: Chemical Geology, v. 409, p. 20–27, doi: 10.1016/j.chemgeo.2015.05.004.

Wang, Y., Storms, J.E.A., Martinius, A.W., Karssenberg, D., and Abels, H.A., 2020, Evaluating alluvial stratigraphic response to cyclic and non-cyclic upstream forcing through process-based alluvial architecture modelling: Basin Research, p.

bre.12454, doi: 10.1111/bre.12454.

Whittaker, A.C., Duller, R.A., Springett, J., Smithells, R.A., Whitchurch, A.L., and

Allen, P.A., 2011, Decoding downstream trends in stratigraphic grain size as a

function of tectonic subsidence and sediment supply: Geological Society of

America Bulletin, v. 123, p. 1363–1382, doi: 10.1130/B30351.1.

5. CONCLUSIONS

In this study, I reconstructed flow depth, slope, discharge, and flow competency of ancient fluvial systems from field measurements of grain size and cross-stratification set thickness and integrate the reconstructions with measured detrital zircon age and size from the Cutler Group fluvial - aeolian system in the foredeep and forebulge of the Paradox Basin. Our results show that gravel- and sand-bedded channels can transport detrital zircon grains without sorting them by size or age, but sorting is more likely to sort detrital zircon grains in silty environments. Variability in the Cutler Group fluvial provenance data is not related to sorting. 3-way multi-dimensional scaling confirms that sorting did not affect provenance data. Rather, I detect changes in provenance of sediment from subtly distinct sources within the Uncompahgre Uplift, suggesting at least three alluvial fans draining distinct catchments into the proximal basin. Active salt uplift likely routed fans into NW-flowing axial fluvial systems between salt walls in the medial foredeep of the basin.

Paleohydraulic reconstruction and provenance analysis also show that sorting did not affect provenance results from fluvial and aeolian deposits in the foredeep to forebulge of the Cutler Group. These results indicate that sediment recycling and predominance of fluvial or aeolian depositional systems varies between the forebulge and foredeep, likely controlled by aggradation rate in both systems. In the fluvial system, where sediment supply and subsidence rate are high, aggradation rate was likely high and caused less sediment recycling. Fluvial sediment supply and subsidence rate were

likely highest in the foredeep, where fluvial sediment recycling is minimal, and lowest on the forebulge, where fluvial sediment recycling is prevalent. In the aeolian system, sediment recycling is minimal on the forebulge, where extrabasinal sediment supply was high, and prevalent in the medial basin, where salt-cored anticlines likely acted as barricades to the wind-blown sediment supply.

Effects of sorting on detrital zircon provenance data can be detected by combining paleohydraulic reconstruction and provenance methods. In fluvial systems, sorting likely only occurs in silty environments where basal shear stress is too low to move all detrital zircon in suspension. This study demonstrates the value of the methods for detailed reconstruction of ancient fluvial and aeolian systems. The allogenic forces that shaped fluvial and aeolian interactions in the Permian Cutler Group likely affect fluvial and aeolian interactions in ancient and modern environments. Detailed reconstructions are used in petroleum and water exploration to inform the composition and expected locations and trends of high quality reservoir rocks in a basin. Reconstructions of ancient fluvial and aeolian interactions can also be used to interpret ancient planetary surface processes and environmental conditions that may have affected early life forms in our solar system. Detailed provenance studies can be utilized in a variety of geoscience studies, and the results of this study further refine the methodology needed to confidently interpret sediment provenance.

APPENDIX A

FACIES ANALYSIS

Facies F_g includes 1 to 10 meter thick structureless conglomerate beds with sharp

erosional bases (Fig. 5; Table 18). Beds are tabular and laterally continuous, or lenticular

and fill scours up to 2 meters deep. Gravel is subrounded to rounded granite, gneiss, and

biotite-quartz schist pebble- and cobble-sized clasts, but some beds contain boulders.

Conglomerate beds fine upward into low angle and trough cross-stratified pebbly

sandstone. This facies is observed only at the Gateway site. Facies F_g is equivalent to

previously reported facies and environments: fan head trench deposits (Campbell, 1980);

laterally continuous stream flood facies (Mack and Rasmussen, 1984); facies Gm

braided and anastamosed fluvial channel deposits (Eberth and Miall, 1991); bar deposits

(Cain and Mountney, 2009); subaqueous debris flows, hyperconcentrated flood flows,

and traction flow deposits (Soreghan et al., 2009); and channel bar and high

concentration flood deposits (Allred, 2016). Tabular laterally continuous beds of F_g are

deposits from sheetfloods, and lenticular scour filling beds as deposits from traction flow

in fluvial channels. Also present northeast of the Gateway location, but not included in

this facies, are matrix supported cobble-boulder conglomerates interpreted to be

deposited by debris flows (Mack and Rasmussen, 1984; Soreghan et al., 2009).

Facies F_{la} includes low-angle cross-stratified conglomerate, pebbly sandstone,

and medium- to coarse-grained sandstone beds (Fig. 5; Table 18). Beds are tabular and

laterally continuous for hundreds of meters with internal scours and conglomerate lags,

or are lenticular less than 50 meters wide. Beds have a sharp erosional base and a

gradational upper contact. Low-angle cross-stratification sets are decimeter to 2 meters

thick, and lenticular beds contain only a few sets of low angle cross-stratification sets.

Low-angle cross-stratified sets are normally graded, with bottomsets and scour troughs defined by clast-supported conglomerates or single-grain layers of gravel lag, foresets defined by very coarse to medium-lower sandstone, and rarely preserved topsets defined by fine sandstone and silty-sandstone. Laterally discontinuous beds can be followed 10s to 100s of meters and are up to 9 meters thick. Granule to cobble size clasts are subrounded to rounded, and are composed of granite, biotite-quartz schist, and gneiss in the proximal basin at Gateway, Richardson Amphitheater, and Paradox Valley, and a mix of granite, gneiss, and mudstone rip-up clasts in the medial basin. At Kane Springs and Lisbon Valley which are situated furthest from the Uncompahgre Uplift, granite and metamorphic clasts were not observed. F_{la} is present at all locations, but median grain size decreases basinward. Facies F_{la} is similar to previously described facies: finer grained conglomerates (Campbell, 1980); braided stream deposits (Mack and Rasmussen, 1984); facies Sla braided fluvial channel deposits (Eberth and Miall, 1991); low angle planar cross-bedded sandstone formed by lateral migration of in-channel and point bars (Cain and Mountney, 2009); hyperconcentrated flow and traction flow deposits (Soreghan et al., 2009); and fluvial channel bar migration deposits (Allred, 2016). F_{la} are LAS formed by migration of bars in fluvial channels. This facies is key because the height and grain size of LAS with preserved topsets were measured for use in paleohydraulic reconstruction and were sampled for detrital zircon geochronology.

Facies F_t includes pebbly sandstone and sandstone with 2 to 50 centimeter thick, normally graded trough cross-stratification sets (Table 18). Viewed perpendicular to flow direction, cross-strata appear tabular with tangential bottomsets. Beds have sharp

178

erosional bases and gradational upper contacts, and are 1 – 10 meters thick with internal

scours up to 2 meters deep (Fig. 5). The conglomerate or gravel lag is the thickness of a

few clasts at the base of channel scours and cross-bed troughs. Foresets are normally

graded, and the median grain size ranges between sites from very fine to very coarse

sandstone. F_t sets are occasionally superimposed on low-angle cross-beds of F_{la}.

Laminae of the troughs are 1 – 10 millimeters thick and often have red and white

banding. F_t is present at all locations, but grain size decreases basinward and gravel lag

is rare at Kane Springs, Lisbon Valley, and Big Spring Canyon. Facies F_t is similar to

previously proposed facies, including: finer grained conglomerates (Campbell, 1980);

braided stream deposits (Mack and Rasmussen, 1984); facies Sti and Stii from braided

and anastamosed fluvial channel, sheet splay, and crevasse splay deposits (Eberth and

Miall, 1991); sandy bar form migration deposits (Cain and Mountney, 2009);

hyperconcentrated flow and traction flow deposits (Soreghan et al., 2009); and fluvial

channel bar migration deposits (Allred, 2016). F_t was formed by migration of 3D dunes

in fluvial channels. The height and grain size of dune trough cross-stratification sets in F_t

were measured for use in paleohydraulic reconstruction and were sampled for detrital

zircon geochronology.

Facies F_{ppl} includes 10 cm – 6 m thick tabular beds of planar parallel laminated

medium to coarse grained micaceous sandstone with interspersed granules and pebbles

(Fig. 5; Table 18). Bedding surfaces have parting lineations and, rarely, pebbly

sandstone has imbricated pebbles. Beds are laterally continuous and have either sharp,

flat bases or gradational bases overlying facies F_{la}. F_{ppl} is observed at Richardson

179

Amphitheater, Paradox Valley, and Moab Valley, is rare at Gateway, Castle Valley and Lisbon Valley, and not observed at Kane Springs. Facies F_{ppl} is similar to previously reported facies and environments, including: distal braided deposits and coarse grained meandering deposits (Campbell, 1980); braided stream deposits (Mack and Rasmussen, 1984); facies Sh and Sl braided and anastamosed fluvial channel, sheet splay, and crevasse splay deposits (Eberth and Miall, 1991); upper flow regime fluvial channel or sheetflood deposits (Cain and Mountney, 2009); hyperconcentrated flow and traction flow deposits (Soreghan et al., 2009); and sheetflood deposits (Allred, 2016). F_{ppl} was formed in the upper flow regime of fluvial channels, possibly in fast flowing shallow water on top of bars, where it conformably overlies facies $F_{la,}$ and in crevasse-splays where it is laterally continuous and interbedded with overbank deposits.

Facies F_r includes current ripple cross-laminated sets of friable silty sandstone less than 6 centimeters thick (Table 18). Beds can be traced for hundreds of meters, but may be incised by F_g, F_{la}, or Ft. Facies F_r either has sharp upper and lower contacts with mudstone, or a gradational basal contact overlying facies F_{la}, F_t, or F_{ppl}. F_r is present at all locations except Gateway. Climbing ripples are present at Castle Valley and Lisbon Valley. F_r is similar to previously reported facies and environments, including: fine grained meandering fluvial deposits (Campbell, 1980); facies Sr sheet splay, crevasse channel, and floodplain deposits (Eberth and Miall, 1991); current ripple laminated sandstone (Cain and Mountney, 2009); and sheetflood deposits (Allred, 2016). F_r is interpreted to be formed by ripple migration in unidirectional flow on channel bar tops

where it overlies F_{la}, F_t, or F_{ppl}, and by ripple migration in unidirectional flow of fluvial overbank deposits where interbedded with mudstone.

Facies S_m includes structureless, fine upper to very fine lower grain size, poorly to well sorted sandstone beds that are less than 50 centimeters thick (Table 18). Structureless sandstone beds of S_m have sharp, flat basal contacts and sharp upper contacts. Beds are tabular and laterally continuous. Beds are often incised by facies F_g, F_{la}, or Ft. Facies S_m is similar to previously reported facies: Sm with bedding destroyed (Eberth and Miall, 1991); rapidly deposited or destroyed bedding sandstone (Cain and Mountney, 2009); high-density turbidity flow deposits (Soreghan et al., 2009); and levee overbank and unconfined sheetflow deposits (Allred, 2016). S_m was rapidly deposited fluvial overbank deposits or sandstone with bedding destroyed by bioturbation.

Facies M_m includes structureless or crudely laminated silty mudstone (Table 18). Facies M_i includes 1 – 20 centimeter thick beds of very fine to coarse grained, current ripple cross-laminated and planar parallel laminated sandstone beds interbedded with structureless or crudely laminated silty mudstone of similar thickness. Thin sandstone beds of M_i are occasionally lenticular, but more often tabular. Facies M_m and M_i are present at all locations, but increase in abundance and thickness away from the uplift. Five to 25 meter thick units of M_m and M_i are present at Castle Valley, Moab Valley, and Lisbon Valley, and form slopes with poor exposure. M_m and M_i are under- and overlain by both fluvial and aeolian deposits at Moab Valley, Kane Springs, and Lisbon Valley. M_m and M_i are similar to previously reported facies and environments: distal braided and fine meandering fluvial facies (Campbell, 1980); braided stream overbank

181

deposits (Mack and Rasmussen, 1984); overbank-interdune deposits (Langford and Chan, 1989); facies Fl crevasse channel and fluvial floodplain suspension deposits (Eberth and Miall, 1991); and fluvial suspension deposits of Cain and Mountney (2006). M_m and M_i are interpreted to be fluvial floodplain suspension deposits and aeolian interdune deposits in a wet dune field.

Facies P includes structureless to crudely laminated silty and very fine sandstone beds with abundant round an irregular shaped carbonate nodules up to 10 centimeters in diameter (Table 18). Nodules share a sand matrix with their host rock, but are enriched in calcite cement. Nodular beds are present at all locations, but are most well developed at Richardson Amphitheater, Moab Valley, Kane Springs, and Lisbon Valley. Facies P is similar to: pedogenic features (Mack and Rasmussen, 1984), facies Lp paleosols (Eberth and Miall, 1991), nodular calcrete deposits formed during substrate stabilization (Cain and Mountney, 2006), and paleosols formed during periods of nondeposition on a fluvial floodplain (Allred, 2016). Facies P is interpreted to be bioturbated paleosols with diagenetic calcite nodules formed on a fluvial floodplain.

Facies A_{la} includes moderately to well sorted, very fine to fine sandstone with low-angle cross-stratification sets $0.5 - 2$ m thick (Table 18). Facies A_{la} lacks steeply dipping cross-stratification and relatively coarser grained wedge-shaped beds at the top and base of cross-stratification sets. A_{la} has inversely graded mm-scale laminae consistent with climbing translatent strata or wind-ripple laminae (Hunter, 1977; Kocurek, 1991). Beds of A_{la} are typically 0.5 to 2 meters thick, but one unit at Lisbon Valley is 3.5 meters thick. Near the top of the section at Lisbon Valley, two beds of A_{la}

contain crinkly laminations. A_{la} is present at Moab Valley, Kane Springs, and Lisbon Valley. Facies A_{la} is similar to aeolian sandstone (Campbell and Steele-Mallory, 1979) and aeolian wind-ripple deposits (Cain and Mountney, 2009). Facies A_{la} is interpreted to be formed by migration of wind-ripples on aeolian sandsheets.

Facies A_t includes moderately- to well-sorted very fine to fine sandstone with steeply dipping tabular cross-stratification sets that are frequently greater than 1 meter thick (Table 18). In facies A_t the medium-sized sand grains occasionally form wedge shaped bottomsets that are coarser than the tabular foresets. A_t is present at Moab Valley, Lisbon Valley, and Kane Springs locations. Facies A_t is similar to eolian sandstone (Campbell and Steele-Mallory, 1979) and aeolian grain flow deposits of (Cain and Mountney, 2009). Facies A_t is interpreted to be formed by grain flows on the lee side of migrating aeolian dunes.

Facies C_s includes laterally continuous, thin, tabular sandy packstone and grainstone carbonate beds with sparse gastropod and brachiopod fossils (Table 18). Bedding surface tops are commonly bioturbated and burrowed. Facies C_s is present at Moab Valley, Kane Springs, and Lisbon Valley locations in association with facies A_{la} and A_t. Facies C_s is similar to marine sandstone (Campbell and Steele-Mallory, 1979). Facies C_s is interpreted to be shallow marine carbonate deposits that contain sand reworked from underlying aeolian and fluvial deposits.

Facies U includes orange colored very fine to coarse sandstone beds with a variety of sedimentary structures (Table 18). Facies U contains planar parallel laminated, trough cross-stratified, tabular cross-stratified, or structureless sandstone, and both

183

laterally continuous and lenticular beds are observed. Some units of facies U at Gateway

contain lenticular channel-form beds with trough cross-stratification and granule to

pebble-sized lag in the troughs (Fig. 5). Beds are less than 2 meters thick. Facies U is

observed at Gateway, Richardson Amphitheater, and Castle Valley locations. Facies

similar to our facies U have been variably interpreted as fluvial and eolian deposits in a

medial-braided stream environment (Campbell, 1980), sheetflood deposits with minor

pedogenic features (Mack and Rasmussen, 1984), loessite and fluvially reworked

loessite (Soreghan et al., 2008), and eolian suspension, fluvial traction, or lacustrine

deposits (Soreghan et al., 2009). Facies U is either eolian loessite or fluvial overbank

deposits.

Table 18: Facies charts

Depositional Environment	Subenvironment	Facies	Code	Structures and geometry	Interpretation	G	RA	PM	PV	CV	MV	LV	KS	BS
Fluvial	Channel	Inverse graded extraformational boulder and cobble conglomerate and massive conglomerate	Fg	Subrounded to rounded, inverse grading, clast supported and matrix supported diamictite. Beds 1-10 meters thick, clast supported conglomerates fill scour troughs.	Alluvial fan debris flow, sheetflood, and channel deposits	x								
		Low-angle cross-bedded conglomerate, pebbly sandstone, and sandstone	Fla	Subrounded to rounded, low-angle, fining upward cross-bed sets decimeter to 2 meters thick. Scoured bases and internal lenticular channel form geometry. Grain size decreases basinward.	Lateral accretion sets formed by migration of lower flow regime bars in fluvial channels	x	x	x	x	x	x	x	x	
		Trough cross-bedded conglomerate, pebbly sandstone, and sandstone	Ft	Subrounded to rounded, fining upward trough cross-bed sets 2 centimeters to 50 centimeters thick. Scoured bases and internal lenticular channel form geometry. Occasionally superimposed on low-angle cross-beds. Grain size decreases basinward.	Formed by migration of lower flow regime 3-D dunes in fluvial channels	x	x	x	x	x	x	x	x	
		Planar parallel laminated sandstone	Fppl	Planar parallel laminations of very fine to coarse grain sandstone and rare imbricated gravel. Parting lineations (primary current lineations) common on exposed bedding planes.	Formed in upper-flow regime in braided streams	x					x			
	Fluvial overbank and floodplain	Ripple and dune cross laminated sandstone	Fr	Ripple cross laminated very fine to fine grain sandstone, commonly silty and friable. Cross laminae sets typically less than 6 cm but up to 20 cm.	Formed by migration of ripples and dunes in unidirectional fluvial overbank flows	x	x	x	x	x	x	x	x	x

185

Table 18: Facies charts continued

Environment	Sub-environment	Facies	Code	Description	Interpretation
Fluvial and aeolian	Fluvial floodplain and aeolian interdune	Massive sandstone	Sm	Mostly structureless fine upper to very fine lower grain sandstone with some crude laminations. Tabular beds are typically less than 50 cm thick.	Rapidly deposited or bioturbated fluvial overbank deposits
		Massive mudstone	Mm	Mostly structureless silty mudstone with occasional crude planar parallel laminations	Bioturbated fluvial overbank and floodplain deposits
		Interbedded sandstone and mudstone	Mi	Very fine-coarse thin sandstone beds, asymmetrical ripples, current ripple cross-lamination and planar parallel laminations. Silty and sandy mudstone beds, crudely laminated, occasional planar parallel laminations. Laterally continuous, some internal sandstone beds lenticular.	Fluvial overbank deposits and aeolian interdune deposits
		Nodular paleosol	P	Structureless or crudely laminated silty and very fine grain sandstone with abundant carbonate nodules up to 10 cm in diameter	Bioturbated paleosol with diagenetic carbonate nodules
Aeolian	Dune field	Low-angle crossbedded sandstone	Ala	Moderately well to well sorted very fine to fine grain sandstone with low-angle planar cross-stratification.	Migration of wind ripples on aeolian sandsheets
		Tabular and trough crossbedded sandstone	At	Moderately well to well sorted very fine to fine grain sandstone with steeply dipping (>10°) tabular crossbed sets commonly greater than 1 meter thick. The coarsest sand forms wedges in the bottomsets.	Deposited by grainflows on aeolian dunes
Marine	Shallow marine	Sandy carbonate	Cs	Thin, sandy carbonate beds. Gastropod and brachiopod fossils are common at Moab Fault and Lisbon Valley, tops are commonly bioturbated. Tabular geometry, laterally continuous.	Shallow marine carbonate
Unidentified		Unidentified laterally continuous sandstone	U	Planar parallel laminated, tabular and trough cross-bedded or structureless, flat non-erosional base, top scoured into by overlying deposits, laterally continuous for 100s of meters.	

APPENDIX B

COMPREHENSIVE DETRITAL ZIRCON PROVENANCE ANALYSIS

The 526 Ma, 1440 Ma, and 1727 Ma age groups present in our detrital samples are locally present in basement rocks of the UU (Mose and Bickford, 1969; Bickford and Cudzilo, 1975; Olson et al., 1977; Livaccari et al., 2001; Jessup et al., 2006; Schoene and Bowring, 2006; Whitmeyer and Karlstrom, 2007; Jones et al., 2009; Daniel et al., 2013; Aronoff et al., 2016). Input from more distant sediment sources, such as 500 – 800 Ma rocks in Peri-Gondwanan terranes along the Appalachian – Marathon – Ouachita orogenic belt and 520 – 540 Ma rocks in the Wichita Mountains of Oklahoma (Wortman et al., 2000; Moecher and Samson, 2006; Abati et al., 2010; Thomas et al., 2016), is not required to explain provenance of the Undifferentiated Cutler fluvial deposits. Non-unique minor age groups present in our samples are also present in the majority of Pennsylvanian – Triassic sedimentary rocks of the western US, and might be derived from local recycling of the Pennsylvanian Ingleside and Lyons Formations of the Eagle Basin, the Molas and Hermosa Formations of the Paradox Basin, or the Permian Cedar Mesa or White Rim formations of the Paradox Basin (Dickinson and Gehrels, 2003; Lawton et al., 2015; Nair et al., 2018; Leary et al., 2020). 291 – 490 Ma, 497 – 682 Ma, and 928 – 1299 Ma detrital zircon found in the Undifferentiated Cutler, Cedar Mesa, White Rim, and Halgaito formations and other Pennsylvanian-Permian sedimentary rocks in the western USA are interpreted to have come from the Appalachian region, or the Ellesmerian orogen in the Arctic (Soreghan et al., 2002; Dickinson and Gehrels, 2003, 2009; Gehrels et al., 2011; May et al., 2013; Sweet et al., 2013; Link et al., 2014; Thomas et al., 2016; Nair et al., 2018; Leary et al., 2020). 1813 – 2494 Ma detrital zircon could have come from many North American rocks, including the Little Belt arc,

Selway terrane, Elves Chasm gneiss, Slave craton, Rae craton, Hearne craton, Superior craton, and Trans-Hudson orogeny, and Penokean orogeny (Whitmeyer and Karlstrom, 2007; Nair et al., 2018; Leary et al., 2020). 2603 – 3587 Ma detrital zircon could be derived from the Wyoming province to the north or Mojave terrane to the west, or recycled from any number of North American sedimentary and metasedimentary rocks that contain detrital zircon of these ages (Whitmeyer and Karlstrom, 2007; Nair et al., 2018; Leary et al., 2020).

The Organ Rock, Moenkopi, and Chinle age signatures are each distinct and multimodal (Fig. 17; Table 15). The Organ Rock sample (CPF_070) from Hite, UT, where the contact between the Cedar Mesa formation and overlying Organ Rock formation is clear, has broad peaks of ages between 1300 – 1500 Ma and 1600 – 1860 Ma that are consistent with derivation from local basement sources. This sample also has several age groups between 291 – 490 Ma and 497 – 682 Ma, which are rare in our samples from the Undifferentiated Cutler Formation. 300 – 490 Ma, 497 – 682 Ma, and 950 – 1300 Ma ages are abundant in the underlying Cedar Mesa Formation and overlying White Rim Formation (Dickinson and Gehrels, 2003; Lawton et al., 2015). The prevalence of locally derived 1300 – 1500 Ma and 1600 – 1860 Ma UU zircon in the Organ Rock Formation at Hite, UT might be an indication that it is the distal equivalent of our Undifferentiated Cutler Formation fluvial system in which fluvial-aeolian interactions might have introduced abundant 291 – 490 Ma and 497 – 682 Ma aeolian derived zircon into the fluvial system, but 950 – 1300 Ma zircon prevalent in the Cedar Mesa and White Rim aeolian systems is not present in the Organ Rock sample.

Further investigation is needed to determine the spatial patterns of fluvial-aeolian interactions in the Cutler Group. 300 – 490 Ma, 497 – 682 Ma, and 950 – 1300 Ma age groups are also abundant in other Permian strata of the Colorado Plateau, and have been interpreted to be derived from the Appalachian region or the Ellesmerian orogen (Dickinson and Gehrels, 2003, 2009; Gehrels et al., 2011; Gehrels and Pecha, 2014; Leary et al., 2020).

At Richardson Amphitheater, the Moenkopi Formation overlies our section above an angular unconformity (Allred, 2016). The Moenkopi sample (CPF_068) has local basement (520 – 530 Ma, 1300 – 1500 Ma, and 1600 – 1860 Ma) and Appalachian or Ellesmerian age groups (291 – 490 Ma and 497 – 682 Ma) similar to the Organ Rock, but also contains 928 – 1299 Ma age groups, consistent recycling of Grenville age signature, potentially derived from Appalachia or the Ellesmerian orogen (Dickinson and Gehrels, 2003, 2009; Gehrels et al., 2011; Gehrels and Pecha, 2014; Leary et al., 2020). Overlying the Moenkopi, our Chinle Formation sample (18PX02) from Moab Valley is dominated the 291 – 490 Ma, 497 – 682 Ma, and 928 – 1299 Ma age groups, as well as a Late Triassic age group with a peak at 214 Ma defining a maximum depositional age, thus confirming Norian depositional age (Irmis et al., 2011). This young age peak is defined by 3 grains. The youngest grain age is 213±5.8 Ma. This sample has fewer grains from the local basement sources than underlying formations (1300 – 1500 Ma, n= 8; 1600 – 1860 Ma, n = 8) suggesting that during deposition of the Chinle Formation, the local Granite-Rhyolite Province and Yavapai-Mazatzal basement rocks were limited sediment sources, potentially because they were being buried.

APPENDIX C

FLUVIAL – AEOLIAN DETRITAL ZIRCON U-PB AGE DATA
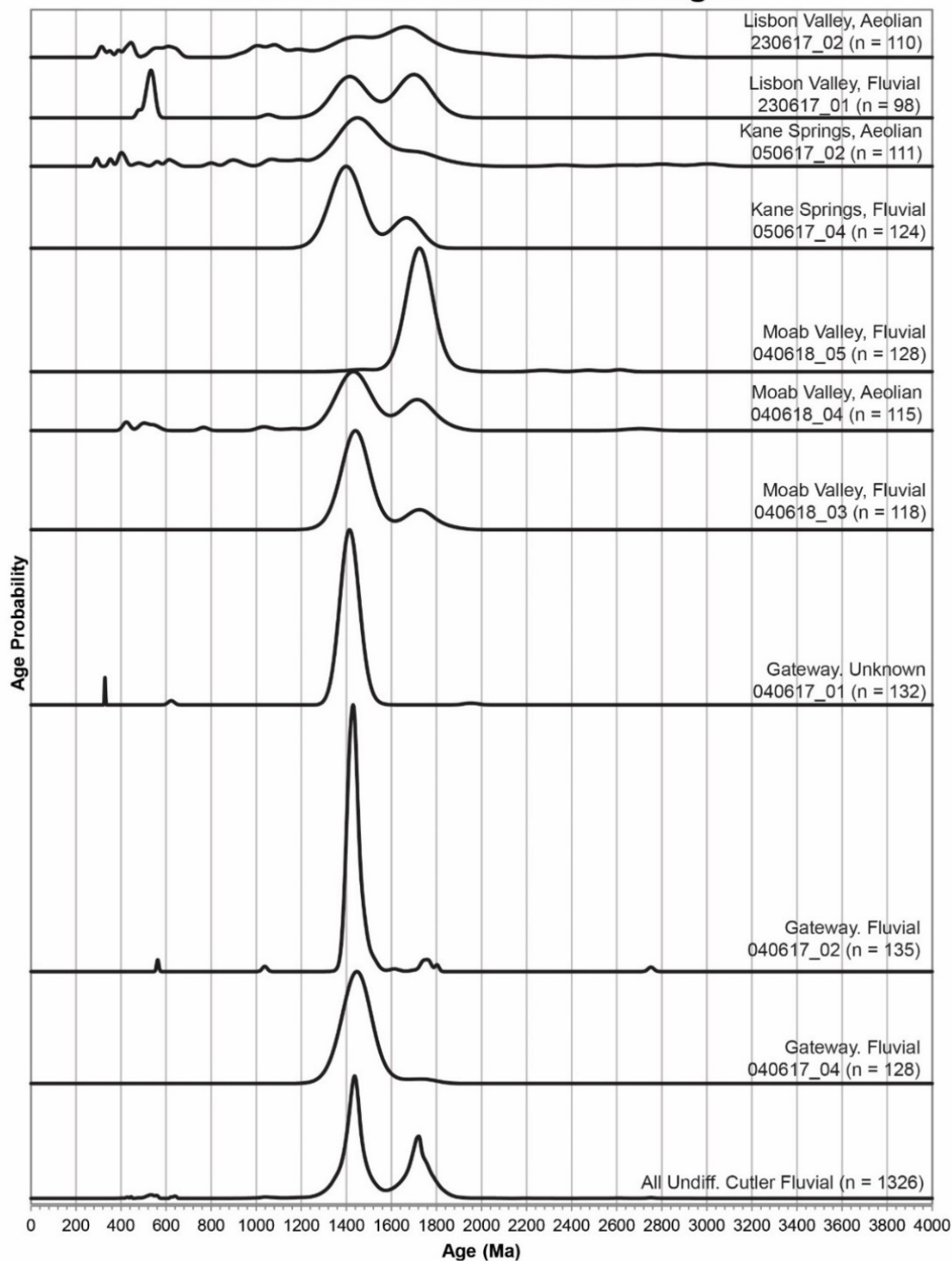
Undiff. Cutler Detrital Zircon Ages

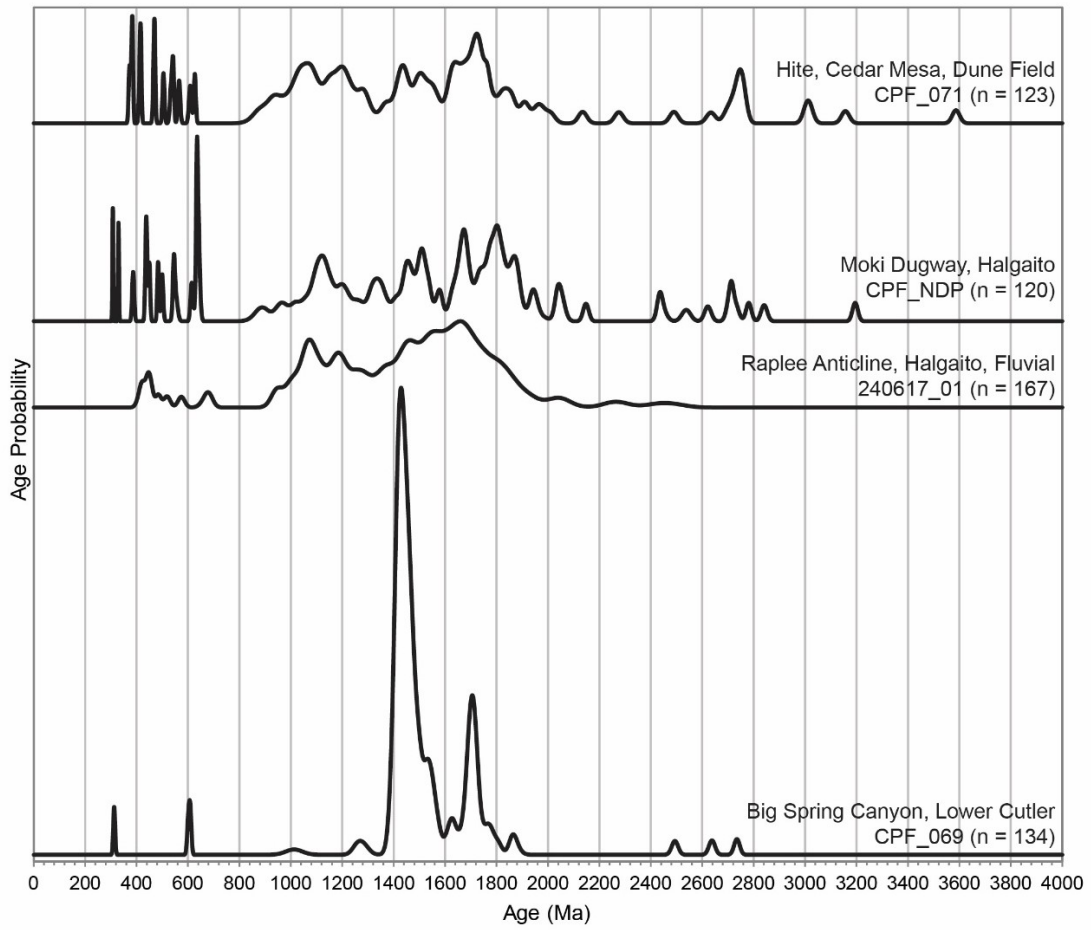**Figure 27: Fluvial and aeolian Cutler Group detrital zircon age PDPs.**

Figure 28: Fluvial and aeolian Cutler Group detrital zircon age PDPs, continued.

Table 19: Mean Cross Correlation Coefficient values for detrital zircon PDP comparison, calculated with DZStats (Saylor and Sundell, 2016). Sample names: 1 – All Undiff. Cutler Fluvial; 2 – 040617_04, Gateway, Fluvial; 3 – 040617_02, Gateway, Fluvial; 4 – 040617_01, Gateway, Unknown; 5 – 040618_03, Moab Valley, Fluvial;6 - 040618_04, Moab Valley, Aeolian; 7 - 040618_05, Moab Valley, Fluvial; 8 - 050617_04, Kane Springs, Fluvial; 9 - 050617_02, Kane Springs, Aeolian; 10 - 230617_01, Lisbon Valley, Fluvial; 11 - 230617_02, Lisbon Valley, Aeolian; 12 – CPF_069, Big Spring Canyon, Lower Cutler, Fluvial; CPF_071, Hite, Cedar Mesa, Aeolian; 240617_01, Raplee Anticline, Halgaito, Fluvial; CPF_NDP, Moki Dugway, Halgaito, Loess.

	1	2	3	4	5	6	7	8	9	10	11	12	13	14	15
1	1.00	0.63	0.64	0.61	0.71	0.69	0.18	0.59	0.48	0.52	0.33	0.63	0.15	0.21	0.10
2	0.63	1.00	0.68	0.81	0.97	0.76	0.00	0.70	0.69	0.43	0.21	0.64	0.11	0.18	0.10
3	0.64	0.68	1.00	0.80	0.68	0.46	0.00	0.41	0.37	0.23	0.10	0.78	0.10	0.07	0.03
4	0.61	0.81	0.80	1.00	0.78	0.55	0.00	0.61	0.45	0.32	0.12	0.65	0.10	0.08	0.05
5	0.71	0.97	0.68	0.78	1.00	0.82	0.02	0.72	0.70	0.50	0.28	0.67	0.15	0.21	0.11
6	0.69	0.76	0.46	0.55	0.82	1.00	0.20	0.80	0.73	0.73	0.49	0.62	0.18	0.33	0.19
7	0.18	0.00	0.00	0.00	0.02	0.20	1.00	0.10	0.07	0.37	0.34	0.07	0.09	0.13	0.15
8	0.59	0.70	0.41	0.61	0.72	0.80	0.10	1.00	0.65	0.68	0.39	0.49	0.13	0.31	0.14
9	0.48	0.69	0.37	0.45	0.70	0.73	0.07	0.65	1.00	0.49	0.40	0.45	0.12	0.35	0.16
10	0.52	0.43	0.23	0.32	0.50	0.73	0.37	0.68	0.49	1.00	0.55	0.36	0.19	0.30	0.16
11	0.33	0.21	0.10	0.12	0.28	0.49	0.34	0.39	0.40	0.55	1.00	0.20	0.18	0.41	0.20
12	0.63	0.64	0.78	0.65	0.67	0.62	0.07	0.49	0.45	0.36	0.20	1.00	0.13	0.12	0.07
13	0.15	0.11	0.10	0.10	0.15	0.18	0.09	0.13	0.12	0.19	0.18	0.13	1.00	0.14	0.07
14	0.21	0.18	0.07	0.08	0.21	0.33	0.13	0.31	0.35	0.30	0.41	0.12	0.14	1.00	0.11
15	0.10	0.10	0.03	0.05	0.11	0.19	0.15	0.14	0.16	0.16	0.20	0.07	0.07	0.11	1.00

Table 20: Fluvial and aeolian detrital zircon age statistics.

	040617_02 G_Fluvial	040617_04 G_Fluvial	040617_01 G_Unknown	041018_03 MV_Fluvial	040618_04 MV_Aeolian	041018_05 MV_Fluvial
n	135	150	131	118	115	128
D50	84	101	96	116	93	122
std dev	24	24	23	31	21	42
D97	165	152	150	182	153	222
relative 1440%	95%	94%	100%	83%	64%	2%
relative 1727%	5%	6%	0%	17%	34%	98%
relative 526%	1%	0%	0%	0%	2%	0%
Max UU	100%	100%	100%	100%	87%	100%
Min from UU	95%	91%	98%	97%	51%	95%
non-UU%	5%	9%	2%	3%	13%	5%

Table 20: Continued

	050617_04 KS_Fluvial	050617 -02 KS_Aeolian	230617_01 LV_Fluvial	230617_02 LV_Aeolian	CPF069 BS - Fluvial	CPF070 Organ Rock
n	131	111	98	110	134	122
D_{50}	65	56	69	52	71	57
std dev	29	15	24	13	18	9
D_{97}	134	95	138	88	115	79
relative 1440%	76%	74%	43%	39%	75%	43%
relative 1727%	24%	25%	45%	54%	25%	55%
relative 526%	0%	1%	12%	7%	0%	2%
Max UU	100%	62%	100%	54%	100%	100%
Min from UU	97%	26%	95%	18%	81%	43%
non-UU%	3%	38%	5%	46%	19%	57%

Table 20: Continued

	Cedar Mesa - Aeolian	Raplee Halgaito - Fluvial	Moki Halgaito - Unknown
n	123	167	120
D_{50}	75	66	59
std dev	16	10	10
D_{97}	111	90	80
relative 1440%	32%	42%	35%
relative 1727%	59%	55%	60%
relative 526%	9%	3%	5%
Max UU	36%	41%	36%
Min from UU	0%	5%	0%
non-UU%	64%	59%	64%

APPENDIX D

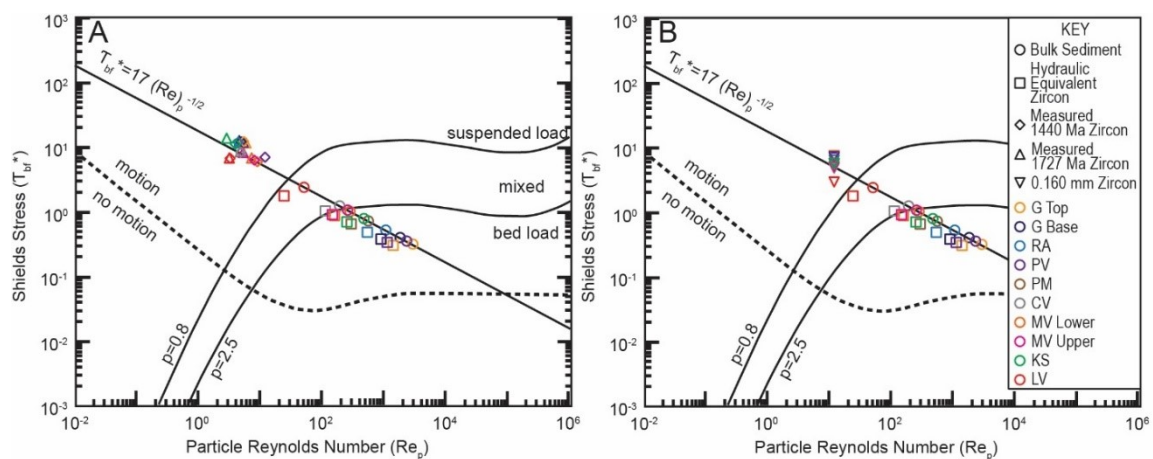FLUVIAL - AEOLIAN PALEOHYDRAULIC RECONSTRUCTION DATA

Figure 29: Rouse curves on a modified shields diagram show that the fluvial system was capable of transporting all zircon in suspension.

Table 21: Aeolian paleohydraulic reconstruction results.

		Bulk Sediment (Quartz)		
Sample	Facies	Bulk Sediment (μm)	w/u* (u*t of nearest aeolian)	w/u* - (u*i of Cedar Mesa D_{97})
Foredeep Fluvial - G, RA, CV, PV, MV, KS, LV	Fluvial	3470	36.2	35.9
G - 040617_02	Fluvial	7940	60.8	55.2
G - 040617_01	Unknown	156	2.6	2.3
MV - 040618_03	Fluvial	1690	24.4	24.0
MV - 040618_04	Aeolian	218	3.9	3.8
MV - 040618_05	Fluvial	159	2.4	2.4
KS - 050617_04	Fluvial	237	4.7	4.3
KS - 050617_02	Aeolian	156	2.6	2.3
LV - 230617_01	Fluvial	420	9.2	8.3
LV - 230617_02	Aeolian	156	2.6	2.3
BS - CPF_069	Fluvial	440	8.8	8.7
Hi - CPF_071	Aeolian	223	4.0	3.9
Raplee - 240617_01	Fluvial	156	2.6	2.3
Moki - CPF_NDP	Unknown	78	0.8	0.7

Table 21: Continued

Sample	Facies	zircon n	Measured Zircon (D50)				Measured Zircon (D97)		
			zircon D_{50} size (μm)	w/u* (u*t of nearest aeolian)	w/u* - (u*i of Cedar Mesa D_{97})		zircon D_{97} size (μm)	w/u* (u*t of nearest aeolian)	w/u* - (u*i of Cedar Mesa D_{97})
Foredeep Fluvial - G, RA, CV, PV, MV, KS, LV	Fluvial	1037	94	1.7	1.7		196	5.2	5.1
G - 040617_02	Fluvial	285	92	1.8	1.6		165	4.4	4.0
G - 040617_01	Unknown	131	96	1.9	1.7		150	3.9	3.5
MV - 040618_03	Fluvial	118	116	2.4	2.4		182	4.7	4.6
MV - 040618_04	Aeolian	115	93	1.7	1.7		153	3.7	3.6
MV - 040618_05	Fluvial	128	122	2.6	2.6		222	6.1	6.0
KS - 050617_04	Fluvial	131	65	1.0	0.9		134	3.3	3.0
KS - 050617_02	Aeolian	111	56	0.7	0.7		95	1.9	1.7
LV - 230617_01	Fluvial	98	69	1.1	1.0		138	3.4	3.1
LV - 230617_02	Aeolian	110	52	0.7	0.6		88	1.7	1.5
BS - CPF_069	Fluvial	300	71	1.0	1.0		115	2.4	2.3
Hi - CPF_071	Aeolian	300	75	1.2	1.1		111	2.2	2.2
Raplee - 240617_01	Fluvial	67	65	1.0	0.9		90	1.7	1.6
Moki - CPF_NDP	Unknown	300	59	0.8	0.7		80	1.4	1.3

APPENDIX E

COEFFICIENT OF VARIATION OF DUNE CROSS-STRATIFICATION

THICKNESS MEASUREMENTS

Table 22: Coefficient of variation values calculated from dune cross-stratification set thickness show that in the foredeep the fluvial system was aggradational and the aeolian system was not.

Location	Number of Measurements	Standard Deviation	Mean	Coefficient of Variance
Fluvial	348	0.08	0.13	0.64
Aeolian	13	1.08	1.29	0.84